



PhD

PROGRAM IN TRANSLATIONAL  
AND MOLECULAR MEDICINE

**DIMET**

UNIVERSITY OF MILANO-BICOCCA  
SCHOOL OF MEDICINE AND FACULTY OF SCIENCE

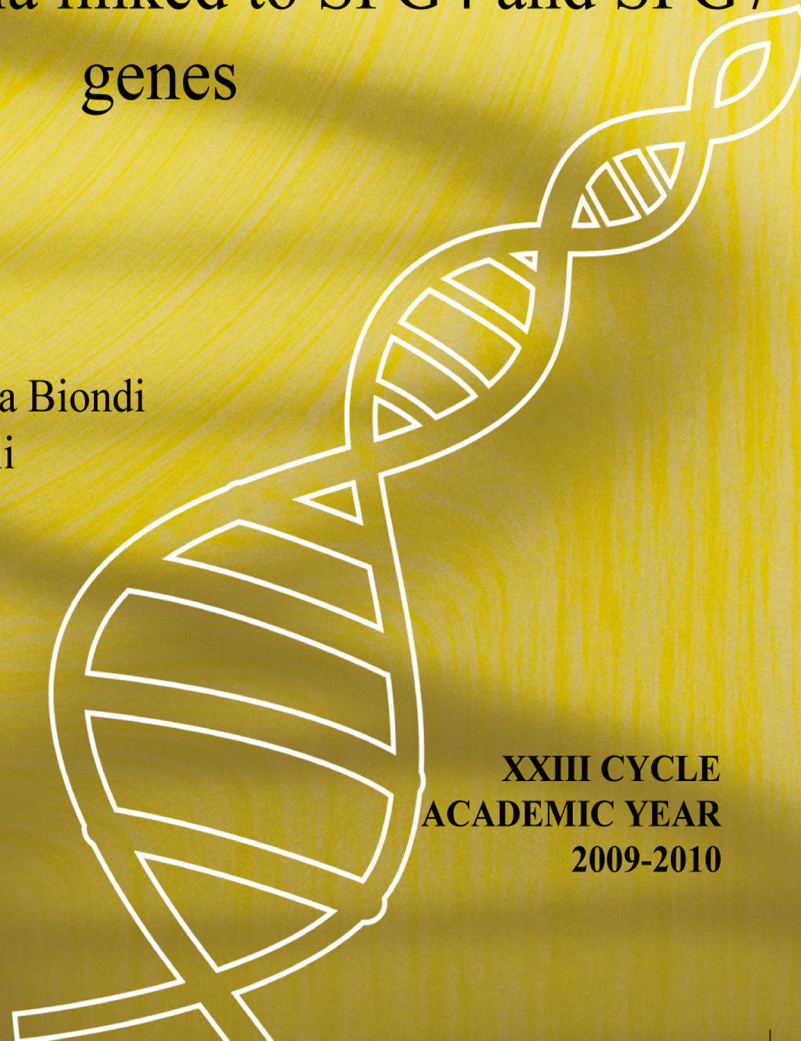
Dissecting the pathogenesis of hereditary  
spastic paraplegia linked to SPG4 and SPG7  
genes

Coordinator: Prof. Andrea Biondi  
Tutor: Prof. Elena Rugarli

Dr. Giuseppe Mancuso  
Matr. No. 033422

XXIII CYCLE  
ACADEMIC YEAR  
2009-2010

DIMET - Dr. Giuseppe Mancuso - A.A. 2009-10



*“We are the recipients of scientific method.  
We can each be a creative and active part of it if we so desire.”*

***Kary Mullis***

*to Mom and Dad*



# Table of Content

<b>TABLE OF CONTENT</b> -----	<b>4</b>
<b>INTRODUCTION</b> -----	<b>12</b>
HEREDITARY SPASTIC PARAPLEGIA-----	12
<i>Table 1</i> -----	13
<i>Figure 1</i> -----	16
HSP GENES INVOLVED IN MICROTUBULE DYNAMICS AND INTRACELLULAR MEMBRANE TRAFFIC-----	17
<i>SPG4/SPAST</i> -----	18
<i>Figure 2</i> -----	21
<i>SPG3A</i> -----	21
<i>SPG31/REEP1</i> -----	22
<i>SPG10/KIF5A</i> -----	23
<i>SPG20</i> -----	23
<i>SPG6/NIPA1</i> -----	24
<i>SPG17</i> -----	24
<i>SPG21</i> -----	25
<i>SPG15/ZFYVE26</i> -----	25
<i>SPG11</i> -----	26
<i>SPG8/KIAA1096</i> -----	26
MITOCHONDRIAL FORMS OF HSP-----	27
<i>SPG7</i> -----	27
<i>SPG13/HSPD1</i> -----	30
<i>Figure 3</i> -----	31
OTHER HSP GENES AND RELATED PATHWAYS-----	32
<i>SPG1/L1CAM</i> -----	32
<i>SPG2</i> -----	32
<i>SPG5/CYP7B1</i> -----	33

SPG35 -----	33
SPG39 -----	33
SPG42/SLC33A -----	34
SPG44/GJC2 -----	34
SPG48/KIAA0415 -----	35
REFERENCES -----	36
<b>AIM OF THE THESIS -----</b>	<b>51</b>
<b>A CRYPTIC PROMOTER IN THE FIRST EXON OF THE SPG4 GENE DIRECTS THE SYNTHESIS OF THE 60 KDA SPASTIN ISOFORM -----</b>	<b>52</b>
ABSTRACT -----	53
<i>Background:</i> -----	53
<i>Results:</i> -----	53
<i>Conclusions:</i> -----	54
BACKGROUND -----	55
RESULTS -----	59
<i>Translation of the 60 kDa spastin isoform does not depend on an IRES -----</i>	<i>59</i>
<i>A minimal ubiquitous SPG4 promoter -----</i>	<i>60</i>
<i>A tissue specific cryptic promoter in the first exon of SPG4 -----</i>	<i>62</i>
<i>Two phenotype modifier polymorphisms lie within the cryptic promoter -----</i>	<i>64</i>
<i>Identification of an endogenous SPG4 transcript specific for the short spastin     isoform -----</i>	<i>65</i>
DISCUSSION -----	67
CONCLUSIONS -----	72
METHODS -----	73
<i>Constructs:</i> -----	73
<i>Site-directed Mutagenesis:</i> -----	74
<i>DNA sequencing:</i> -----	75
<i>Luciferase assays:</i> -----	75
<i>In vitro transcription:</i> -----	76
<i>Cell culture, DNA and mRNA transfection and immunofluorescence:</i> -----	77

<i>SDS-PAGE and immunoblotting:</i>	77
<i>5' RACE:</i>	78
<i>Bioinformatics analysis:</i>	79
<i>Statistical analysis:</i>	79
AUTHORS' CONTRIBUTION	80
ACKNOWLEDGEMENTS	80
FIGURES	81
<i>Figure 1 - Schematic representation of the SPG4 first exon</i>	81
<i>Figure 2 - Experiments with dicistronic vectors reveal a cryptic promoter</i>	82
<i>Figure 3 - Analysis of the SPG4 minimal promoter</i>	84
<i>Figure 4 - Identification of a cryptic promoter in SPG4 exon 1</i>	86
<i>Figure 5 - The cryptic promoter mediates expression of the short spastin isoform in vivo</i>	88
<i>Figure 6 - The role of c.131C&gt;T and c.134C&gt;A polymorphisms on the cryptic promoter activity</i>	90
<i>Figure 7 - An endogenous SPG4 transcript specific for the 60 kDa spastin isoform</i>	92
ADDITIONAL FILES	94
<i>Figure S1 - Bioinformatic analysis of SPG4 transcription start sites based on cap analysis of gene expression</i>	94
REFERENCES	96
<b>PLEIOTROPIC EFFECTS OF SPASTIN ON NEURITE GROWTH DEPENDING ON EXPRESSION LEVELS</b>	<b>101</b>
ABSTRACT	102
INTRODUCTION	103
MATERIALS AND METHODS	106
<i>Patients and SPG4 mutation analysis:</i>	106
<i>Constructs:</i>	106
<i>Cell cultures:</i>	106
<i>Gene silencing:</i>	107

<i>Live cell imaging of EB3-GFP movement:</i> -----	108
<i>Overexpression experiments:</i> -----	108
<i>Immunoblotting:</i> -----	109
<i>Real-time PCR:</i> -----	109
RESULTS-----	111
<i>Reduced MT dynamics in spastin-depleted NSC34 cells</i> -----	111
<i>Spastin knock down affects axonal growth in primary hippocampal neurons</i> -----	113
<i>Effect of spastin overexpression on neurite extension and MT stability</i> -----	115
<i>Mild increase of spastin levels enhances neurite elongation and branching in NSC34 cells</i> -----	116
<i>SPG4 mutant alleles potentially leading to premature termination of translation do not produce truncated spastin isoforms</i> -----	118
DISCUSSION-----	121
ACKNOWLEDGMENTS-----	126
FIGURES-----	127
<i>Figure 1. Spastin RNA interference reduces MT dynamics in NSC34 cells</i> ----	127
<i>Figure 2. Silencing of spastin in hippocampal primary neurons affects neurite outgrowth</i> -----	129
<i>Figure 3. Spastin overexpression in hippocampal neurons</i> -----	131
<i>Figure 4. Spastin overexpression in NSC34 immortalized neurons leads to defects in neurite elongation and maintenance</i> -----	133
<i>Figure 5. Spastin upregulation at low levels in NSC34 cells leads to cell protrusions, neurite elongation and branching</i> -----	135
<i>Figure 6. Lack of truncated abnormal spastin isoform in SPG4 patients</i> ----	137
SUPPLEMENTARY MATERIALS AND METHODS-----	139
<i>HSP patients</i> -----	139
<i>Constructs</i> -----	140
<i>Real-time PCR</i> -----	140
SUPPLEMENTARY FIGURES-----	141
<i>S1. Validation of Spg4 gene silencing</i> -----	141

<i>S2. Morphometric analyses in spastin-silenced neurons</i> -----	143
<i>S3. Spastin overexpression affects acetylated and detyrosinated MTs</i> -----	144
<i>S4. Expression of spastin under the endogenous promoter leads to decreased levels of acetylated tubulin</i> -----	146
<i>S5. Validation of the ability of the spastin antibody to detect truncated spastin isoforms</i> -----	147
VIDEO DESCRIPTION-----	149
<i>Video 1.</i> -----	149
<i>Video 2.</i> -----	149
SUPPLEMENTARY TABLE. -----	149
<i>SPG4 mutations analyzed in this study</i> -----	149
REFERENCES-----	150
SUPPLEMENTARY REFERENCES -----	156

## **REGULATION OF OPA1 PROCESSING AND MITOCHONDRIAL FUSION BY M-AAA**

### **PROTEASE ISOENZYMES AND OMA1 ----- 157**

ABSTRACT -----	158
INTRODUCTION-----	159
RESULTS -----	162
<i>AFG3L1 and AFG3L2 are required for mitochondrial fusion</i> -----	162
<i>The m-AAA protease controls the stability of L-OPA1</i> -----	163
<i>Respiratory activity of m-AAA protease deficient mitochondria</i> -----	165
<i>A dominant negative mutant of AFG3L2</i> -----	167
<i>OMA1 mediates OPA1 processing in the absence of m-AAA proteases</i> -----	168
<i>Tissue-specific destabilization of L-OPA1 in Afg3l2<sup>-/-</sup> mice</i> -----	172
<i>Mitochondrial dysfunction induces OPA1 processing by OMA1</i> -----	173
DISCUSSION -----	175
MATERIAL AND METHODS-----	181
<i>Generation of immortalized MEFs lines.</i> -----	181
<i>Downregulation of m-AAA protease subunits and OMA1</i> -----	181
<i>Expression of AFG3L2 variants and OMA1</i> -----	182



<i>Assessment of cell growth</i> -----	182
<i>Fluorescence microscopy</i> -----	183
<i>Transmission electron microscopy</i> -----	183
<i>Polarographic measurements</i> -----	184
<i>Inhibitor studies</i> -----	184
<i>Antibodies</i> -----	185
<i>Online Supplemental Material</i> -----	185
ACKNOWLEDGEMENTS-----	186
ABBREVIATIONS-----	186
FIGURE LEGENDS-----	187
<i>Figure 1. Fragmentation of mitochondria in MEFs depleted of AFG3L1 and AFG3L2.</i> -----	187
<i>Figure 2. AFG3L1 and AFG3L2 are required for mitochondrial fusion.</i> -----	189
<i>Figure 3. Destabilization of long OPA1 isoforms in the absence of the m-AAA protease.</i> -----	191
<i>Figure 4. Expression of dominant negative AFG3L2<sup>E408Q</sup> inhibits cell proliferation and impairs mitochondrial morphology and OPA1 processing.</i> -----	193
<i>Figure 5. OMA1 degrades OPA1 in AFG3L1/AFG3L2-deficient MEFs.</i> -----	195
<i>Figure 6. Impaired OPA1 processing in Afg3l2<sup>-/-</sup>-mice.</i> -----	197
<i>Figure 7. Mitochondrial dysfunction induces OPA1 processing by OMA1.</i> ---	199
<i>Figure 8. Two peptidases regulate OPA1 cleavage at S1.</i> -----	201
SUPPLEMENTAL FIGURE LEGENDS-----	202
<i>Supplemental Figure S1.</i> -----	202
<i>Supplemental Figure S2.</i> -----	203
<i>Supplemental Figure S3.</i> -----	204
<i>Figure S4.</i> -----	206
<i>Figure S5.</i> -----	209
REFERENCES-----	210

<b>ALTERNATIVE SPLICING OF SPG7, A GENE INVOLVED IN HEREDITARY SPASTIC PARAPLEGIA, ENCODES A VARIANT OF PARAPLEGIN TARGETED TO THE ENDOPLASMIC RETICULUM.</b>	<b>217</b>
ABSTRACT	218
INTRODUCTION	219
RESULTS:	222
1. <i>An alternative Paraplegin isoform localizes to the Endoplasmic Reticulum.</i>	222
2. <i>The catalytic domain of Paraplegin2 is exposed inside ER lumen.</i>	224
3. <i>Paraplegin2 needs a partner to form an high molecular weight complex</i>	225
4. <i>Paraplegin2 is endogenously synthesized in mouse brain and forms an high molecular weight complex.</i>	226
5. <i>Paraplegin2 interacts with Seipin, an ER protein involved in HSP.</i>	227
MATERIALS AND METHODS:	229
1. <i>RT-PCR and cloning.</i>	229
2. <i>Immunofluorescence analysis and live imaging microscopy.</i>	229
3. <i>SDS-page protection assay, subcellular fractionation and gel filtration assay.</i>	230
4. <i>Immunoprecipitation assay</i>	231
5. <i>Antibodies</i>	232
DISCUSSION:	233
FIGURE LEGENDS:	237
<i>Figure 1:</i>	237
<i>Figure 2:</i>	239
<i>Figure 3:</i>	241
<i>Figure 4:</i>	243
<i>Figure 5:</i>	245
<i>Figure 6:</i>	247
<i>Supplementary Figure 1:</i>	249
REFERENCES	251

<b>CONCLUSIONS</b>	<b>257</b>
SPG4 AND SPASTIN: RELEVANCE FOR TRANSLATIONAL RESEARCH	257
SPG7 AND PARAPLEGIN: RELEVANCE FOR TRANSLATIONAL RESEARCH	260
REFERENCES	264
<b>PUBLICATIONS</b>	<b>269</b>
<b>ACKNOWLEDGMENTS</b>	<b>270</b>
<i>Ringraziamenti in italiano</i>	272

# Introduction

## Hereditary Spastic Paraplegia

Hereditary Spastic Paraplegia (HSP) define inherited neurodegenerative conditions that are grouped together because they share the principal clinic feature of progressive spasticity of lower limbs. The presence or the absence of other neurological or non-neurological phenotypes leads to the division of HSPs into two main groups: pure and complicated forms [1-4]. Nowadays several molecular evidences have been reported suggesting this division is not entirely clearcut, but it still remains as a clinical useful classification.

The first histopathological analysis on HSP patients was performed by Strümpell and revealed degeneration of the lateral corticospinal tracts disproportionately affecting the lumbar region, with less obvious involvement of the anterior corticospinal tracts [5, 6]. More recent studies reported a length-dependent neurodegeneration, also called “dying back” axonopathy, involving distal ends of sensory and motor axons in the spinal cord. The spinocerebellar tracts are also involved, but to a lesser degree. Moreover, loss of Betz cells, loss of cells in Clarke’s column and anterior horn cell degeneration are infrequent findings [7-10]. Finally, a recent post mortem analysis on HSP patients showed a significant reduction in axonal area and

density at all spinal cord levels examined [11]. The gross pathological findings therefore reflect the clinical phenotype observed in HSP.

From a genetic point of view, both pure and complicated HSPs can be inherited in autosomal dominant (AD), autosomal recessive (AR) or X-linked inheritance pattern and show considerable genetic locus heterogeneity [7]. At the time of writing 20 HSP genes have been identified and 21 more have been mapped to chromosomal location (Table 1) [12]. Although our knowledge of the genetics of HSP is not yet complete, these discoveries have formed the basis of a genetic classification. Notably, the mechanism by which alteration in several genes with totally different functions leads to the same pathogenetic phenotype is still unclear and its study will be fundamental in allowing the rational development of therapeutic approaches for this group of conditions (Figure 1).

The identification of HSP genes also permit to sort them into functional groups. The two larger categories obtained from this grouping analysis comprehend proteins involved in membrane traffic processes and those involved in mitochondrial functions.

*Table 1*

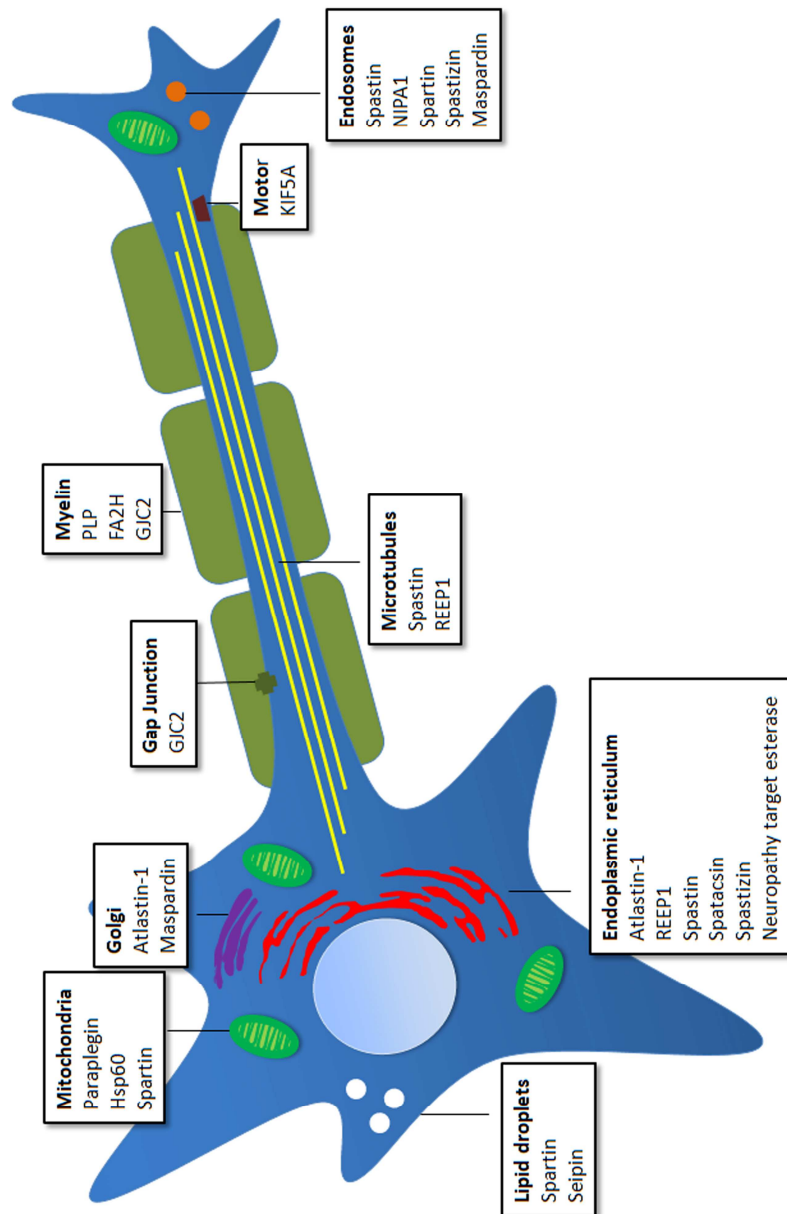
List of known HSP genes, loci and associated proteins, obtained from the OMIM database (<http://www.ncbi.nlm.nih.gov/sites/entrez>).

ACRONYM	INHERITANCE	LOCATION	PHENOTYPE	PROTEIN	FUNCTION
SPG1/L1CAM	X-linked	Xq28	Complicated	L1CAM	Development and guidance of the corticospinal tract
SPG2	X-linked	Xq21-22	Complicated	PLP	Axon-glia interaction
SPG3A/ATL1	AD	14q11-q21	Pure	Atlastin	Endoplasmic Reticulum morphogenesis
SPG4	AD	2p24-21	Pure	Spastin	Microtubule severing
SPG5/CYP7B1	AR	8p12-q13	Pure	CYP7B1	Cholesterol and Neurosteroid metabolism
SPG6/NIPA1	AD	15q11.1	Pure	NIPA1	Membrane trafficking, BMP signaling
SPG7	AR	16q24.3	Pure/Complicated	Paraplegin	Mitochondrial protease
SPG8/KIAA0196	AD	8q23-24	Pure	Strumpellin/KIAA0196	Endosomal trafficking related to Actin dynamics
SPG9	AD	10q23-24	Complicated		
SPG10/KIF5A	AD	12q13	Pure	KIF5A	Anterograde motor protein
SPG11	AR	15q13	Pure	Spatacsin	Membrane trafficking (?)
SPG12	AD	19q13	Pure		
SPG13/HSPD1	AD	2q24	Pure	HSP60	Mitochondrial chaperone
SPG14	AR	3q27-28	Complicated		
SPG15/ZFYVE26	AR	14q22-q24	Complicated	ZFYV26 (Spastizin)	Membrane trafficking (?)
SPG16	X-linked	Xq11.2	Complicated		
SPG17/BSC12	AD	11q12-q14	Complicated	Seipin	Lipid droplets metabolism
SPG18	AR	8p12-p11 21			
SPG19	AD	9q33-q34	Pure		
SPG20	AR	13q12.3	Complicated	Spartin	Endosomal and lipid droplets trafficking (?)
SPG21	AR	15q22.31	Complicated	Masparidin	Membrane Trafficking

ACRONYM	INHERITANCE	LOCATION	PHENOTYPE	PROTEIN	FUNCTION
SPG23	AR	1q24-q32	Complicated		
SPG24	AR	13q14	Pure		
SPG25	AR	6q23.3-q24.1	Complicated		
SPG26	AR	12p11.1-q14	Complicated		
SPG27	AR	10q22.1-q24.1	Pure		
SPG28	AR	14q21.3-q22.3	Pure		
SPG29	AD	1p31.1-21.1	Complicated		
SPG30	AR	2q37.3	Complicated		
SPG31/REEP1	AD	2p11.2	Pure	REEP1	ER-microtubule interaction
SPG32	AR	14q12-q21	Complicated		
SPG34	X-linked	Xq24-q25	Pure		
SPG35	AR	16q21-q23.1	Complicated	FA2H	hydroxylation of myelin galactocerebroside lipid components
SPG39	AR	19p13.3	Complicated	NTE	Phospholipid homeostasis
SPG41	AD	11p14.1-p11.2			
SPG42/SLC33A	AD	3q24	Pure	SLC33A1	Acyl-CoA transporter
SPG43	AR	11p13.11-q12	Complicated		
SPG44/GJC2	AR	1q41-q42	Complicated	Connexin 47	Gap junction protein
SPG45	AR	10q24.3-q25.1	Complicated		
SPG48/KIAA0415	AR	7p22.2	Complicated	KIAA0415	DNA repair

Figure 1

Schematic representation of a motor neuron, with the subcellular localization of the known HSP genes.





## **HSP genes involved in microtubule dynamics and intracellular membrane traffic**

The membrane traffic/transport cluster is the largest functional group of HSP proteins and the most relevant in terms of disease incidence. Members of this family are Spastin, Atlastin, REEP1, KIF5A, NIPA1, Masparidin and Spartin. In addition, other HSP proteins like Seipin, Spatacsin and Spastizin could also be related with this group. Intracellular membrane traffic is the targeted movement of cargo molecules between membrane-bound compartments based on small membrane bound vesicles. This phenomena involve complex processes like co-ordinated membrane modeling, membrane scission, motor proteins mediated transport of vesicle along the cytoskeleton, membrane recognition and docking and membrane fusion dynamics [13]. Within cells these processes occur in two main pathways, the secretory and the endocytic. In the first case, newly synthesized proteins are transported from ER to Golgi and then to the trans-Golgi network, where they are sorted for delivery to secretory granules, plasma membrane or endosomes. In the second case, transmembrane proteins of the plasma membrane are delivered to early endosomes where they may be recycled to the plasma membrane or sent to several intracellular location including Golgi, late endosomes and lysosomes [14].

### *SPG4/SPAST*

The SPG4 gene encodes for Spastin, a protein that belongs to the AAA family (ATPases Associated with various cellular Activity). AAA proteins are involved in several biological processes such as DNA replication and recombination, transcription, organelle biogenesis, proteolysis and microtubule regulation, but they all use ATP hydrolysis to dismantle or unfold protein complexes [15, 16]. In particular Spastin is part of the subfamily-7 of AAA proteins, like Katanin, a microtubule severing protein, and SKD1, a component of endosomal trafficking machinery. Interestingly, Spastin appears to combine both functions. In addition to the AAA domain, Spastin present other regions that are really important for its function (Figure 2). In the N-terminal portion of the protein are in fact localized the Microtubule Interacting and Trafficking (MIT) domain and the Microtubule Binding Domain (MTBD). The MIT domain was identified for the first time in the Sortin Nexin SNX15 and then in other proteins involved in trafficking pathways like the previously cited SKD1 [17] and in the HSP related protein Spartin [18]. This domain consist of an asymmetric 3-helix bundle that binds amphipatic helices called MIT-interacting motifs (MIMs). A biochemical role for MIT was connected to a group of structurally related proteins, the Charged Multivesicular Body Proteins (CHMPs), components of the Endosomal Sorting Complex Required for Transport (ESCRT) machinery [19, 20]. After the MIT domain, Spastin presents a 32 amino acids region encoded by exon 4. However, this little portion may be absent due to

alternative splicing of SPG4 mRNA without apparent alteration in the protein activity.

Finally, to complete the Spastin structural overview, two different isoforms of the protein have been described, starting from two different Methionine in position 1 and 87. This two proteins have a different expression pattern in mouse tissues [21], with a strong enrichment of the longest one in the nervous system. The first 86 amino acids, exclusively present in the long Spastin, form a hydrophobic region that functions as a Nuclear Export Signal (NES) [21], but has also been suggested as a transmembrane anchor. Under overexpression conditions, the two Spastin isoforms have also a different subcellular localization, with the longest one that forms discrete punctate structures in the cytoplasm and the shorter one that instead appears more diffuse and also present in the nucleus [21].

Several evidences confirmed Spastin as a microtubule severing protein. Microtubules (MTs) are dynamic polymers that undergo remarkable alterations in organization and distribution during cellular events such as mitosis, migration or neurite outgrowth. MT dynamics is largely accomplished through rapid assembly and disassembly of the MTs at their plus ends [13]. MT severing represents an additional process for cytoskeletal dynamics in which MT are cutted along their length [22]. The first microtubule severing protein identified was a Spastin highly homologous AAA protein called Katanin P60 [23].

Cells transfected for Spastin present disrupted microtubule cytoskeleton showing sparse and short MTs with recognizable ends and this peculiar phenotype was also reproducible using a *Drosophila* system [24, 25]. Otherwise, the formal proof that Spastin severs MTs was obtained by *in vitro* assays using recombinant Spastin together with immobilized rhodamine-labeled MTs [26, 27].

As most of the AAA+ protein do, also Spastin forms a hexameric structure in its active form and this oligomerization occurs in an ATP-dependent manner [28, 29]. In this hexameric state, pore loop residues of Spastin bind the C-terminal tail of Tubulin pulling it through the central pore of the complex and generating a mechanical force that destabilizes the tubulin-tubulin interactions.

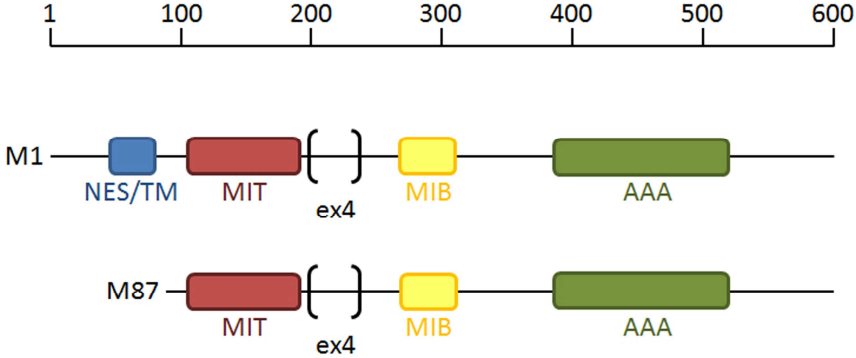
Mutation in Spastin are distributed along the entire gene with the exception of the alternatively spliced exon 4. The mutational spectrum comprehend all types of mutations, including large scale rearrangements [30].

With its N-terminal region, Spastin interact with several partners. With the exception of NA14, that is a protein of the centrosome [31], all the other interactors are integral membrane or membrane associated proteins: Protrudin/ZFYVE27 is a protein involved in neurite extension and directional membrane trafficking [32-34], CHMP1B is a component of the ESCRT complex [35], GP25L2 is a protein involved in ER-to-Golgi traffick [35] and Reticulon1 is a protein involved in ER morphogenesis [36]. More interesting, the HSP related protein Atlastin was published as a Spastin interactor and

have been characterized as a ER morphogenesis related factor [37, 38].

Figure 2

Schematic representation of Spastin isoforms, starting from methionine 1 or 87. Exon 4 can be subject to alternative splicing and is depicted in brackets. Abbreviations : NES/TM, putative nuclear export signal, transmembrane region; MIT, microtubule-interacting and trafficking domain; MTB, microtubule binding domain ; AAA, AAA domain.



SPG3A

SPG3A is the gene that encodes for Atlastin, a GTPase protein member of the dynamine/guanylate binding family. Due to high homology, two additional protein of this family were named Atlastin-2 and Atlastin-3 [39]. Subcellular localization studies have suggested that Atlastin is an integral protein of the early secretory pathway membrane, with a topology that exposes both C- and N- terminal

region in the cytosol [39]. Moreover, this protein has a GTPase function and forms homo-holigomers *in vivo* [39]. One of the pathways associated with Atlastin is the ER morphogenesis, in particular ER membrane curvature processes fundamental for tubular ER formation [40] and in *Drosophila* it was also reported as a factor promoting homotypic fusion of ER membranes in a GTP depending manner [41]. The interaction of the C-terminal region of Atlastin with Spastin suggests a coupling between ER modeling events and cytoskeletal regulation, also important for ER morphogenesis [42].

#### *SPG31/REEP1*

The SPG31 gene encodes for Receptor Expression Enhancing Protein 1 (REEP1), a mammalian homologue of the DP1/Yop1p family. The subcellular localization of REEP1 is controversial due to the presence of different articles that report it as a mitochondrial, but also as an ER protein [43, 44]. Otherwise, a recent study demonstrates that REEP1 localizes prominently to the tubular ER, where it interacts with both Atlastin and Spastin through an intramembrane, hydrophobic hairpin domain. Unexpectedly, REEP1 also mediates interaction of the tubular ER with microtubules, which identifies REEP1 as a member of a novel protein family within the DP1/Yop1p superfamily [45]. Moreover, a truncated REEP1 protein resulting from a pathogenic *SPG31* mutation does not bind microtubules and it disrupts the ER network [45].

### *SPG10/KIF5A*

The SPG10 gene encodes for KIF5A protein, a member of the kinesin superfamily. Kinesins are motor proteins that use energy obtained from ATP hydrolysis to move cargoes along MT [46]. *In vivo*, KIF5 proteins form tetrameric complexes with kinesin light chain (KLC) proteins. These tetramers are called Kinesin-I. The ATPase and the MT binding domains are contained in the N-terminal portion of the protein, termed motor domain, while C-terminal binds KLC and cargo proteins [46]. Even if specific KIF5A cargoes have not been identified yet, it has been characterized as an anterograde motor protein for neurofilaments [46, 47]. In the secretory pathway KIF5s are involved in ER-to-Golgi and Golgi-to-ER traffic, but also in Golgi to plasma membrane transport, while in the endosomal pathway they play a role in transport of recycling endosomes and lysosomes [46, 48].

### *SPG20*

The SPG20 gene encodes for Spartin. The characterization of this protein present a lot of controversial results in term of subcellular localization and function. Under overexpression conditions Spartin was in fact published as a mitochondrial protein [49], but also as a cytosolic protein recruited to endosomes by Epidermal Growth Factor (EGF) stimulation [50]. Finally, a third overexpression study defined Spartin as a cytoplasmatic protein recruited on Lipid Droplets (LD) under LD induction stimuli based on oleic acid treatment [51]. These last findings were confirmed by analysis performed on the

endogenous protein [52]. The MIT domain contained in Spartin [18] give also a clue about a role of the protein in endosome, suggesting a close connection between these compartments and the LD.

#### *SPG6/NIPA1*

The SPG6 gene encodes for NIPA1, a polytopic integral membrane protein that localizes to plasma membrane, endosomes and possibly on Golgi apparatus [53, 54]. The protein appears to be a functional magnesium transporter [54]. Studies examining the effect of NIPA1 mutations involved in the disease (T45R and G106R) have shown that they affect traffic of the protein through the secretory pathway by trapping the mutant in the ER [54-56]. A study made in *C. elegans* suggested the hypothesis that this entrapment could lead to the pathogenesis of the disease through a gain-of-function induction of ER Unfolded Protein Response (UPR) and consequent cell death [55], but experiments in mammalian cells couldn't reproduce these data [56]. Another hypothesis arising from study of the *Drosophila* homologue of NIPA1 linked instead the pathogenesis of the disease to an impairment in Bone Morphogenic Protein (BMP) signaling [57].

#### *SPG17*

SPG17 gene encodes for Seipin, a protein anchored to ER membrane due to the presence of two transmembrane domains that form an ER lumen loop [58]. This protein is expressed in motor neurons of the spinal cord and in the cortex of brain, consistently with the cellular



target of the disease [58]. Seipin deficiency clearly affect lipid metabolism both in yeast, where an impairment in LD formation has been reported, and in humans, where recessive loss of function mutation leads to Berardinelli-Seip lipodistrophy [59-61]. However, this function seems not to be related with HSP pathogenesis. The mutations found in patients with Silver Syndrome HSP (N88S and S90L) in fact act in an autosomal dominant matter and seem to be characterized by a gain-of-function pathogenetic mechanism. These mutation alter a glycosylation motif promoting Seipin polyubiquitination, a phenomena that leads to protein aggregation, ER stress and cell death [58, 62]. However, all these ER stress condition were obtained using overexpression approaches and may not reproduce properly endogenous conditions.

#### *SPG21*

The SPG21 gene encodes for Maspardin, also termed Acid Cluster Protein 33 (ACP33) [63]. This protein localizes to endosomes and binds to the cytoplasmatic tail of the CD4 immune receptor, regulating its signaling activity [63].

#### *SPG15/ZFYVE26*

The SPG15 gene encodes for Spastizin, an endosomal protein containing a FYVE (found in Fab1p, YOTB, Vac1p and EEA1) zinc finger domain [64]. This domain binds specifically to Phosphotidyl Inositol 3

Phosphate, a phospholipid found in endosomal membranes and is often required for protein binding to this organelle [65].

#### *SPG11*

The SPG11 gene encode for Spatacsin, a four transmembrane domain protein that may be involved in membrane trafficking. It shows a histological expression pattern in brain very similar to the Spastizin one and if this is considered in the context of the similar phenotype in disease, it can suggest a functional relationship between the two proteins [66, 67].

#### *SPG8/KIAA1096*

The SPG8 gene encodes for Strumpellin, a protein that also localizes to the endosomal compartment [12]. Recently this protein has been characterized as part of a 500 kDa complex in which are present also FAM21, KIAA1033, WASH and CCDC53. In cells, this complex regulate Actin dynamics through WASH-Arp2/3 pathway, suggesting a role of endosomal trafficking related to Actin dynamics in the pathogenesis of the disease [68].

## **Mitochondrial forms of HSP**

Even if several HSP proteins have been published as mitochondrial, for most of them like REEP1, Spartin and Spatacsin [44, 49, 67] further analysis opened to different hypothesis. The only two HSP proteins that up to now have been described as 100% mitochondrial located are Paraplegin and HSP60.

### *SPG7*

The SPG7 gene encodes for Paraplegin, a 795 amino acids mitochondrial protein with a N-terminal mitochondrial targeting sequence (MTS), two transmembrane domains, a AAA domain and a metal dependent proteolytic domain. This last domain belongs to the M41 family of peptidases and contains the HEXXH metal binding motif in the proteolytic center. Paraplegin is a subunit of the *m*-AAA protease, a hexameric complex located in the inner membrane of the mitochondria that exposes the active region composed by AAA and proteolytic domains into the mitochondrial matrix (*m*- stands for matrix). The human *m*-AAA protease has a native molecular mass of approximately 900 kDa and may be composed either by Paraplegin and AFGL2 or only by AFG3L2, depending if AFG3L2 hetero- or homo-oligomerizes [69].

The *m*-AAA protease has been mainly studied in *S. Cerevisiae* where it is composed by the two subunits Yta10p and Yta12p, presumably present in equimolar amount and able to assemble only in a hetero-oligomeric fashion [70]. In yeast the *m*-AAA protease plays a

fundamental role during mitochondrial biogenesis and its inactivation or depletion lead to the inability to grow on non-fermentable carbon sources [71]. The YTA10p-Yte12p complex actively extracts transmembrane segments and pulls solvent-exposed domains across the membrane before exerting its proteolytic activity. This process is driven by the AAA domain that acts both as a chaperon to recognize and bind short N-terminal and C-terminal matrix misfolded domains of membrane protein, but also as an ATP motor to dislocate the substrate from the membrane. Respiratory chain proteins and F1Fo ATPase subunits have been described as substrates for *m*-AAA protease [71] and therefore this protease is defined as a key component of a quality control system that mitochondria use to conduct the surveillance of proteins of the inner membrane and to degrade in a selective manner non assembled or damaged peptides. Moreover, an additional role of yeast *m*-AAA protease involves the ability to mediate proteolytic maturation of specific proteins. The main substrate described in yeast is MRPL32, a component of mitochondrial ribosomal complex [72]. This substrate is synthesized as a precursor protein that is imported within mitochondria and then processed by *m*-AAA protease, remaining in tight association with mitochondrial inner membrane. This maturation is required for correct assembly of MRPL32 in the ribosomal complex and a defect in this processing event affects severely the mitochondrial protein synthesis, providing an explanation for the respiratory deficiency found in strains depleted for Yta10p and Yte12p [72]. Reconstruction experiments performed in *S. Cerevisiae* by deleting the yeast *m*-AAA

and expressing the mammalian one evidence also another important role for this protease. Mouse AFG3L2 in fact mediates its own maturation upon mitochondrial import and also processed newly imported Paraplegin [73] (Figure 3). Furthermore, these studies have suggested a role of the mammalian *m*-AAA protease in the processing of the dynamin-like GTPase Opa1 [74, 75], a protein involved in inner membrane fusion, in regulation of cristae morphology and in protecting cells from apoptosis. Mitochondria contain several mature Opa1 isoforms that arise through the combination of alternative splicing events and proteolytic maturation. A combination of long and short Opa1 is required for mitochondrial fusion and cristae maintenance [76]. The formation of short isoforms of Opa1 is impaired in yeast strains deleted for the *m*-AAA protease, but is restored upon mammalian subunits expression [74, 75]. Notably, no strong evidences have been reported so far about the role of *m*-AAA protease in Opa1 process in mammalian cells.

A mouse model of HSP due to Paraplegin deficiency was generated by constitutive inactivation of the *Spg7* gene [77]. These mice reproduce perfectly the late-onset complex phenotype of patients affected by AR HSP due to Paraplegin mutation, showing progressive motor impairments and a distal axonopathy affecting long motor and sensory spinal axons and peripheral and optic nerves. Notably, the beginning of the motor impairment in the knock out mice correlates with the appearance of enlarged and structurally abnormal mitochondria in the synaptic terminals of motor neurons. This mitochondrial alteration became worse with aging, but affects only

the axons of neurons that will degenerate, with no appearance in shorter axons and glial cells [77]. Moreover, the accumulation of morphologically abnormal mitochondria is followed by occurrence of segmental distension of axons formed by accumulation of neurofilaments and organelles, suggesting that also the impairment in the axonal transport seems to play an important role in neurodegeneration [77].

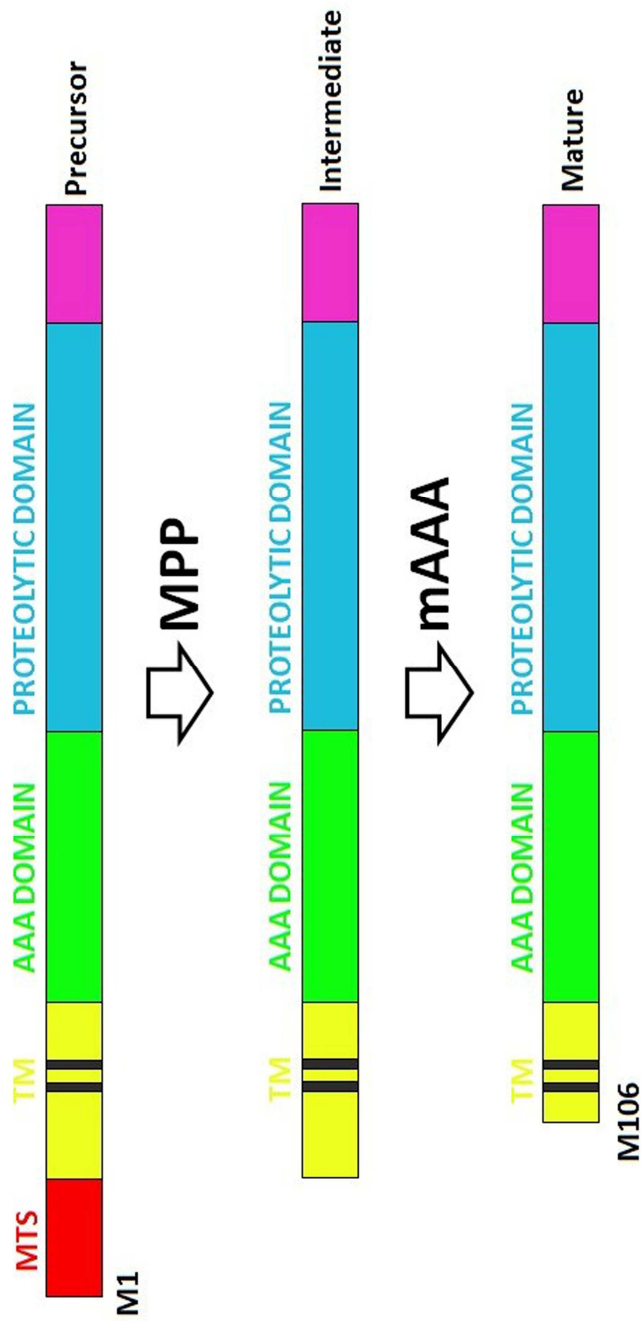
The *Spq7<sup>-/-</sup>* model was used to assess if replacement of Paraplegin specifically in axonal mitochondria could rescue the degeneration phenotype [78]. This study was performed by AAV2 viral vectors intramuscular injection and consequent delivery of Paraplegin cDNA to spinal motor neurons. The data obtained show statistical significant decrease in the number of swollen or degenerating axons and in the number of axons containing abnormal mitochondria, but also a considerable improvement in mice motor ability [78].

#### *SPG13/HSPD1*

The SPG13 gene encodes for the mitochondrial chaperonin HSP60, one of the main molecular chaperonines assisting mitochondrial proteins to achieve their native conformation. . Together with the mt-HSP70 machinery, HSP60 can specifically recognize non-native folding intermediates and stabilises them against aggregation. Albeit mt-HSP70 mediates the folding of the vast majority of newly imported mitochondrial proteins, the HSP60 system is required for the complete folding of a subset of proteins [79].

Figure 3

Schematic representation of Paraplegin structure and processing.



## **Other HSP genes and related pathways**

### *SPG1/L1CAM*

The SPG1 gene encodes for L1CAM, a transmembrane glycoprotein expressed during development on the surface of long axons and growth cones, including those of the corticospinal tracts. L1CAM mediates cell adhesion, neurite outgrowth, axon pathfinding and fasciculation through homophilic and heterophilic binding with a variety of extracellular and transmembrane molecules. It plays also an important role in mediating guidance of corticospinal axons through the pyramidal decussation [80, 81].

### *SPG2*

The SPG2 gene encodes for PLP1, a protein highly expressed in oligodendrocytes. This protein and its splicing variant DM20 constitute the 50% of myelin proteins. PLP1 is involved in stabilization and maintenance of the myelin sheath and it plays a major role in axonal-myelin interactions, whereas DM20 is assumed to be involved in oligodendrocyte maturation [82, 83]. The function of the protein has been studied in a range of spontaneous and genetically engineered animal models including the spontaneous mutant rumpshaker mouse (*RSH*). This model displays a relatively benign phenotype with tremor and preserved lifespan [84].



### *SPG5/CYP7B1*

The CYP7B1 gene encodes for a 7 $\alpha$ -hydroxylase involved in the acidic pathway of formation of primary bile acids from cholesterol. The role of this enzyme in the brain is to catabolize 27-OH-Cholesterol and also to provide the metabolic route for 7-OH-Dehydroepiandrosterone, a neurosteroid with important neuroprotective actions. Thus the pathogenic effect of the mutation may arise from toxic accumulation of oxysterol or from loss of neuroprotective effect of DHEA-related neurosteroids [85].

### *SPG35*

The SPG35 gene encodes for Fatty Acid 2-hydroxylase (FA2H). Mutations in this protein decrease enzymatic activity of the protein in vitro suggest that abnormal hydroxylation of myelin galactocerebroside lipid components can lead to a severe progressive phenotype, with a clinical presentation of complicated HSP and radiological features of leukodystrophy [86]. FA2H was also linked to regulation in cAMP-induced cell cycle exit [87].

### *SPG39*

The SPG39 gene encodes for Neuropathy Target Esterase (NTE), a protein closely involved in organophosphate (OP)-induced delayed neuropathy (OPIDN), a disease in which OP toxicity causes degeneration of the longest upper and lower motor neuron axons. The pathogenetic mechanism that leads to the disease could be

either related to direct OP-induced inhibition of NTE, or to the generation of OP-NTE neurotoxic complexes, or to a combination of these two events [88]. Depletion of NTE from mouse brain results in a neurodegenerative phenotype characterized by axonal degeneration and late onset hind-limb ataxia [89] and a close related phenotype can also be observed in flies mutated in the NTE homologue gene Swiss Cheese (SWS) [90]. Even if the function of NTE and its relation to axonal degeneration are still not completely clear, recent studies showed that both NTE and SWS localize to the endoplasmic reticulum: NTE is a phospholipase that regulates membrane phospholipid metabolism [91, 92] and SWS is also an interactor of PKA-C3 and mediate its recruitment to ER [93, 94].

#### *SPG42/SLC33A*

The SLC33A gene encodes for an acetyl-CoA transporter that translocate its substrate into the lumen of Golgi apparatus, where acetyl-CoA is transferred to the sialyl residues of gangliosides and glycoproteins. This protein modification can play an important role in outgrowth and maintenance of axons of the corticospinal tracts. Knock-down analysis performed on the Zebrafish orthologous for SLC33A cause defective axonal outgrowth from the spinal cord [95].

#### *SPG44/GJC2*

The SPG44 gene encodes for the gap junction protein Connexin 47 (Cx47). Protein with mutation involved in complicated HSP (99C>G)

forms gap junction plaques at cell borders similar to wild-type Cx47 in transfected cells, but fails to form functional homotypic channels in scrape-loading and dual whole-cell patch clamp assays [96].

#### *SPG48/KIAA0415*

The SPG48 gene encodes for the KIAA0415 protein, a putative helicase that interacts with Spatacsin and Spastizin. This gene was recently discovered using a genome-scale approach for studying homologous recombination DNA double-strand break repair (HRDSBR). The data proposed by the authors show an induced sensitivity of KIAA0415 mutant cells to DNA damaging drugs, connecting HSPs to DNA repair dynamics [97].

## References

1. Harding AE: **Classification of the hereditary ataxias and paraplegias.** *Lancet* 1983, **1**(8334):1151-1155.
2. Reid E: **Pure hereditary spastic paraplegia.** *J Med Genet* 1997, **34**(6):499-503.
3. McDermott C, White K, Bushby K, Shaw P: **Hereditary spastic paraparesis: a review of new developments.** *J Neurol Neurosurg Psychiatry* 2000, **69**(2):150-160.
4. Fink JK: **Advances in hereditary spastic paraplegia.** *Curr Opin Neurol* 1997, **10**(4):313-318.
5. Strümpell A: **Beiträge zur Pathologie des Rückenmarks;** 1880.
6. Strümpell A: **Ueber eine bestimmte Form der primären kombinierten Systemerkrankung des Rückenmarks;** 1886.
7. Harding AE: **The hereditary ataxias and related disorders.;** 1984.
8. Schwarz GA, Liu CN: **Hereditary (familial) spastic paraplegia; pathologic study of a case.** *Trans Am Neurol Assoc* 1955(80th Meeting):54-56.
9. Behan WM, Maia M: **Strumpell's familial spastic paraplegia: genetics and neuropathology.** *J Neurol Neurosurg Psychiatry* 1974, **37**(1):8-20.
10. Bruyn RP: **The neuropathology of hereditary spastic paraparesis.** *Clin Neurol Neurosurg* 1992, **94 Suppl**:S16-18.

11. Deluca GC, Ebers GC, Esiri MM: **The extent of axonal loss in the long tracts in hereditary spastic paraplegia.** *Neuropathol Appl Neurobiol* 2004, **30**(6):576-584.
12. Reid E. REI: **Scriver's Online Metabolic and Molecular Bases of Inherited Diseases.** In: *Hereditary Spastic Paraplegia.* Edited by Valle B, Vogelstein, Kinzler, Antonarakis, Ballabio; 2010.
13. Alberts B JA, Lewis J, Raff M, Roberts K and Walter P: **Molecular Biology of the Cell:** Garland Science; 2007.
14. Mellman I, Warren G: **The road taken: past and future foundations of membrane traffic.** *Cell* 2000, **100**(1):99-112.
15. Hanson PI, Whiteheart SW: **AAA+ proteins: have engine, will work.** *Nat Rev Mol Cell Biol* 2005, **6**(7):519-529.
16. Neuwald AF, Aravind L, Spouge JL, Koonin EV: **AAA+: A class of chaperone-like ATPases associated with the assembly, operation, and disassembly of protein complexes.** *Genome Res* 1999, **9**(1):27-43.
17. Rigden DJ, Liu H, Hayes SD, Urbe S, Clague MJ: **Ab initio protein modelling reveals novel human MIT domains.** *FEBS Lett* 2009, **583**(5):872-878.
18. Ciccarelli FD, Proukakis C, Patel H, Cross H, Azam S, Patton MA, Bork P, Crosby AH: **The identification of a conserved domain in both spartin and spastin, mutated in hereditary spastic paraplegia.** *Genomics* 2003, **81**(4):437-441.
19. Row PE, Liu H, Hayes S, Welchman R, Charalabous P, Hofmann K, Clague MJ, Sanderson CM, Urbe S: **The MIT domain of**

**UBPY constitutes a CHMP binding and endosomal localization signal required for efficient epidermal growth factor receptor degradation.** *J Biol Chem* 2007, **282**(42):30929-30937.

20. Tsang HT, Connell JW, Brown SE, Thompson A, Reid E, Sanderson CM: **A systematic analysis of human CHMP protein interactions: additional MIT domain-containing proteins bind to multiple components of the human ESCRT III complex.** *Genomics* 2006, **88**(3):333-346.
21. Claudiani P, Riano E, Errico A, Andolfi G, Rugarli EI: **Spastin subcellular localization is regulated through usage of different translation start sites and active export from the nucleus.** *Exp Cell Res* 2005, **309**(2):358-369.
22. Baas PW, Karabay A, Qiang L: **Microtubules cut and run.** *Trends Cell Biol* 2005, **15**(10):518-524.
23. McNally FJ, Vale RD: **Identification of katanin, an ATPase that severs and disassembles stable microtubules.** *Cell* 1993, **75**(3):419-429.
24. Errico A, Ballabio A, Rugarli EI: **Spastin, the protein mutated in autosomal dominant hereditary spastic paraplegia, is involved in microtubule dynamics.** *Hum Mol Genet* 2002, **11**(2):153-163.
25. Roll-Mecak A, Vale RD: **The Drosophila homologue of the hereditary spastic paraplegia protein, spastin, severs and disassembles microtubules.** *Curr Biol* 2005, **15**(7):650-655.

26. Salinas S, Carazo-Salas RE, Proukakis C, Cooper JM, Weston AE, Schiavo G, Warner TT: **Human spastin has multiple microtubule-related functions.** *J Neurochem* 2005, **95**(5):1411-1420.
27. Evans KJ, Gomes ER, Reisenweber SM, Gundersen GG, Lauring BP: **Linking axonal degeneration to microtubule remodeling by Spastin-mediated microtubule severing.** *J Cell Biol* 2005, **168**(4):599-606.
28. Pantakani DV, Swapna LS, Srinivasan N, Mannan AU: **Spastin oligomerizes into a hexamer and the mutant spastin (E442Q) redistribute the wild-type spastin into filamentous microtubule.** *J Neurochem* 2008, **106**(2):613-624.
29. White SR, Evans KJ, Lary J, Cole JL, Lauring B: **Recognition of C-terminal amino acids in tubulin by pore loops in Spastin is important for microtubule severing.** *J Cell Biol* 2007, **176**(7):995-1005.
30. Fonknechten N, Mavel D, Byrne P, Davoine CS, Cruaud C, Bonsch D, Samson D, Coutinho P, Hutchinson M, McMonagle P *et al*: **Spectrum of SPG4 mutations in autosomal dominant spastic paraplegia.** *Hum Mol Genet* 2000, **9**(4):637-644.
31. Errico A, Claudiani P, D'Addio M, Rugarli EI: **Spastin interacts with the centrosomal protein NA14, and is enriched in the spindle pole, the midbody and the distal axon.** *Hum Mol Genet* 2004, **13**(18):2121-2132.
32. Mannan AU, Krawen P, Sauter SM, Boehm J, Chronowska A, Paulus W, Neesen J, Engel W: **ZFYVE27 (SPG33), a novel**

- spastin-binding protein, is mutated in hereditary spastic paraplegia.** *Am J Hum Genet* 2006, **79**(2):351-357.
33. Martignoni M, Riano E, Rugarli EI: **The role of ZFYVE27/protrudin in hereditary spastic paraplegia.** *Am J Hum Genet* 2008, **83**(1):127-128; author reply 128-130.
34. Shirane M, Nakayama KI: **Protrudin induces neurite formation by directional membrane trafficking.** *Science* 2006, **314**(5800):818-821.
35. Reid E, Connell J, Edwards TL, Duley S, Brown SE, Sanderson CM: **The hereditary spastic paraplegia protein spastin interacts with the ESCRT-III complex-associated endosomal protein CHMP1B.** *Hum Mol Genet* 2005, **14**(1):19-38.
36. Mannan AU, Boehm J, Sauter SM, Rauber A, Byrne PC, Neesen J, Engel W: **Spastin, the most commonly mutated protein in hereditary spastic paraplegia interacts with Reticulon 1 an endoplasmic reticulum protein.** *Neurogenetics* 2006, **7**(2):93-103.
37. Sanderson CM, Connell JW, Edwards TL, Bright NA, Duley S, Thompson A, Luzio JP, Reid E: **Spastin and atlastin, two proteins mutated in autosomal-dominant hereditary spastic paraplegia, are binding partners.** *Hum Mol Genet* 2006, **15**(2):307-318.
38. Evans K, Keller C, Pavur K, Glasgow K, Conn B, Luring B: **Interaction of two hereditary spastic paraplegia gene products, spastin and atlastin, suggests a common pathway**



- for axonal maintenance.** *Proc Natl Acad Sci U S A* 2006, **103**(28):10666-10671.
39. Zhu PP, Patterson A, Lavoie B, Stadler J, Shoeb M, Patel R, Blackstone C: **Cellular localization, oligomerization, and membrane association of the hereditary spastic paraplegia 3A (SPG3A) protein atlastin.** *J Biol Chem* 2003, **278**(49):49063-49071.
40. Voeltz GK, Prinz WA, Shibata Y, Rist JM, Rapoport TA: **A class of membrane proteins shaping the tubular endoplasmic reticulum.** *Cell* 2006, **124**(3):573-586.
41. Orso G, Pendin D, Liu S, Toso J, Moss TJ, Faust JE, Micaroni M, Egorova A, Martinuzzi A, McNew JA *et al*: **Homotypic fusion of ER membranes requires the dynamin-like GTPase atlastin.** *Nature* 2009, **460**(7258):978-983.
42. Vedrenne C, Hauri HP: **Morphogenesis of the endoplasmic reticulum: beyond active membrane expansion.** *Traffic* 2006, **7**(6):639-646.
43. Saito H, Kubota M, Roberts RW, Chi Q, Matsunami H: **RTP family members induce functional expression of mammalian odorant receptors.** *Cell* 2004, **119**(5):679-691.
44. Zuchner S, Wang G, Tran-Viet KN, Nance MA, Gaskell PC, Vance JM, Ashley-Koch AE, Pericak-Vance MA: **Mutations in the novel mitochondrial protein REEP1 cause hereditary spastic paraplegia type 31.** *Am J Hum Genet* 2006, **79**(2):365-369.

45. Park SH, Zhu PP, Parker RL, Blackstone C: **Hereditary spastic paraplegia proteins REEP1, spastin, and atlastin-1 coordinate microtubule interactions with the tubular ER network.** *J Clin Invest* 2010, **120**(4):1097-1110.
46. Hirokawa N, Noda Y: **Intracellular transport and kinesin superfamily proteins, KIFs: structure, function, and dynamics.** *Physiol Rev* 2008, **88**(3):1089-1118.
47. Xia CH, Roberts EA, Her LS, Liu X, Williams DS, Cleveland DW, Goldstein LS: **Abnormal neurofilament transport caused by targeted disruption of neuronal kinesin heavy chain KIF5A.** *J Cell Biol* 2003, **161**(1):55-66.
48. Gupta V, Palmer KJ, Spence P, Hudson A, Stephens DJ: **Kinesin-1 (uKHC/KIF5B) is required for bidirectional motility of ER exit sites and efficient ER-to-Golgi transport.** *Traffic* 2008, **9**(11):1850-1866.
49. Lu J, Rashid F, Byrne PC: **The hereditary spastic paraplegia protein spartin localises to mitochondria.** *J Neurochem* 2006, **98**(6):1908-1919.
50. Bakowska JC, Jupille H, Fatheddin P, Puertollano R, Blackstone C: **Troyer syndrome protein spartin is mono-ubiquitinated and functions in EGF receptor trafficking.** *Mol Biol Cell* 2007, **18**(5):1683-1692.
51. Eastman SW, Yassaee M, Bieniasz PD: **A role for ubiquitin ligases and Spartin/SPG20 in lipid droplet turnover.** *J Cell Biol* 2009, **184**(6):881-894.

52. Edwards TL, Clowes VE, Tsang HT, Connell JW, Sanderson CM, Luzio JP, Reid E: **Endogenous spartin (SPG20) is recruited to endosomes and lipid droplets and interacts with the ubiquitin E3 ligases AIP4 and AIP5.** *Biochem J* 2009, **423**(1):31-39.
53. Rainier S, Chai JH, Tokarz D, Nicholls RD, Fink JK: **NIPA1 gene mutations cause autosomal dominant hereditary spastic paraplegia (SPG6).** *Am J Hum Genet* 2003, **73**(4):967-971.
54. Goytain A, Hines RM, El-Husseini A, Quamme GA: **NIPA1(SP6), the basis for autosomal dominant form of hereditary spastic paraplegia, encodes a functional Mg<sup>2+</sup> transporter.** *J Biol Chem* 2007, **282**(11):8060-8068.
55. Zhao J, Matthies DS, Botzolakis EJ, Macdonald RL, Blakely RD, Hedera P: **Hereditary spastic paraplegia-associated mutations in the NIPA1 gene and its Caenorhabditis elegans homolog trigger neural degeneration in vitro and in vivo through a gain-of-function mechanism.** *J Neurosci* 2008, **28**(51):13938-13951.
56. Tsang HT, Edwards TL, Wang X, Connell JW, Davies RJ, Durrington HJ, O'Kane CJ, Luzio JP, Reid E: **The hereditary spastic paraplegia proteins NIPA1, spastin and spartin are inhibitors of mammalian BMP signalling.** *Hum Mol Genet* 2009, **18**(20):3805-3821.
57. Wang X, Shaw WR, Tsang HT, Reid E, O'Kane CJ: **Drosophila spichthyin inhibits BMP signaling and regulates synaptic**

- growth and axonal microtubules.** *Nat Neurosci* 2007, **10**(2):177-185.
58. Ito D, Fujisawa T, Iida H, Suzuki N: **Characterization of seipin/BSCL2, a protein associated with spastic paraplegia 17.** *Neurobiol Dis* 2008, **31**(2):266-277.
59. Boutet E, El Mourabit H, Prot M, Nemani M, Khallouf E, Colard O, Maurice M, Durand-Schneider AM, Chretien Y, Gres S *et al*: **Seipin deficiency alters fatty acid Delta9 desaturation and lipid droplet formation in Berardinelli-Seip congenital lipodystrophy.** *Biochimie* 2009, **91**(6):796-803.
60. Payne VA, Grimsey N, Tuthill A, Virtue S, Gray SL, Dalla Nora E, Semple RK, O'Rahilly S, Rochford JJ: **The human lipodystrophy gene BSCL2/seipin may be essential for normal adipocyte differentiation.** *Diabetes* 2008, **57**(8):2055-2060.
61. Szymanski KM, Binns D, Bartz R, Grishin NV, Li WP, Agarwal AK, Garg A, Anderson RG, Goodman JM: **The lipodystrophy protein seipin is found at endoplasmic reticulum lipid droplet junctions and is important for droplet morphology.** *Proc Natl Acad Sci U S A* 2007, **104**(52):20890-20895.
62. Ito D, Suzuki N: **Seipinopathy: a novel endoplasmic reticulum stress-associated disease.** *Brain* 2009, **132**(Pt 1):8-15.
63. Zeitlmann L, Sirim P, Kremmer E, Kolanus W: **Cloning of ACP33 as a novel intracellular ligand of CD4.** *J Biol Chem* 2001, **276**(12):9123-9132.
64. Hanein S, Martin E, Boukhris A, Byrne P, Goizet C, Hamri A, Benomar A, Lossos A, Denora P, Fernandez J *et al*:

**Identification of the SPG15 gene, encoding spastizin, as a frequent cause of complicated autosomal-recessive spastic paraplegia, including Kjellin syndrome.** *Am J Hum Genet* 2008, **82**(4):992-1002.

65. Birkeland HC, Stenmark H: **Protein targeting to endosomes and phagosomes via FYVE and PX domains.** *Curr Top Microbiol Immunol* 2004, **282**:89-115.
66. Stevanin G, Azzedine H, Denora P, Boukhris A, Tazir M, Lossos A, Rosa AL, Lerer I, Hamri A, Alegria P *et al*: **Mutations in SPG11 are frequent in autosomal recessive spastic paraplegia with thin corpus callosum, cognitive decline and lower motor neuron degeneration.** *Brain* 2008, **131**(Pt 3):772-784.
67. Stevanin G, Santorelli FM, Azzedine H, Coutinho P, Chomilier J, Denora PS, Martin E, Ouvrard-Hernandez AM, Tessa A, Bouslam N *et al*: **Mutations in SPG11, encoding spatacsin, are a major cause of spastic paraplegia with thin corpus callosum.** *Nat Genet* 2007, **39**(3):366-372.
68. Jia D, Gomez TS, Metlagel Z, Umetani J, Otwinowski Z, Rosen MK, Billadeau DD: **WASH and WAVE actin regulators of the Wiskott-Aldrich syndrome protein (WASP) family are controlled by analogous structurally related complexes.** *Proc Natl Acad Sci U S A* 2010, **107**(23):10442-10447.
69. Koppen M, Metodiev MD, Casari G, Rugarli EI, Langer T: **Variable and tissue-specific subunit composition of mitochondrial m-AAA protease complexes linked to**

- hereditary spastic paraplegia. *Mol Cell Biol* 2007, 27(2):758-767.**
70. Arlt H, Tauer R, Feldmann H, Neupert W, Langer T: **The YTA10-12 complex, an AAA protease with chaperone-like activity in the inner membrane of mitochondria. *Cell* 1996, 85(6):875-885.**
71. Arlt H, Steglich G, Perryman R, Guiard B, Neupert W, Langer T: **The formation of respiratory chain complexes in mitochondria is under the proteolytic control of the m-AAA protease. *EMBO J* 1998, 17(16):4837-4847.**
72. Nolden M, Ehses S, Koppen M, Bernacchia A, Rugarli EI, Langer T: **The m-AAA protease defective in hereditary spastic paraplegia controls ribosome assembly in mitochondria. *Cell* 2005, 123(2):277-289.**
73. Koppen M, Bonn F, Ehses S, Langer T: **Autocatalytic processing of m-AAA protease subunits in mitochondria. *Mol Biol Cell* 2009, 20(19):4216-4224.**
74. Duvezin-Caubet S, Koppen M, Wagener J, Zick M, Israel L, Bernacchia A, Jagasia R, Rugarli EI, Imhof A, Neupert W *et al*: **OPA1 processing reconstituted in yeast depends on the subunit composition of the m-AAA protease in mitochondria. *Mol Biol Cell* 2007, 18(9):3582-3590.**
75. Ishihara N, Fujita Y, Oka T, Mihara K: **Regulation of mitochondrial morphology through proteolytic cleavage of OPA1. *EMBO J* 2006, 25(13):2966-2977.**

76. Frezza C, Cipolat S, Martins de Brito O, Micaroni M, Beznoussenko GV, Rudka T, Bartoli D, Polishuck RS, Danial NN, De Strooper B *et al*: **OPA1 controls apoptotic cristae remodeling independently from mitochondrial fusion.** *Cell* 2006, **126**(1):177-189.
77. Ferreirinha F, Quattrini A, Pirozzi M, Valsecchi V, Dina G, Broccoli V, Auricchio A, Piemonte F, Tozzi G, Gaeta L *et al*: **Axonal degeneration in paraplegin-deficient mice is associated with abnormal mitochondria and impairment of axonal transport.** *J Clin Invest* 2004, **113**(2):231-242.
78. Pirozzi M, Quattrini A, Andolfi G, Dina G, Malaguti MC, Auricchio A, Rugarli EI: **Intramuscular viral delivery of paraplegin rescues peripheral axonopathy in a model of hereditary spastic paraplegia.** *J Clin Invest* 2006, **116**(1):202-208.
79. Horwich AL, Fenton WA, Chapman E, Farr GW: **Two families of chaperonin: physiology and mechanism.** *Annu Rev Cell Dev Biol* 2007, **23**:115-145.
80. Kenwrick S, Watkins A, De Angelis E: **Neural cell recognition molecule L1: relating biological complexity to human disease mutations.** *Hum Mol Genet* 2000, **9**(6):879-886.
81. Weller S, Gartner J: **Genetic and clinical aspects of X-linked hydrocephalus (L1 disease): Mutations in the L1CAM gene.** *Hum Mutat* 2001, **18**(1):1-12.
82. Garbern JY, Yool DA, Moore GJ, Wilds IB, Faulk MW, Klugmann M, Nave KA, Siermans EA, van der Knaap MS, Bird

TD *et al*: **Patients lacking the major CNS myelin protein, proteolipid protein 1, develop length-dependent axonal degeneration in the absence of demyelination and inflammation.** *Brain* 2002, **125**(Pt 3):551-561.

83. Inoue K: **PLP1-related inherited dysmyelinating disorders: Pelizaeus-Merzbacher disease and spastic paraplegia type 2.** *Neurogenetics* 2005, **6**(1):1-16.
84. Griffiths IR, Scott I, McCulloch MC, Barrie JA, McPhilemy K, Cattanach BM: **Rumpshaker mouse: a new X-linked mutation affecting myelination: evidence for a defect in PLP expression.** *J Neurocytol* 1990, **19**(2):273-283.
85. Tsaousidou MK, Ouahchi K, Warner TT, Yang Y, Simpson MA, Laing NG, Wilkinson PA, Madrid RE, Patel H, Hentati F *et al*: **Sequence alterations within CYP7B1 implicate defective cholesterol homeostasis in motor-neuron degeneration.** *Am J Hum Genet* 2008, **82**(2):510-515.
86. Dick KJ, Eckhardt M, Paisan-Ruiz C, Alshehhi AA, Proukakis C, Sibtain NA, Maier H, Sharifi R, Patton MA, Bashir W *et al*: **Mutation of FA2H underlies a complicated form of hereditary spastic paraplegia (SPG35).** *Hum Mutat* 2010, **31**(4):E1251-1260.
87. Alderson NL, Hama H: **Fatty acid 2-hydroxylase regulates cAMP-induced cell cycle exit in D6P2T schwannoma cells.** *J Lipid Res* 2009, **50**(6):1203-1208.



88. Chang PA, Wu YJ: **Motor neuron diseases and neurotoxic substances: a possible link?** *Chem Biol Interact* 2009, **180**(2):127-130.
89. Akassoglou K, Malester B, Xu J, Tessarollo L, Rosenbluth J, Chao MV: **Brain-specific deletion of neuropathy target esterase/swisscheese results in neurodegeneration.** *Proc Natl Acad Sci U S A* 2004, **101**(14):5075-5080.
90. Kretzschmar D, Hasan G, Sharma S, Heisenberg M, Benzer S: **The swiss cheese mutant causes glial hyperwrapping and brain degeneration in Drosophila.** *J Neurosci* 1997, **17**(19):7425-7432.
91. Li Y, Dinsdale D, Glynn P: **Protein domains, catalytic activity, and subcellular distribution of neuropathy target esterase in Mammalian cells.** *J Biol Chem* 2003, **278**(10):8820-8825.
92. Quistad GB, Barlow C, Winrow CJ, Sparks SE, Casida JE: **Evidence that mouse brain neuropathy target esterase is a lysophospholipase.** *Proc Natl Acad Sci U S A* 2003, **100**(13):7983-7987.
93. Muhlig-Versen M, da Cruz AB, Tschape JA, Moser M, Buttner R, Athenstaedt K, Glynn P, Kretzschmar D: **Loss of Swiss cheese/neuropathy target esterase activity causes disruption of phosphatidylcholine homeostasis and neuronal and glial death in adult Drosophila.** *J Neurosci* 2005, **25**(11):2865-2873.
94. Bettencourt da Cruz A, Wentzell J, Kretzschmar D: **Swiss Cheese, a protein involved in progressive**

- neurodegeneration, acts as a noncanonical regulatory subunit for PKA-C3. *J Neurosci* 2008, **28**(43):10885-10892.
95. Lin P, Li J, Liu Q, Mao F, Qiu R, Hu H, Song Y, Yang Y, Gao G, Yan C *et al*: **A missense mutation in SLC33A1, which encodes the acetyl-CoA transporter, causes autosomal-dominant spastic paraplegia (SPG42).** *Am J Hum Genet* 2008, **83**(6):752-759.
96. Orthmann-Murphy JL, Salsano E, Abrams CK, Bizzi A, Uziel G, Freidin MM, Lamantea E, Zeviani M, Scherer SS, Pareyson D: **Hereditary spastic paraplegia is a novel phenotype for GJA12/GJC2 mutations.** *Brain* 2009, **132**(Pt 2):426-438.
97. Slabicki M, Theis M, Krastev DB, Samsonov S, Mundwiller E, Junqueira M, Paszkowski-Rogacz M, Teyra J, Heninger AK, Poser I *et al*: **A genome-scale DNA repair RNAi screen identifies SPG48 as a novel gene associated with hereditary spastic paraplegia.** *PLoS Biol* 2010, **8**(6):e1000408.

## **Aim of the thesis**

The aim of this thesis is to analyze and characterize the function of two genes involved in Hereditary Spastic Paraplegia, SPG4 and SPG7, to dissect their role in the pathogenesis of the disease.

SPG4 encodes for Spastin, a microtubule severing protein involved in cytoskeletal dynamics and subcellular trafficking.

On the other hand, SPG7 encodes for Paraplegin, a subunit of the m-AAA protease complex. This protease plays a key role in inner membrane protein quality control and in specific substrate maturation.

Studying two genes with different function can shed light on common pathogenetic mechanisms in an etiologically complex disease such as Hereditary Spastic Paraplegia.

# **A cryptic promoter in the first exon of the SPG4 gene directs the synthesis of the 60 kDa spastin isoform**

Giuseppe Mancuso<sup>1</sup> and Elena I. Rugarli<sup>1,2</sup>

<sup>1</sup> Division of Biochemistry and Genetics, Istituto Neurologico “C. Besta”, Milan, Italy

<sup>2</sup> Department of Neuroscience and Medical Biotechnologies, University of Milano-Bicocca, Milan, Italy

*Published: 9 July 2008*

*BMC Biology 2008, 6:31 doi:10.1186/1741-7007-6-31*

## **Abstract**

### *Background:*

Mutations in *SPG4* cause the most common form of autosomal dominant hereditary spastic paraplegia (HSP), a neurodegenerative disease characterized by weakness and spasticity of the lower limbs due to degeneration of the corticospinal tract. *SPG4* encodes spastin, a microtubule-severing ATPase belonging to the AAA family. Two isoforms of spastin, of 68 and 60 kDa respectively, are variably abundant in tissues, show different subcellular localizations, and interact with distinct molecules. The isoforms arise through alternative initiation of translation from two AUG codons in exon 1, however it is unclear how regulation of their expression may be achieved.

### *Results:*

We present data that rule out the hypothesis that a cap-independent mechanism may be involved in the translation of the 60 kDa spastin isoform. Instead, we provide evidence for a complex transcriptional regulation of *SPG4* that involves both a TATA-less ubiquitous promoter and a cryptic promoter in exon 1. The cryptic promoter covers the 5' UTR and overlaps with the coding region of the gene. By using promoterless constructs in various experimental settings, we find that the cryptic promoter is active in HeLa, HEK293, and motoneuronal NSC34 cells but not in SH-SY-5H neuroblastoma cells. We show that the cryptic promoter directs the synthesis of a *SPG4*

transcript that contains a shorter 5' UTR and translates selectively the 60 kDa spastin isoform. Two polymorphisms (S44L and P45Q), leading to an early-onset severe form of HSP when present in heterozygosity with a mutant allele, fall a few nucleotides downstream the novel transcriptional start site, opening up the possibility that they may exert their modifier effect at the transcriptional level. We provide evidence that at least one of them decreases the activity of the cryptic promoter in luciferase assays.

*Conclusions:*

We have identified a cryptic promoter in exon 1 of the *SPG4* gene that selectively drives the expression of the 60 kDa spastin isoform in a tissue-regulated manner. These data may have implications for the understanding of the biology of spastin and the pathogenic basis of HSP.

## Background

Hereditary spastic paraplegia (HSP) is a genetically heterogeneous disorder characterized by progressive weakness and spasticity of the lower limbs, due to retrograde degeneration of the corticospinal axons [1]. *SPG4*, the gene most commonly involved in autosomal dominant HSP, encodes spastin, an ATPase belonging to the AAA family [2]. Spastin acts as a microtubule-severing protein, suggesting that axonal degeneration in HSP may depend on defective regulation of cytoskeleton dynamics in long axonal tracts [3] [4] [5]. The identification of several spastin molecular interactors involved in cell trafficking led to the proposal that the microtubule-severing activity of spastin may be coupled to specific processes and therefore occur in a regulated manner [6].

Spastin has a complex subcellular localization. It is enriched in the centrosome in interphase and during mitosis, similarly to p60 katanin, another microtubule-severing protein [7] [8]. Low levels of spastin are present in the nucleus of proliferating cells, while neurons show a prevalent cytoplasmic localization [9] [7] [10]. We previously found that one mechanism to regulate targeting of spastin to specific cell compartments is alternative initiation of translation from two AUGs present in exon 1 of the *SPG4* gene [11]. Both spastin isoforms contain a nuclear localization signal (NLS), however the long 68 kDa spastin isoform also bears a nuclear export signal (NES) and is efficiently exported to the cytoplasm in an exportin-dependent fashion. Conversely, the shorter 60 kDa spastin isoform localizes to

both the nucleus and the cytoplasm upon overexpression in eukaryotic cells.

Although both spastin isoforms efficiently sever microtubules [4] [5], they display several functional differences. Firstly, the shorter isoform is the most abundant in all tissues examined, while the longer form is efficiently detectable only in brain and spinal cord [11] [12]. Secondly, two proteins, atlastin and NA14, have been shown to interact specifically to the N-terminal region of spastin present in the long isoform but absent in the short isoform [7] [13] [14]. Since atlastin is in turn implicated in HSP, this observation may be of direct relevance to the pathogenesis of the disease. Thirdly, two polymorphisms (S44L and P45Q) acting as phenotype modifiers have been identified in the long-isoform-specific region. Patients carrying a mutated allele of spastin and one of these two polymorphisms on the other allele are affected by a severe disease with early age of onset [15] [16] [17]. Furthermore, a family was described, in which one patient with a late onset mild spastic paraplegia was homozygous for the S44L polymorphism [18].

In vertebrates, initiator codons are recognized most efficiently within the context GCCRCCaugG, with the purine (R) in position -3 and the G in position +4 making the strongest contributions [19]. The main *SPG4* open reading frame (ORF) starts with an AUG that resides in a context that deviates significantly from the consensus motif (TGAaugA). Moreover, an upstream ORF (uORF) overlaps with the main *SPG4* ORF and contains an AUG in a good Kozak's consensus sequence (GTTaugG). It is expected that this uORF would drastically



inhibit translation from the first *SPG4* AUG, while allowing reinitiation at the second AUG that has a G in position +4, and is located at a sufficient distance from the stop codon of the uORF (Figure1). uORFs have been recognized in genes with regulatory function and may offer a mechanism to restrict expression of a toxic product [19] [20]. In some cases, limited access to the main ORF might be anyway achieved by leaky scanning. In summary, the presence of a uORF that overlaps with the main *SPG4* ORF, as well as the sequence context surrounding the first two AUGs in the main ORF, may explain why translation of the long spastin isoform is strongly unfavoured in vivo. Consistent with this model, expression of an *SPG4* cDNA containing the 5' UTR abundantly produces the shorter protein isoform and only in a limited amount the long 68 kDa isoform [11]. Moreover, in vitro transcription-translation assays using a cDNA construct that starts from the first AUG supported translation of both spastin isoforms, likely reflecting leaky scanning from the first AUG [11].

Although the scanning mechanism for initiation of translation can satisfactorily explain our previous data, there might still be the possibility that translation of the short abundant 60 kDa spastin isoform occurs via direct entry of the ribosomes at the downstream AUG codon. Albeit this mechanism is well documented for certain viral genes, it is still quite controversial whether it occurs in mammalian genes [21] [22].

While testing for the presence of an internal ribosome entry site (IRES) in the *SPG4* mRNA, we found evidence for a cryptic promoter in exon 1, responsible for the production of a shorter mRNA specific

for the 60 kDa spastin isoform. This promoter shows some degree of tissue-specificity, providing a way to regulate the production of the different spastin isoforms.

## Results

### *Translation of the 60 kDa spastin isoform does not depend on an IRES*

Translation of the 60 kDa spastin isoform from AUG in position 259-261 may depend on the migration of the translational machinery until it meets this AUG codon that lies in a better Kozak's sequence context than the first AUG (Figure 1). However, the program UTRscan predicts a secondary RNA structure compatible with the presence of an IRES, immediately upstream the second AUG, suggesting that the short spastin isoform could be synthesized through a cap-independent mechanism. To test this possibility, we cloned the *SPG4* cDNA sequence comprised between the first and the second ATG into a widely used dicistronic vector, pRF (construct pRF +4/+258). This vector contains the SV40 promoter directing the expression of a dicistronic RNA encoding the *Renilla* luciferase as the first cistron and the firefly luciferase as the second. This plasmid was transfected in HeLa and SH-SY-5Y neuroblastoma cell lines and the *Renilla* and firefly luciferase activities were measured. The construct pRF +4/+258 displayed a very high firefly activity in HeLa cells, compared to the control empty vector (Figure 2a), consistent with the possibility that the region between the two AUG in the first exon of *SPG4* might contain a functional IRES. This construct was less active in SH-SY-5Y cells.

Although the dicistronic test has been considered the gold standard for testing the existence of functional IRES elements, a major drawback of this approach is that it cannot distinguish between an

IRES activity and the presence of a cryptic promoter [23]. To exclude this possibility, we cloned the same *SPG4* sequence into a promoterless pRF vector (pRF $\Delta$ P), in which the SV40 promoter has been removed (Figure 2b). Both *Renilla* and firefly luciferase activities were almost undetectable when the empty pRF $\Delta$ P vector was transfected, whereas a dramatic increase of the firefly activity was observed for the pRF $\Delta$ P +4/+258 construct in HeLa cells, strongly suggesting the presence of a promoter activity in the first exon of *SPG4* (Figure 2b). Again, the fold of activation was lower in SH-SY-5Y cells (Figure 2b).

The presence of a strong promoter in the region under analysis could mask the presence of the IRES, hampering to detect its functionality. To circumvent this problem, an effective method is direct transfection of the dicistronic RNAs [23]. To this end, in vitro-transcribed capped dicistronic mRNAs were transfected into HeLa cells and the activities of both *Renilla* and firefly luciferases were measured. The firefly activities of both the empty vector and the pRF +4/+258 were barely detectable, while the *Renilla* luciferase activities were comparable, indicating that the first exon of *SPG4* does not contain an IRES element (Figure 2c).

#### *A minimal ubiquitous SPG4 promoter*

The finding of a promoter activity in the region between the two ATGs prompted us to study the regulatory sequences of the *SPG4* gene. Bioinformatic analysis of the genomic region upstream the

transcriptional start site (defined as in the reference sequence AB029006) does not identify any TATA box, but detects several CG boxes and a CAAT box in position -597. Furthermore, sequence comparison between the human and the mouse *SPG4* genomic sequence shows a very high degree of sequence conservation in the 5' UTR of *SPG4* and in a region of 400 bp upstream the putative initiation of transcription, suggesting that this region may contain important regulatory elements (Figure 3a).

To define the minimal genomic region that confers basic expression of the *SPG4* gene, we tested the ability of different fragments of the genomic region upstream the first ATG of the *SPG4* gene to drive the expression of the luciferase gene in transiently transfected HeLa, HEK293 and SH-SY-5Y cells (Figure 3b). The activities of these promoters were measured by a luciferase assay and considered as fold of induction in respect to the activity of the empty vector. We did not find any cell specific difference in the activities of the different fragments in the three cell lines (Figure 3c). The construct that showed higher promoter activity was S -621/-1, containing the highly conserved 400 bp genomic region and the 5' UTR. Inclusion of additional 669 bp upstream of this region led to a certain decrease of promoter activity, while removal of a sequence of approximately 220 bp containing the CAAT box (S -400/+3) did not reduce significantly the promoter activity. Deletion of the 5' UTR and of approximately 200 bp upstream the transcription initiation site (construct S 1290/-424) completely abolished promoter activity, while the removal of only the 5' UTR (S -400/-206) reduced the basal transcriptional

activity (Figure 3c). These experiments identify a region of 400 bp upstream the first ATG as a minimal promoter region active in all cell lines tested and point to a role of the 5' UTR to sustain basic ubiquitous *SPG4* expression.

#### *A tissue specific cryptic promoter in the first exon of SPG4*

The promoter activity observed in the region within the two ATGs in the experiments with the promoterless pRF $\Delta$ P vector, as well as the role of the 5' UTR for basal expression, induced us to examine in detail the potential presence of regulatory sequences in exon 1. To this purpose, we cloned different regions of the first exon of *SPG4* upstream of the firefly luciferase gene and tested their promoter activity in all cell lines (Figure 4a). We found a strong promoter activity both in HeLa and HEK293 cells in the region that starts immediately downstream the putative transcriptional start site and include both ATGs (S -207/+259) (Figure 4b). This activity, although decreased, is still present in constructs that contain only the coding region (S +4/+259), or the 5' UTR (S -207/-1). We define the whole region comprised between the canonical transcriptional start site, as defined in public databases, and the AUG in position 259-261, as cryptic promoter. Notably, the activity of this cryptic promoter appears to display some degree of cell line specificity, being highly functional in HeLa cells and HEK293 and significantly less in SH-SY-5Y cells (Figure 4b), thus confirming our previous observations with the promoterless dicistronic vector.

We used the TRANSFAC program to identify binding sites for known transcription factors in the cryptic promoter region. This allowed us to identify two putative Sp1 binding sites that were conserved in the human and mouse genomes (Figure 4a). Site-directed mutagenesis was employed to insert mutations into the upstream, the downstream, or both Sp1 sites in the construct S -207/+259. Transfection of the mutated constructs showed a significant reduction of the cryptic promoter activity in HeLa cells only when both Sp1 sites are mutagenized (Figure 4c).

We previously showed that when spastin is expressed in mammalian cells, two isoforms are produced, starting from the first and the second methionine [11]. The amount of the shorter isoform increases when the 5' UTR is included in the construct [11]. In vitro transcription-translation experiments suggested that this is largely due to alternative initiation of translation [11]. However, our novel findings suggest that transcriptional regulation could contribute to the production of the shorter isoform through the use of the cryptic promoter. To test this possibility, we removed the CMV promoter from a CMV-spastin-GFP construct and analyzed the ability of the cryptic promoter (in this construct represented only by the region +4/+259) to drive the expression of the short spastin isoform after transfection in different cell lines. We found that a short spastin-GFP isoform, with a size consistent with initiation of translation at the second AUG, is produced in this condition in HeLa, HEK293, and murine spinal motoneuronal NSC34 cells (Figure 5a, b and not shown). To confirm this data, we generated a construct containing

the GFP reporter under the control of the CMV promoter followed by a stop codon and by the coding region of spastin (CMV-EGFP-STOP-Spastin). Such a construct could express spastin only if the region between the first two ATGs functions as promoter. Consistently, transfected cells with high levels of GFP expression showed low levels of spastin expression, detected with a specific anti-spastin antibody (Figure 5c).

In conclusion, both reporter and expression studies with promoterless constructs strongly indicate that the first *SPG4* exon contains a cryptic promoter that may contribute to produce the 60 kDa isoform in several cell types in vivo.

*Two phenotype modifier polymorphisms lie within the cryptic promoter*

The S44L and P45Q (c.131C>T and c.134C>A) polymorphisms in the *SPG4* gene act as phenotype-modifier. Patients that bear one of these polymorphisms and a canonical *SPG4* mutation on the other allele show an early age of onset of HSP and rapid progression of symptoms [15] [16]. Since these nucleotide changes fall into the newly identified cryptic promoter, we tested their capability to affect the promoter activity. The polymorphisms were inserted by mutagenesis in the constructs S -207/+259 and S +4/+259 (Figure 6a). The activity of these mutagenized promoters was tested in HeLa cells and compared with the wild-type constructs. The presence of the c.131C>T substitution significantly diminished the activity of the



promoter of about one half, while no effect was detected with the c.134C>A substitution (Figure 6b). When the substitutions were inserted in the context of a larger promoter, containing also part of the ubiquitous minimal promoter (S -400/+259), no change in activity was observed for either of them (Figure 6b).

*Identification of an endogenous SPG4 transcript specific for the short spastin isoform*

The previous experiments strongly suggest the existence of a cryptic promoter in the first exon of the *SPG4* gene. Differentially regulated alternative transcriptional start sites (TSSs) are a common feature in protein-coding genes and commonly generate alternative N-termini [24]. Genome-wide analyses, using short tags derived from 5' ends of capped RNAs (CAGE), oligocapping methods and full-length cDNA collections, can be publicly accessed in the CAGE analysis web site and in the Database of Transcriptional Start Sites (DBTSS). We searched these databases for TSSs within the human *SPG4* gene. Remarkably, we found that both databases identify an alternative promoter located within exon 1, downstream the first ATG, defined by a clustering of TSSs separated by less than 500 bp. The tags derive from HEK 293 cells, as well as from different tissues including brain. A summary of these data is represented in figure S1.

To gain further experimental proof that the cryptic promoter is responsible for the synthesis of a short *SPG4* mRNA, we performed 5' RACE experiments in both HeLa and SH-SY-5Y cells. Total RNA was

isolated from the cells. Truncated or uncapped RNA molecules were removed by a phosphatase treatment. Subsequently, the caps were eliminated by treatment with tobacco acid pyrophosphatase (TAP), and an adapter oligonucleotide was ligated to the 5' ends. After nested amplification with gene specific primers located downstream the second AUG, we could amplify in HeLa cells a specific product of about 250 bp, which was absent from the minus TAP control reaction (Figure 7a). This product was cloned and sequenced and found to initiate from nucleotide +117. This transcript therefore contains an ORF that starts with AUG 259-261 and encodes the short 60 kDa spastin isoform. Both Sp1 sites are located upstream the beginning of the novel transcript, while the polymorphisms c.131C>T and c.134C>A appear to be positioned a few bases downstream (Figure 7b). Notably, this TSS corresponds to 2 tags identified in HEK293 in the DBTSS database. We could not obtain a similar 5' RACE product in SH-SY-5Y cells, consistent with the lower activity of the cryptic promoter in this cell line (not shown).

## Discussion

Haploinsufficiency of spastin causes hereditary spastic paraplegia, suggesting that tight control of the protein levels is required for axonal integrity. We previously showed that the *SPG4* gene synthesizes two isoforms of spastin (68 kDa and 60 kDa, respectively), depending on alternative initiation of translation from two AUGs in the first exon [11]. Regulation of the expression of protein isoforms simply based on inefficient translation or leaky scanning is however hard to achieve. Here, we report a transcriptional mechanism of *SPG4* regulation that may contribute to the production of different ratio of long and short spastin isoforms in tissues.

We identified a ubiquitous spastin minimal promoter and found evidence for a tissue-specific cryptic promoter in the first exon of the gene. An evolutionary highly conserved region of 400 base pairs upstream the first in frame AUG of the *SPG4* gene was sufficient to provide basal expression in HeLa, HEK293 and SH-SY-5Y cells. This region does not contain a TATA box, but includes several cis-acting GC-rich elements, suggesting that the *SPG4* promoter belongs to the vast category of TATA-less promoters common to mammalian housekeeping genes [25]. Inclusion in the reporter constructs of upstream genomic regions did not significantly increase the transcriptional activity. Furthermore, deletion of a putative CAAT box, not conserved in the mouse, did not decrease substantially the promoter activity. In contrast, a certain drop in activity was found when the majority of the 5' UTR of the gene was removed from all

the constructs tested. A possible explanation is that the 5' UTR itself may contain additional TSS or regulatory elements that cooperate with upstream sequences to allow basal transcription of the *SPG4* gene. Consistently, very high levels of sequence conservation are observed in the 5' UTR among different species from human to chicken.

The latter hypothesis is supported by the finding of a cryptic promoter in the first exon of the *SPG4* gene. The region comprised between the most upstream TSS (corresponding to position -221) and the first ATG, and the region between the first and the second in frame ATGs, both alone and even stronger in combination, are able to drive expression of a reporter gene in promoterless vectors. Collectively, we define these regions in *SPG4* exon 1 as cryptic promoter. Furthermore, promoterless constructs containing only the coding sequence of spastin drove the expression of the shorter spastin isoform in HeLa, HEK293, and in NSC34 cells. These are murine immortalized spinal motoneurons that express both long and short spastin isoforms [11]. This result suggests that the cryptic promoter may also be active in neurons implicated in the human pathology. Remarkably, the cryptic promoter shows some degree of tissue-specificity, as shown by low activity in the neuroblastoma-derived SH-SY-5Y cells.

The presence of shorter capped *SPG4* mRNAs is supported by the successful identification of a novel *SPG4* transcript that starts downstream the first AUG in HeLa cells by 5' RACE experiments. Moreover, our experimental data are consistent with high-

throughput genome-wide studies, which identified a cluster of TSSs within both the human and murine *SPG4* genes located in close proximity to the TSS of the novel transcript identified in our study. The previous results strongly suggest that the *SPG4* gene has multiple core promoters, containing multiple TSSs, the usage of which generate diversity not only in the transcripts but most importantly in the proteins produced. A similar scenario is emerging with more and more frequency from studies of mammalian core promoters [25]. As expected for a broad promoter with multiple TSSs, several CpG islands boxes and multiple binding sites for the transcription factor Sp1 are present in the cryptic promoter. It has been suggested that Sp1 may direct the basal machinery to form a preinitiation complex within a loosely defined window [26]. Mutagenesis of two evolutionary conserved Sp1 sites decreased the activity of the cryptic promoter, suggesting that Sp1 or Sp family members transcription factors may bind to the cryptic promoter. Sp1 elements are required for the expression of many ubiquitous, tissue-specific and viral genes [27]. Interestingly, Sp1 levels decrease with cellular aging [28]. Further studies are however required to define the transcription factors involved in *SPG4* expression.

Western blot analysis strongly indicates that the 60 kDa spastin isoform is the predominant one in many tissues and cells [11] [12]. Based on our data, we propose that a combination of transcriptional and translational mechanisms is employed in concert to modulate the levels of spastin isoforms in cells. At the transcriptional level, cells may synthesize the 60 kDa isoform simply through the production of

a shorter transcript that possesses as first in frame AUG the one in position 259-261. However, an additional mechanism to ensure preferential synthesis of the 60 kDa spastin isoform likely arise during translation, due to several constraints imposed on translation from the first in frame AUG, such as: the presence of a 73% GC-rich 5' UTR, an overlapping uORF, and a poor Kozak's context [19]. Indeed, in our experiments with spastin expression constructs, it is clear that the short spastin isoform is expressed at high levels when the *SPG4* coding sequence is under the control of the CMV promoter, suggesting that translation of this isoform occurs even when the synthesis of a longer mRNA is favoured.

Our study tends to exclude that a cap-independent mechanism through recognition of an IRES might play a role in translation of the spastin 60 kDa short isoform. This latter mechanism has been extensively demonstrated in viral transcripts, and more recently also found in a number of eukaryotic transcripts, whose translation need to occur also in circumstances in which cap-dependent translation is inhibited. Functional IRES elements have been proposed in several eukaryotic genes, but subsequent studies using more sensitive procedures have questioned the validity of several of them [29] [30] [31]. Similarly, we showed by direct RNA transfection of a dicistronic transcript that the predicted IRES in the *SPG4* exon 1 is not functional, further confirming the impreciseness of bioinformatic approaches to predict IRES sequences, and stressing the importance of adequate functional validation.

It remains to be established why several mechanisms have evolved to maintain the levels of the long 68 kDa spastin isoform low in most cells and tissues. This seems apparently in contrast with the evolutionary conservation of the first AUG and even of the uORF in several organisms, and may point to the need of a regulated expression of this isoform, or of a possible toxic effect of this product if expressed at high level.

The identification of the cryptic *SPG4* promoter and of a shorter *SPG4* transcript may have implications in human pathology. We found that a previously reported polymorphism (c.131C>T) that acts as disease modifier falls into the cryptic promoter region and decreases its activity significantly. Notably, this polymorphism lies a few base pairs downstream the TSS of the novel transcript described here and therefore within a bona-fide *SPG4* core promoter. However, a second polymorphism, c.134C>A, did not affect the cryptic promoter activity, casting doubts on whether these polymorphisms actually act transcriptionally. Further studies on cell lines derived from HSP families in which both a mutant *SPG4* allele and the polymorphism segregate are needed to address this issue.

## Conclusions

Our study describes alternative promoter usage and heterogeneity of transcription initiation for the *SPG4* gene. A canonical promoter has features typical of housekeeping genes, while a cryptic promoter in the 5' UTR and coding region of spastin seems to provide tissue-specificity. The usage of these alternative promoters generates *SPG4* mRNAs with 5' UTRs of different length and with different AUGs, driving the production of different spastin isoforms. Our study emphasizes the need to take into account *SPG4* complex transcriptional regulation to achieve a better understanding of the biology of spastin and of the pathogenic effect of mutations or polymorphisms located in the first exon of the gene.



## Methods

### *Constructs:*

In all numeric references in this study, nucleotide +1 corresponds to the A of the first ATG codon, according to [32].

*Dicistronic Constructs (pRF).* The +4/+258 region of *SPG4* was amplified by PCR from human genomic DNA using Pfu Ultra (Stratagene) and cloned *SpeI/NcoI* into pRF and pRFΔP (Fw: 5'-**GCAGTACTTAATTCTCCGGGTGGACGA**-3', Rev: 5'-**ATCCATGGGAGGGCGCGGGAGAAGCG**-3', *SpeI* and *NcoI* sites in bold, respectively). Both dicistronic vectors are a kind gift from Dr. J-T Zhang [30]. For RNA transfection experiments, the dicistronic cassette was excised from pRF +4/+258 using a *BamHI/NheI* digestion and then cloned *BamHI/EcoRV* into the multiple cloning site of pBluescript KS – (Stratagene).

*Spastin Promoter Constructs (S).* All these constructs were obtained by cloning different portions of the human genomic sequence upstream the *SPG4* start codon into the pGL3 vector (Promega). The S-1290/-1 insert was amplified by PCR using Pfu Ultra (Stratagene) from human genomic DNA and cloned in the *XhoI/HindIII* sites of pGL3 vector (Fw: 5'-AT**CTCGAGA**ACCCAGCAGCTCTGGGGGA-3', Rev: 5'-ATA**AGCTT**TCACAGCTCTCACTGCCGCC-3', *XhoI* and *HindIII* sites in bold, respectively). S-621/-1 was obtained from S-1290/-1 by *SmaI/EcoRV* excision and self-ligation. S-207/-1 was obtained from S-1290/-1 by *KpnI/PstI* excision and self ligation. S-1290/-424 was obtained from S-1290/-1 by *HindIII/PstI* excision and self-ligation.

The S-400/+259 insert was amplified by PCR using Pfu Ultra (Stratagene) from human genomic DNA and cloned XhoI/HindIII (Fw: 5'-ATCTCGAGTGGGAACTGTAGTTGAGT-3', Rev: 5'-ATAAGCTTCGGAGCTCCTCCTGGCTG-3', XhoI and HindIII sites in bold, respectively). S-207/+259 was obtained from S-400/+259 by SmaI/PstI excision and self-ligation. S+4/+259 was obtained from S-400/+259 by SmaI/EcoRI excision and self-ligation. S-400/+3 was obtained from S-400/+259 by EcoRI/HindIII excision and self-ligation. S-400/-206 was obtained from S-400/+259 by PstI/Hind III excision and self-ligation.

*Expression constructs.* Spastin-GFP-ΔCMV was obtained from CMV-spastin-GFP vector [3] by digestion with NruI/KpnI and self ligation. Spastin-GFP-ΔM1 was obtained from spastin-GFP vector by digestion with EcoRI/KpnI and self ligation. To obtain the CMV-EGFP-STOP-Spastin construct the *SPG4* coding region was cloned blunt in the NotI site of pEGFP N°2 (Clontech).

*Site-directed Mutagenesis:*

Site-directed mutagenesis was performed by PCR reactions using Pfu Ultra (Stratagene). After amplification, 10 U of Dpn I were added to the PCR product and incubated for 1 hour at 37° C. The mutagenized DNA was transformed into *E. Coli XL1Blue* supercompetent cells. The c.131C>T polymorphism was introduced into S-400/+259, S-207/+259 and S+4/+259 vectors using the following set of oligos: Fw: 5'-GCCCTCCGCCGAGTTGCCGCATAAGCGGAAC-3', Rev: 5'-GTTCCGCTTATGCGGCAACTCGGGCGGAGGGGC-3' (mismatches

reported in bold). The c.134C>A polymorphism was introduced into S-400/+259, S-207/+259 and S+4/+259 vectors using the following set of oligos: Fw: 5'-CCTCCGCCCGAGTCGCAGCATAAGCGGAACCTG-3', Rev: 5'-CAGGTTCCGCTTATGCTGCGACTCGGGCGGAGG-3' (mismatches reported in bold). Mutagenesis of Sp1 sites was introduced in the S-207/+259 construct. The upstream Sp1 site was mutated using this set of oligos: Fw: 5'-AGGAAGGAGAAAGGGGAAGGGCAAGCGGGCAGCGTGCGG-3', Rev: 5'-CCGCACGCTGCCCGCTTGGCCCTTCCCCTTTCTCCTTCCT-3' (mismatches reported in bold). The downstream Sp1 site was mutated using the following set of oligos: Fw: 5'-CCCTTGCTGGCCCCAACCCCAACCGCCGCCGGGCCGGC-3', Rev: 5'-GCCGGCCCGCGCGGGTTGGGGTTGGGGCCAGGCAAGGG-3' (mismatches reported in bold). All mutagenized vectors were controlled by DNA sequencing.

*DNA sequencing:*

DNA sequencing was performed by using a 3100 Genetic Analyzer (Applied Biosystems) and BigDye Terminator v1.1 Cycle Sequencing kit (Applied Biosystems) according to the specifications of the manufacturer.

*Luciferase assays:*

*Renilla* and firefly luciferase activities were measured using the Dual-Luciferase Reporter System (Promega) and a Victor<sup>2</sup> 1420 Multilabel

Counter (Perkin Elmer). 24 hours post-transfection, 20 µl of cell lysate was combined sequentially with FL and RL specific substrates according to the protocol supplied by the manufacturer. Light emission was measured 2 seconds after addition of each of the substrates and integrated over a 10 seconds interval. All experiments were performed in duplicates and were repeated at least three times, using different DNA preparations.

*In vitro transcription:*

pRF and pBS-pRF +4/+258 plasmids were linearized prior to transcription by BamHI restriction, purified by incubation at 50°C for 30 minutes with 10 µg proteinase K and 0.5% SDS, and precipitated with 25 mM EDTA and 300 mM sodium acetate pH 5.2. Capped RNA transcripts were synthesized by using MAXIscript in vitro transcription kit (Ambion) according to the specifications of the manufacturer. Briefly, recombinant T7 or T3 polymerases were used to synthesize mRNA from 2.5 µg linearized DNA and 0.5 mM Ribo m<sup>7</sup> G Cap Analog (Promega) was added to the reaction mix. In vitro transcription was performed by incubation at 37°C for 1 hour in presence of 40 U of RNAsin RNase inhibitor (Promega). Following transcription, reactions were treated with DNase I for 15 minutes at 37°C.

*Cell culture, DNA and mRNA transfection and immunofluorescence:*

HeLa, HEK 293, and NSC34 cells were cultured in Dulbecco's Modified Eagle's Media (Euroclone) supplemented with 10% or 5% fetal bovine serum, 200 U/ml penicillin, 200 µg/ml streptomycin and 2mM glutamine. SH-SY-5Y cells were cultured in Minimum Essential Media (Euroclone) supplemented with 10% Fetalclone III (Hyclone), 200 U/ml penicillin, 200 µg/ml streptomycin and 2mM glutamine. All cultures were grown as monolayer in a humidified incubator at 37°C in an atmosphere of 5% CO<sub>2</sub>.

Transient DNA transfections were performed by using Lipofectamine 2000 (Invitrogen) according to the specifications of the manufacturer. Briefly, 8x10<sup>4</sup> cells were seeded per well of a 24-well plate the day prior to transfection. Cells were transfected with DNA (500 ng) and cultured for additional 24 or 48 hours. In co-transfection experiments, pRL-CMV DNA was added in 1:100 ratio.

mRNA transfections were performed by using Transmessenger Transfection Reagent (Qiagen) according to the specifications of the manufacturer. Briefly, 8x10<sup>4</sup> cells were seeded per well of a 24-well plate the day prior to transfection. Cells were transfected with mRNA (2 µg) and cultured for additional 8 hours.

Immunofluorescences were performed as previously described [3].

*SDS-PAGE and immunoblotting:*

Cells were scraped in phosphate-buffered saline and lysed for 30 minutes in RIPA buffer (50mM Tris-Hcl, 1% NP-40, 0,25% Na-

deoxycholate, 150 mM NaCl, 1 mM EDTA, pH 7,4) and protease inhibitor cocktail (Sigma-Aldrich) in ice. Protein samples were resuspended in SDS sample buffer and subjected to standard SDS-PAGE electrophoresis followed by protein transfer to a polyvinylidene difluoride membrane (Amersham). Spastin was revealed by immunoblotting with S51 polyclonal antibody [7].

*5' RACE:*

Total RNA was extracted from cells using TRIzol (Invitrogen) according to the specifications of the manufacturer. Rapid amplification of 5' cDNA ends was carried out using a FirstChoice RLM-RACE kit (Ambion) according to the manufacturer's instructions with the following exceptions. The outer PCR reaction was carried out with 10 pmol gene-specific outer primer (5'-ACCATTCCACAGCTTGCTCCTTCT-3'), 1.25 units of Pfu Ultra (Stratagene) and 1.5 ng first-strand cDNA reaction. The PCR conditions were as follows: (1×) 94°C, 3 min; (35×) 94°C, 30 s; 55°C, 30 s; 72°C, 90 s; and (1×) 72°C, 10 min. The inner PCR reaction was carried out with 10 pmol gene-specific inner primer (5'-CG**CAAGCTT**AGGCCTGTTTGTGGAAGACTCGGACG-3', BamHI site in bold), using the same conditions as for the outer PCR. PCR products were separated on 2% agarose gel, cloned BamHI into a pBluescript KS – vector (Stratagene) and sequenced.

*Bioinformatics analysis:*

Conservation studies were performed by using the Human BLAT Search database (<http://genome.ucsc.edu/cgi-bin/hgBlat>). Alignments between human and mouse sequences were performed by using mVISTA (<http://genome.lbl.gov/vista/mvista/submit.shtml>) with the following parameters: Min\_Y (Minimum Y value on the mVISTA plot) 40%, Min\_id (Minimum conservation identity) 50%, Min\_length (Minimum length for a CNS) 50bp. IRES prediction was performed by using UTRscan ([www.ba.itb.cnr.it/BIG/UTRScan](http://www.ba.itb.cnr.it/BIG/UTRScan)). Transcription factors binding sites were predicted using two different matrixes. MATCH<sup>tm</sup> (<http://193.43.101.40/cgi-bin/biobase/transfac/10.2/bin/start.cgi>) parameters: Profile: vertebrates, Cut-off selection: [minimize the sum of both error rates](#). PATCH<sup>tm</sup> (<http://193.43.101.40/cgi-bin/biobase/transfac/10.2/bin/start.cgi>) parameters: sites selection: vertebrate sites, Minimum length of site: 10bp, Maximum number of mismatches: 0, Mismatch penalty: 100, Lower score boundary: 87,5. Bioinformatic analysis of 5' full-length *SPG4* cDNAs was performed using the CAGE analysis web site (<http://fantom3.gsc.riken.jp>) and the Database of Transcriptional Start Sites (<http://dbtss.hgc.jp>).

*Statistical analysis:*

Data are expressed as the mean +/- the standard error of the mean. Statistical analysis was performed using a two-way unpaired Student's t test.

### **Authors' Contribution**

GM carried out all the experiments. EIR conceived and coordinated the study and wrote the manuscript. All authors read and approved the final manuscript.

### **Acknowledgements**

The authors wish to thank Dr. J-T Zhang for kindly providing the pRF vectors, Elena Riano and Germana Meroni for critical discussion and helpful suggestions. This work was supported by grants from the European Union (LSHM-CT-2003-503382 to E.I.R.) and Italian Telethon Foundation (GGP05057 to E.I.R.).



## Figures

*Figure 1 - Schematic representation of the SPG4 first exon*

Translation of spastin initiates from two in-frame start codons (+1, and +259). A uORF overlaps with the first in frame AUG and may serve to divert some ribosomes to the downstream start site.

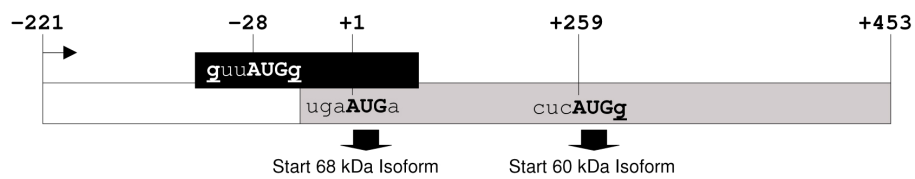
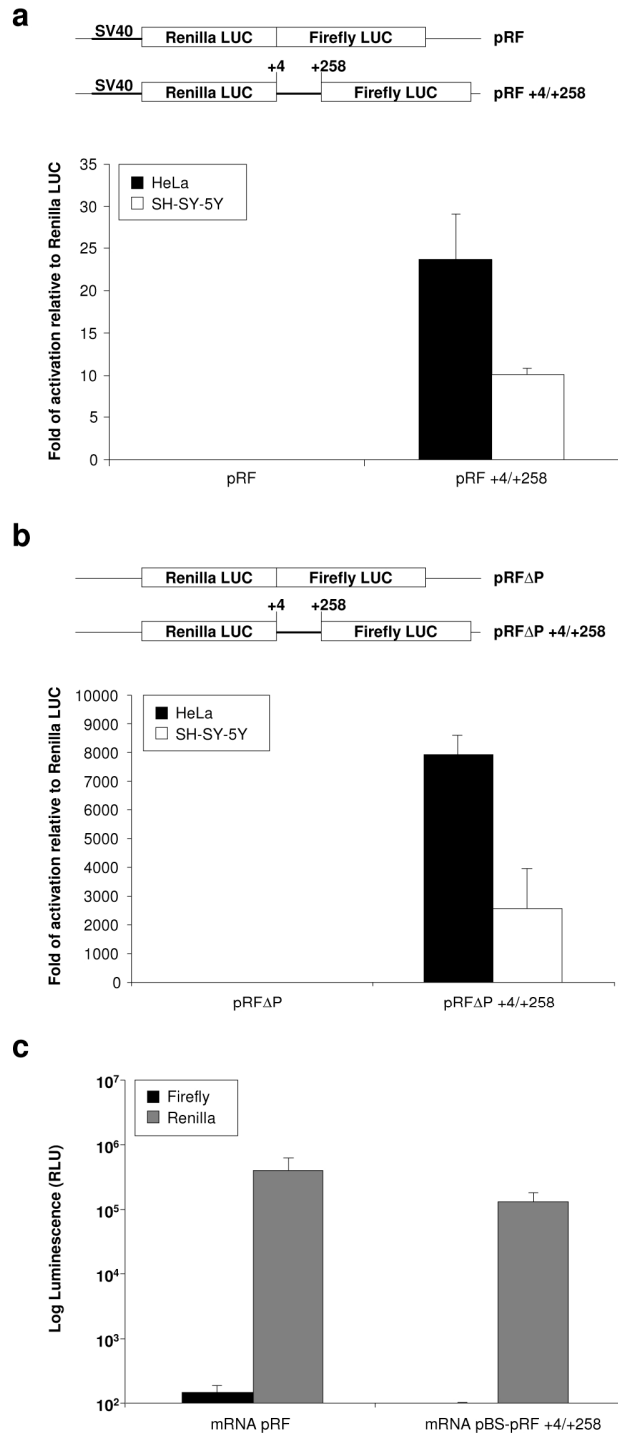


Fig.1

*Figure 2 - Experiments with dicistronic vectors reveal a cryptic promoter*

a) The sequence under analysis was cloned in a dicistronic vector between two different luciferases, from *Renilla* and firefly. HeLa and SH-SY-5Y cells were transfected with the indicated constructs. Cell lysates were prepared 24 hours post-transfection and the activity of the firefly luciferase was normalized to that of the *Renilla* luciferase. For each construct at least 3 independent experiments were performed. b) The same sequence was cloned into a vector lacking the SV40 promoter (pRF $\Delta$ P). Cell lysates were prepared 24 hours post-transfection and the activity of the firefly luciferase was normalized to that of the *Renilla* luciferase. For each construct at least 3 independent experiments were performed. c) In vitro transcribed dicistronic mRNAs were synthesized from the indicated linearized constructs. HeLa cells were transfected with the capped dicistronic mRNAs, and 8 hours after transfection *Renilla* and firefly activities were measured. Error bars represent SEM.



**Fig.2**

*Figure 3 - Analysis of the SPG4 minimal promoter*

a) Sequence comparison using mVISTA between human and mouse genomic regions upstream the first ATG of *SPG4* demonstrates extensive sequence conservation. b) Schematic representation of the constructs used. Different genomic sequences were cloned upstream the firefly luciferase reporter gene. The arrow indicates the TSS of the reference *SPG4* sequence. The position of a putative CAAT box is shown. c) HeLa, SH-SY-5Y and HEK293 cells were co-transfected with the indicated constructs and with a CMV-*Renilla* luciferase plasmid. Cell lysates were prepared 24 hours post-transfection and the activity of the firefly luciferase was normalized to that of the *Renilla* luciferase. For each construct at least 3 independent experiments were performed, using different DNA preparations. Error bars represent SEM.

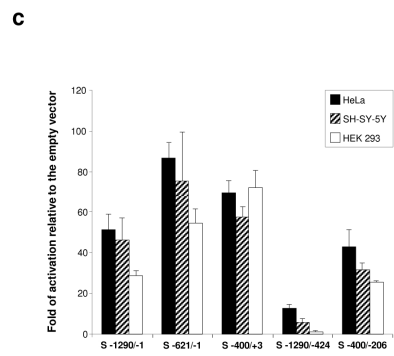
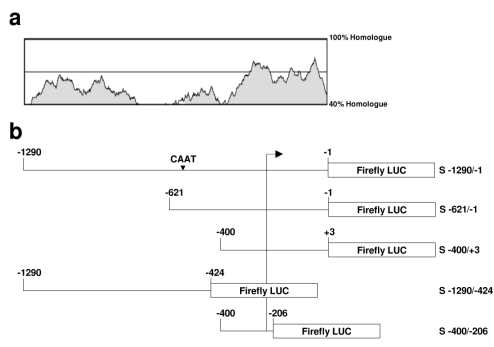


Fig.3

*Figure 4 - Identification of a cryptic promoter in SPG4 exon 1*

a) Schematic representations of the firefly luciferase reporter constructs used. The position of the predicted Sp1 sites is indicated.

b) HeLa, SH-SY-5Y and HEK293 cells were co-transfected with the indicated constructs and with a CMV-*Renilla* luciferase plasmid. Cell lysates were prepared 24 hours post-transfection and the activity of the firefly luciferase was normalized to that of the *Renilla* luciferase. For each construct at least 3 independent experiments were performed, using different DNA preparations.

c) Mutation of each and both predicted Sp1 sites were generated in the S -207/+259 construct and tested in HeLa cells as described above (n=3). Error bars represent SEM. The p value of Student's t test is shown.

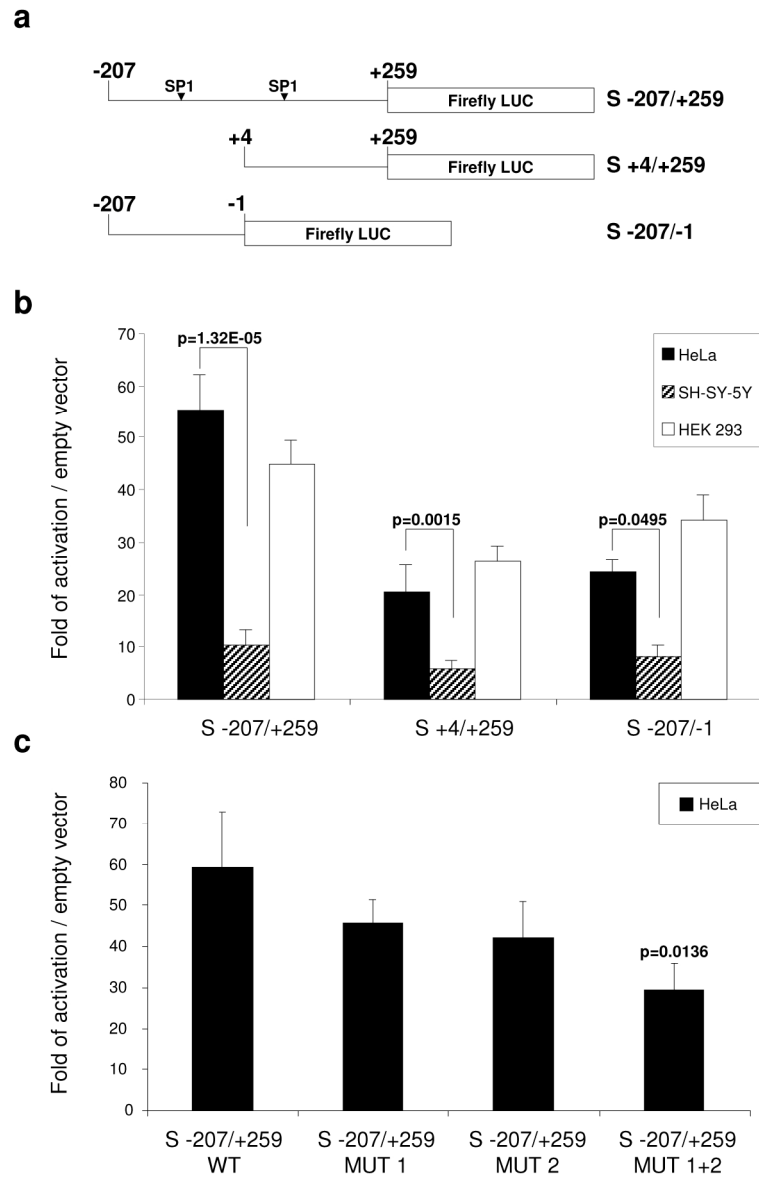


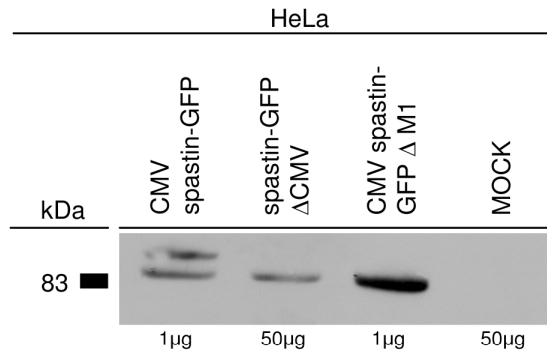
**Fig.4**

*Figure 5 - The cryptic promoter mediates expression of the short spastin isoform in vivo*

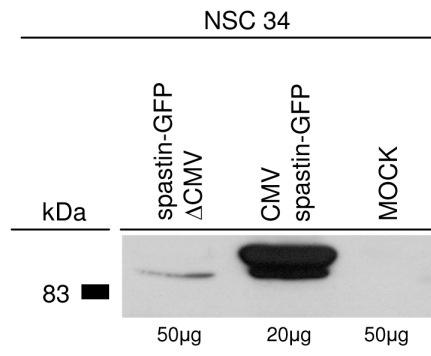
a) HeLa cells were transfected with a CMV-spastin-GFP, a CMV-spastin- $\Delta$ M1, or a spastin-GFP- $\Delta$ CMV construct. Cell lysates were prepared 48 hours post-transfection and subjected to SDS-PAGE. Immunoblotting for transfected spastin was performed with the S51 polyclonal antibody. The CMV-spastin-GFP plasmid drives expression of two spastin isoforms, starting from the first and second methionine, as previously described [11]. Consistently, the CMV-spastin- $\Delta$ M1 construct produces only the shorter isoform. Notably, the promoterless spastin construct synthesizes the short isoform, albeit at lower level, indicating that the cryptic promoter of spastin is active in vivo. Below each lane, it is indicated the amount of transfected cell lysate loaded. b) Similar results were obtained in the murine immortalized motoneuronal cell line NSC34. c) The empty CMV-EGFP vector and CMV-EGFP-STOP-spastin construct were transfected in HeLa cells. Immunofluorescence was performed 48 hours after transfection. Transfected cells were detected by EGFP epifluorescence, while spastin was revealed using the S51 polyclonal antibody. Cells expressing high levels of GFP also synthesize low levels of spastin. Note the different pattern of GFP (diffuse) and spastin staining (discrete, as previously described [11]).



**a**



**b**



**c**

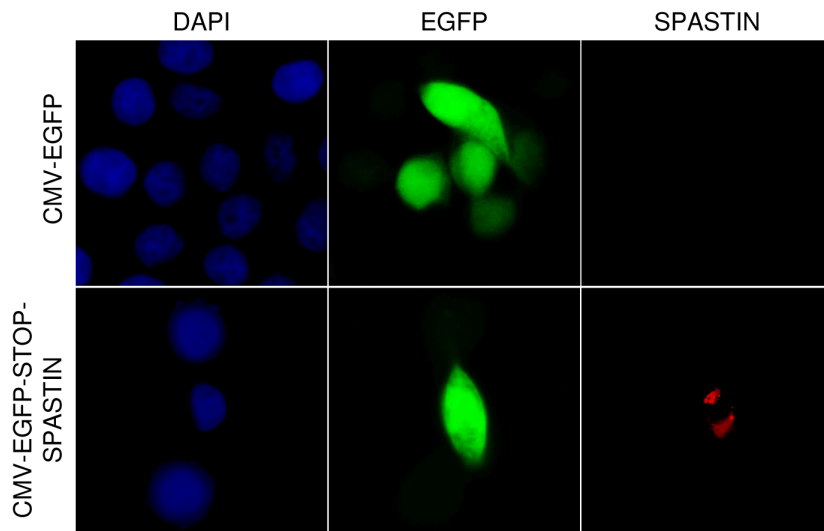
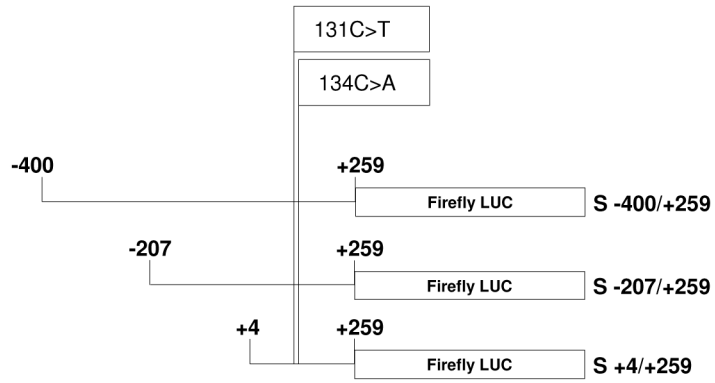


**Fig.5**

*Figure 6 - The role of c.131C>T and c.134C>A polymorphisms on the cryptic promoter activity*

a) Schematic representations of the firefly luciferase reporter constructs used. The position of both polymorphisms is indicated. b) HeLa cells were transfected with the indicated constructs together with a plasmid containing CMV-*Renilla* luciferase. Cell lysates were prepared 24 hours post-transfection and the activity of the firefly luciferase was normalized to that of the *Renilla* luciferase. For each construct at least 3 independent experiments were performed, using different DNA preparations. Error bars represent SEM. The p value of Student's t test is shown.

**a**



**b**

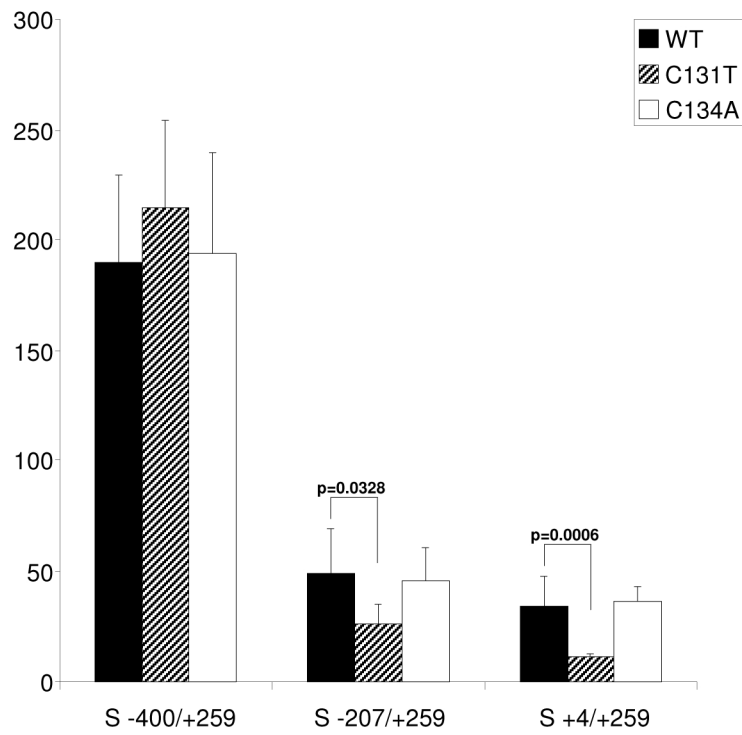


**Fig.6**

*Figure 7 - An endogenous SPG4 transcript specific for the 60 kDa spastin isoform*

a) 5' RACE performed on total RNA extracted from HeLa cells detects a specific product of about 250 bp that is lacking in the minus TAP control sample. b) Sequence of the *SPG4* first exon starting from the transcriptional start site, as defined in public databases, and ending with the second ATG in position 259-261. Sp1 sites are underlined, position of the c.131C>T and c.134C>A polymorphisms and of the two in frame ATGs is shown in bold, while arrows indicate the traditional and the novel transcriptional start site found in this study.

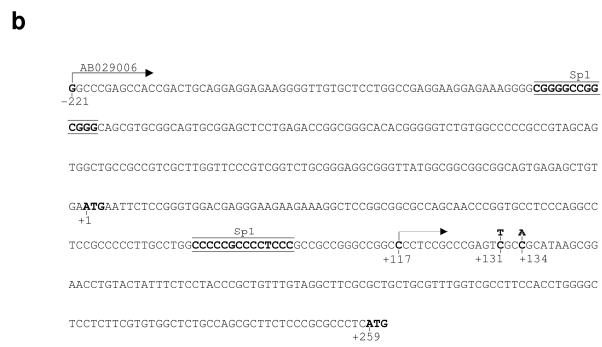
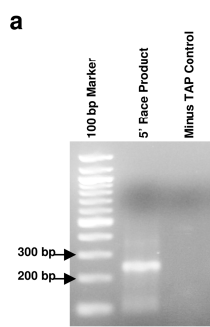


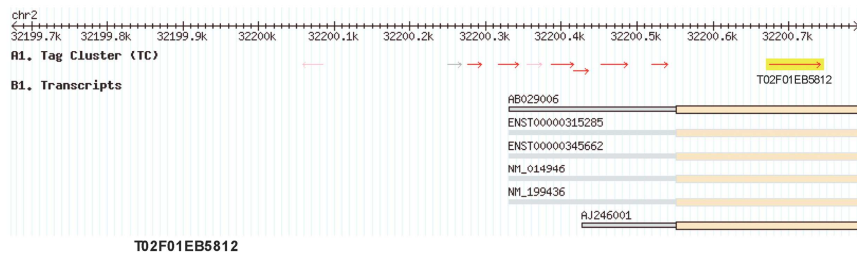
Fig.7

## **Additional files**

*Figure S1 - Bioinformatic analysis of SPG4 transcription start sites based on cap analysis of gene expression*

a) Position of *SPG4* tag clusters (TC, red arrows) shown in the CAGE database, in respect to the reference transcripts. The *SPG4* promoter appears to belong to a broad type that can initiate transcription over a large region, resulting in a population of mRNAs with different lengths. Notably, in the case of *SPG4*, these different transcripts may correspond to different coding regions. Indeed the T02F01EB5812 cluster maps between the first and second ATG. It corresponds to 14 mapped tags deriving from different libraries, including nervous tissues. b) Inspection of the *SPG4* alternative promoter region from the DBTSS database in HEK 293 cells. TSS positions are indicated by red lines. The coding sequence is highlighted in yellow.

**a**



Library	Category	Tags
pancreas	malignancy	4
Hep G2	liver	1
Hep G2	liver	1
liver	malignancy	1
CRL-2429 CCD-1112Sk p16	skin	1
kidney medulla	kidney	1
large intestine	malignancy	1
cerebrum, parietal lobe white matter	brain	1
cerebrum, occipital lobe white matter	brain	1
cerebrum, occipital cortex	brain	1
cecum	malignancy	1

Supplementary Figure 1

## References

1. Fink JK: **Hereditary spastic paraplegia**. *Curr Neurol Neurosci Rep* 2006, **6**(1):65-76.
2. Hazan J, Fonknechten N, Mavel D, Paternotte C, Samson D, Artiguenave F, Davoine CS, Cruaud C, Durr A, Wincker P *et al*: **Spastin, a new AAA protein, is altered in the most frequent form of autosomal dominant spastic paraplegia**. *Nature Genet* 1999, **23**:296-303.
3. Errico A, Ballabio A, Rugarli EI: **Spastin, the protein mutated in autosomal dominant hereditary spastic paraplegia, is involved in microtubule dynamics**. *Hum Mol Genet* 2002, **11**(2):153-163.
4. Evans KJ, Gomes ER, Reisenweber SM, Gundersen GG, Lauring BP: **Linking axonal degeneration to microtubule remodeling by Spastin-mediated microtubule severing**. *J Cell Biol* 2005, **168**(4):599-606.
5. Salinas S, Carazo-Salas RE, Proukakis C, Cooper JM, Weston AE, Schiavo G, Warner TT: **Human spastin has multiple microtubule-related functions**. *J Neurochem* 2005, **95**(5):1411-1420.
6. Salinas S, Carazo-Salas RE, Proukakis C, Schiavo G, Warner TT: **Spastin and microtubules: Functions in health and disease**. *J Neurosci Res* 2007.
7. Errico A, Claudiani P, D'Addio M, Rugarli EI: **Spastin interacts with the centrosomal protein NA14, and is enriched in the**



- spindle pole, the midbody and the distal axon.** *Hum Mol Genet* 2004, **13**(18):2121-2132.
8. McNally FJ, Okawa K, Iwamatsu A, Vale RD: **Katanin, the microtubule-severing ATPase, is concentrated at centrosomes.** *J Cell Sci* 1996, **109**(Pt 3):561-567.
  9. Wharton SB, McDermott CJ, Grierson AJ, Wood JD, Gelsthorpe C, Ince PG, Shaw PJ: **The cellular and molecular pathology of the motor system in hereditary spastic paraparesis due to mutation of the spastin gene.** *J Neuropathol Exp Neurol* 2003, **62**(11):1166-1177.
  10. Yu W, Qiang L, Solowska JM, Karabay A, Korulu S, Baas PW: **The Microtubule-severing Proteins Spastin and Katanin Participate Differently in the Formation of Axonal Branches.** *Molecular biology of the cell* 2008.
  11. Claudiani P, Riano E, Errico A, Andolfi G, Rugarli EI: **Spastin subcellular localization is regulated through usage of different translation start sites and active export from the nucleus.** *Exp Cell Res* 2005, **309**(2):358-369.
  12. Solowska JM, Morfini G, Falnikar A, Himes BT, Brady ST, Huang D, Baas PW: **Quantitative and functional analyses of spastin in the nervous system: implications for hereditary spastic paraplegia.** *J Neurosci* 2008, **28**(9):2147-2157.
  13. Sanderson CM, Connell JW, Edwards TL, Bright NA, Duley S, Thompson A, Luzio JP, Reid E: **Spastin and atlastin, two proteins mutated in autosomal-dominant hereditary spastic**

- paraplegia, are binding partners.** *Hum Mol Genet* 2006, **15**(2):307-318.
14. Evans K, Keller C, Pavur K, Glasgow K, Conn B, Luring B: **Interaction of two hereditary spastic paraplegia gene products, spastin and atlastin, suggests a common pathway for axonal maintenance.** *Proc Natl Acad Sci U S A* 2006, **103**(28):10666-10671.
  15. Chinnery PF, Keers SM, Holden MJ, Ramesh V, Dalton A: **Infantile hereditary spastic paraparesis due to codominant mutations in the spastin gene.** *Neurology* 2004, **63**(4):710-712.
  16. Svenson IK, Kloos MT, Gaskell PC, Nance MA, Garbern JY, Hisanaga S, Pericak-Vance MA, Ashley-Koch AE, Marchuk DA: **Intragenic modifiers of hereditary spastic paraplegia due to spastin gene mutations.** *Neurogenetics* 2004, **5**(3):157-164.
  17. McDermott CJ, Burness CE, Kirby J, Cox LE, Rao DG, Hewamadduma C, Sharrack B, Hadjivassiliou M, Chinnery PF, Dalton A *et al*: **Clinical features of hereditary spastic paraplegia due to spastin mutation.** *Neurology* 2006, **67**(1):45-51.
  18. Lindsey JC, Lusher ME, Mc Dermott CJ, White KD, Reid E, Rubinsztein DC, Bashir R, Hazan J, Shaw PJ, Bushby KMD: **Mutation analysis of the spastin gene (SPG4) in patients with hereditary spastic paraparesis.** *J Med Genet* 2000, **37**:759-765.

19. Kozak M: **Pushing the limits of the scanning mechanism for initiation of translation.** *Gene* 2002, **299**(1-2):1-34.
20. Morris DR, Geballe AP: **Upstream open reading frames as regulators of mRNA translation.** *Mol Cell Biol* 2000, **20**(23):8635-8642.
21. Kozak M: **A second look at cellular mRNA sequences said to function as internal ribosome entry sites.** *Nucleic Acids Res* 2005, **33**(20):6593-6602.
22. Komar AA, Hatzoglou M: **Internal ribosome entry sites in cellular mRNAs: mystery of their existence.** *J Biol Chem* 2005, **280**(25):23425-23428.
23. Van Eden ME, Byrd MP, Sherrill KW, Lloyd RE: **Demonstrating internal ribosome entry sites in eukaryotic mRNAs using stringent RNA test procedures.** *Rna* 2004, **10**(4):720-730.
24. Carninci P, Sandelin A, Lenhard B, Katayama S, Shimokawa K, Ponjavic J, Semple CA, Taylor MS, Engstrom PG, Frith MC *et al*: **Genome-wide analysis of mammalian promoter architecture and evolution.** *Nature genetics* 2006, **38**(6):626-635.
25. Sandelin A, Carninci P, Lenhard B, Ponjavic J, Hayashizaki Y, Hume DA: **Mammalian RNA polymerase II core promoters: insights from genome-wide studies.** *Nat Rev Genet* 2007, **8**(6):424-436.
26. Smale ST, Kadonaga JT: **The RNA polymerase II core promoter.** *Annu Rev Biochem* 2003, **72**:449-479.
27. Suske G: **The Sp-family of transcription factors.** *Gene* 1999, **238**(2):291-300.

28. Oh JE, Han JA, Hwang ES: **Downregulation of transcription factor, Sp1, during cellular senescence.** *Biochem Biophys Res Commun* 2007, **353**(1):86-91.
29. Bert AG, Grepin R, Vadas MA, Goodall GJ: **Assessing IRES activity in the HIF-1alpha and other cellular 5' UTRs.** *Rna* 2006, **12**(6):1074-1083.
30. Han B, Zhang JT: **Regulation of gene expression by internal ribosome entry sites or cryptic promoters: the eIF4G story.** *Mol Cell Biol* 2002, **22**(21):7372-7384.
31. Wang Z, Weaver M, Magnuson NS: **Cryptic promoter activity in the DNA sequence corresponding to the pim-1 5'-UTR.** *Nucleic Acids Res* 2005, **33**(7):2248-2258.
32. den Dunnen JT, Antonarakis SE: **Mutation nomenclature extensions and suggestions to describe complex mutations: a discussion.** *Human mutation* 2000, **15**(1):7-12.

# Pleiotropic effects of spastin on neurite growth depending on expression levels

Elena Riano<sup>1</sup>, Monica Martignoni<sup>1</sup>, Giuseppe Mancuso<sup>1</sup>, Daniele Cartelli<sup>2</sup>, Francesca Crippa<sup>3</sup>, Irene Toldo<sup>4</sup>, Gabriele Siciliano<sup>5</sup>, Daniela Di Bella<sup>1</sup>, Franco Taroni<sup>1</sup>, Maria Teresa Bassi<sup>3</sup>, Graziella Cappelletti<sup>2</sup>, and Elena I. Rugarli<sup>1,6</sup>

<sup>1</sup> Division of Biochemistry and Genetics, Istituto Neurologico “C. Besta”, Milan, Italy

<sup>2</sup> Department of Biology, University of Milan, Milan, Italy

<sup>3</sup> E. Medea Scientific Institute, Laboratory of Molecular Biology, Bosisio Parini, Italy

<sup>4</sup> Department of Pediatrics, University of Padua, Padua, Italy

<sup>5</sup> Department of Neuroscience, S. Chiara Hospital, University of Pisa, Pisa, Italy.

<sup>6</sup> Department of Neuroscience and Medical Biotechnologies, University of Milano-Bicocca, Milan, Italy

*Published: 2009*

*Journal of Neurochemistry. (2009) 108, 1277–1288*

## **Abstract**

Hereditary spastic paraplegia (HSP) is characterized by weakness and spasticity of the lower limbs, owing to degeneration of corticospinal axons. The most common form is due to heterozygous mutations in the *SPG4* gene, encoding spastin, a microtubule-severing protein. Here, we show that neurite growth in immortalized and primary neurons responds in pleiotropic ways to changes in spastin levels. Spastin depletion alters the development of primary hippocampal neurons leading to abnormal neuron morphology, dystrophic neurites, and axonal growth defects. By live imaging with EB3-GFP, a microtubule plus-end tracking protein, we ascertained that the assembly rate of microtubules is reduced when spastin is down-regulated. Spastin overexpression at high levels strongly suppresses neurite maintenance, while slight spastin up-regulation using an endogenous promoter enhances neurite branching and elongation. Spastin severing activity is exerted preferentially on stable acetylated and detyrosinated microtubules. We further show that *SPG4* nonsense or splice site mutations found in HSP patients result in reduced spastin levels, supporting haploinsufficiency as the molecular cause of the disease. Our study reveals that *SPG4* is a dosage-sensitive gene, and broadens the understanding of the role of spastin in neurite growth and microtubule dynamics.

## Introduction

Hereditary spastic paraplegia (HSP) is characterized by weakness and spasticity of the lower limbs owing to dying-back of the axons of the corticospinal tracts (Fink 2006). The gene most commonly mutated in autosomal dominant HSP, *SPG4*, exemplifies the importance of cytoskeletal remodeling for axon homeostasis. *SPG4* encodes spastin, an ATPase belonging to the AAA (ATPases Associated with diverse cellular Activities) family (Hazan *et al.* 1999). Spastin is involved in microtubule (MT)-severing (Errico *et al.* 2002, Evans *et al.* 2005, Roll-Mecak & Vale 2005, Salinas *et al.* 2005), a process by which long MTs can be fractured into shorter tracks. Spastin forms a ring-shaped hexamer containing a central pore and six radiating arms that may dock onto the MTs (White *et al.* 2007, Roll-Mecak & Vale 2008). Structural data on *Drosophila* spastin are consistent with a model in which spastin pulls the C terminus of tubulin through its central pore generating a mechanical force that destabilizes tubulin-tubulin interactions within the MT lattice (Roll-Mecak & Vale 2008). Depending on different usage of two AUG codons in the first exon, and alternative splicing of exon 4, four spastin isoforms can be detected, the most abundant in tissues being the one retaining exon 4 and starting from the second methionine (Claudiani *et al.* 2005). MT-severing plays an important role during meiosis and mitosis to release MTs from the centrosome, and is thought to be essential in neurons, where the capacity of a MT to move is strictly related to its length (Baas *et al.* 2006). Spastin is enriched in the centrosome in

interphase and during mitosis, in the cytokinesis structure midbody, and in the growth cones and branching points of neurons, all regions characterized by extensive cytoskeletal remodeling (Errico *et al.* 2004, Yu *et al.* 2008). A recent study has identified an important role of spastin in the formation of axonal branches (Yu *et al.* 2008). It is therefore an attractive hypothesis that HSP due to *SPG4* mutations arises through disturbances of the dynamics of MTs in the long central motor axons. These axons can reach the length of 1 meter in an adult individual, contain more than 99% of the cytoplasm of the cell, and are dependent on efficient transport of organelles, cytoskeletal components, and lipid constituents synthesized in the cell body.

To date, up to 150 mutations of all types have been found in HSP patients along the *SPG4* gene. Approximately 15-25% of these are missense mutations, while the vast majority are clearly loss-of-function mutations, such as nonsense or splice site mutations, deletions and insertions causing frameshifts (Depienne *et al.* 2007). Missense mutations do not appear to induce phenotypes different from exon rearrangements. All together, genetic analysis of patients argues for haploinsufficiency as the basis of the disease. The view that spastin haploinsufficiency causes HSP is also supported by the available mouse model (Tarrade *et al.* 2006). Homozygous *Spg4*<sup>-/-</sup> mice displayed a late-onset motor deficit associated with focal axonal swelling in the lumbar spinal cord with accumulation of organelles and cytoskeletal components. Heterozygous *Spg4*<sup>+/-</sup> mice have a milder phenotype, suggesting a dosage effect.



Here we show that neurite growth and stability are extremely susceptible to small changes in spastin levels. Moreover, we provide evidence that no truncated spastin isoforms are detectable in cell lines from HSP patients carrying *SPG4* mutations.

## Materials and methods

### *Patients and SPG4 mutation analysis:*

Blood specimens were obtained from the probands, family members, and control subjects after signing the informed consent. The Institutional Ethical Committees of Istituto Neurologico “C. Besta” and IRCCS E. Medea approved this study.

Genomic DNA from peripheral blood leukocytes was prepared with isoquick Nucleic Acid Extraction kit (ORCA Research, Bothell, WA). All *SPG4* coding exons were amplified from patients’ DNA and directly sequenced. Mutation nomenclature refers to the A of the initiator ATG as nucleotide +1. A total of 150 control individuals from the Italian population were recruited as control subjects and checked for the nucleotide changes under examination.

### *Constructs:*

Spastin-GFP and Spastin<sup>K388R</sup>-GFP were previously described (Errico *et al.* 2002). EB3-GFP was a kind gift from N. Galjart (Stepanova *et al.* 2003). The CMV-EGFP-STOP-5’UTR-spastin was generated by cloning the *SPG4* cDNA including the coding region and 125 bp of 5’ UTR blunt in the *NotI* site of pEGFP-N2 vector (Clontech).

### *Cell cultures:*

A monolayer of cortical glial cells was grown as described (Goslin & Banker 1990). Hippocampi from 18-day-old fetal mice were

mechanically dissociated. Dissociated neurons were plated on poly-L-lysine-treated glass coverslip (1 mg/ml) at a density of 25,000 cells/cm<sup>2</sup>, in DMEM (50%, Highclone) and HAM's F12 (50%, Invitrogen), supplemented with 5 mM Hepes buffer, 0.6% glucose, 25 µg/ml insuline and N1 supplement. After 24 hours the coverslips were transferred, face down, to dishes containing the monolayer of cortical glial cells. NSC34 cells were kindly provided by Dr Neil R. Cashman (McGill University, Montreal, Canada) and were cultured in DMEM with 5% defined FBS. Lymphoblastoid cell lines were cultured in RPMI 1640 (Gibco) supplemented with 20% fetal clone 1 (Hyclone), 2% pyruvate (Gibco) and 1% of non essential aminoacids (Gibco).

*Gene silencing:*

Stealth™ siRNAs were synthesized by Invitrogen with the following sequences:

MSS11: 5'-CCAGUGAGAUGAGAAAUAUUCGAUU-3';

MSS12: 5'-GGAAUGUGGACAGCAAUCUUGCUAA-3';

MSS13: 5'-GGAAUGGUAUAAGAAAGGUAUCGAA-3';

SCR11: 5'-CCAGAGGUAAGAUAAUUAGCGUAUU-3';

C: StealthRNAi negative control LO GC (Invitrogen).

siRNA duplexes (100 nM) together with 2 µg of an empty GFP vector for 250,000 cells were transfected in primary neurons at the time of plating using the Microporator MP-100 apparatus (Digital Bio). Neurons were processed for immunofluorescence after 72 hours. Morphometric measurements were performed on a total of 106

transfected neurons with SCR11, 101 with the C, 74 with MSS11, 31 with MSS12, and 31 with MSS13. At least 4 independent experiments were performed.

*Live cell imaging of EB3-GFP movement:*

NSC34 cells were cotransfected with EB3-GFP and SCR11 or MSS11 and analyzed after 72 hours. Cultures were transferred to a live cell imaging workstation composed of an inverted microscope (Nikon Eclipse TE2000-S + BD CARV II), a heated (37°C) chamber and a Nikon Plan Apo VC 100X/1.40 oil objective. Images were collected every 5 s for a total time of 5 min with a cooled camera (QUANTEM 512 SC) driven by Metamorph software (Molecular Devices Ltd.), obtaining 61 frame length movies. Velocity and number of EB3-GFP dashes was calculated by using the Kymograph function of Metamorph software. Statistical analysis was performed on the average velocity of comets in individual axons obtained from independent experiments.

*Overexpression experiments:*

For overexpression experiments, NSC34 cells and hippocampal neurons were transfected with lipofectamine 2000 (Invitrogen). Immunofluorescence was performed as described (Errico *et al.* 2002). Antibodies against MAP2, tyrosinated tubulin, and acetylated tubulin were from Sigma-Aldrich. Antibody against detyrosinated tubulin was from Chemicon. Antibody against GFP was purchased by ABCAM. Secondary antibodies were from Dako and Invitrogen. Cells were

stained using DAPI (1 $\mu$ g/ml, Roche) and mounted in Vectashield H1000 (Vector Laboratories), or Fluorsave (Calbiochem). Immunofluorescences were examined using an Axioplan microscope (Zeiss) and images acquired with an AxioCam CDD camera and Axiovision digital imaging software (Zeiss). Confocal microscopy was performed with a Bio-Rad Radiance 2100 confocal microscope at 1,024 x 1,024-pixel resolution. For quantification of neurite length we used a cut-off length of 30  $\mu$ m.

*Immunoblotting:*

Total proteins from lymphoblastoid cell lines were extracted in lysis buffer containing 40 mM HEPES-NaOH (pH 7.6), 150 mM NaCl, 0.5% Triton X-100, 10 mM MgCl<sub>2</sub>, 1 mM Na<sub>3</sub>VO<sub>4</sub>, 1 mM EDTA and protease inhibitor cocktail (Sigma-Aldrich). Proteins from NSC34 cells were solubilized in RIPA buffer (Claudiani *et al.* 2005). Protein samples were resuspended in SDS sample buffer and subjected to standard SDS-PAGE electrophoresis. The anti spastin S51 antibody has been previously described and is raised against a spastin epitope containing amino acids 87 to 354 (Errico *et al.* 2004). Secondary antibodies were from Amersham Pharmacia. To normalize we employed antibodies against calnexin (Stressgen).

*Real-time PCR:*

RNA extraction was performed using TRIzol<sup>®</sup> (Invitrogen), following the manufacturer specifications. cDNA was synthesized using

SuperScript™ First-Strand Synthesis System (Invitrogen). Real-time amplification was performed using SYBR® Green PCR Master Mix (Applied Biosystem, Foster City, CA) in an ABI PRISM 7000 Sequence Detection System. cDNA synthesized from 140 ng of RNA was used in each reaction. Primers for GAPDH were used as gene standard reference. Primer sequences are available upon request. Each PCR reaction was performed in triplicate with the following profile: one cycle at 50 °C for 2 min, one cycle at 95 °C for 10 min and then 40 cycles at 95 °C for 15 s and 60 °C for 1 min (two-step protocol). The experiment was repeated three independent times.

## Results

### *Reduced MT dynamics in spastin-depleted NSC34 cells*

Primary cortical neurons derived from *Spg4*<sup>-/-</sup> mice grew normally, but in approximately 5% of the cases developed neurite swellings, selectively localized to a specialized region of the axon, at the border between stable and dynamic MTs (Tarrade *et al.* 2006). The low penetrance of this phenotype can be explained by a protecting environment established *in vivo* after constitutive removal of the *Spg4* gene through up-regulation of other MT-severing molecules. To further study the role of spastin in neurite growth and stability, we employed a combination of overexpression and depletion strategies in cultured neurons. Abrupt silencing of spastin by RNA interference (RNAi) would not allow compensatory mechanisms to be established, while overexpression of spastin at different levels may reveal how neurons react to variations in spastin dosage.

We tested three different small interfering RNA (siRNA) directed against the murine *Spg4* gene (MSS11, MSS12, and MSS13) in NSC34 cells, immortalized motor neurons derived from the fusion of mouse embryonic day 12-14 spinal cord and neuroblastoma cells, which express both spastin isoforms (Cashman *et al.* 1992, Claudiani *et al.* 2005). As control, we used both a universal control siRNA (C) and a scrambled sequence corresponding to MSS11 (SCR11). After transfection in NSC34 cells, all three siRNAs were effective in significantly reducing *Spg4* transcript and spastin protein levels for at least 110 hours after transfection (Fig. S1). Furthermore, we

confirmed that spastin RNAi does not lead to activation of an interferon response by analyzing the expression levels of transcripts for proteins constituents of the IFN pathway (Fig. S1 and not shown). This is especially important when using RNAi to silence protein expression in neurons, since it has been shown that activation of an interferon-response in primary neurons can lead to synapse and dendritic spine retraction (Alvarez *et al.* 2006).

As a first step, we used RNAi to silence spastin expression in NSC34 cells and studied the effects on the MT cytoskeleton. MT-severing contributes to MT dynamics by providing cells with short MTs highly susceptible to transport, and by promoting the growth of MTs by means of treadmilling, a process whereby MTs add subunits to one end while simultaneously losing subunits from the other end (Baas *et al.* 2005). Spastin-silenced cells are therefore expected to contain longer, less motile, and more stable MTs. We did not observe any significant difference in the amount of acetylated tubulin (associated with older, stable MTs) or tyrosinated tubulin (a marker of newly formed MTs) in interfered compared to control cells by immunofluorescence (not shown). We then used EB3-GFP to visualize the plus ends of polymerizing MTs. EB3 is a member of a group of proteins that associate with MT plus ends during their assembly, and then spontaneously dissociate, and thus is visible as a moving comet in live-microscopy (Stepanova *et al.* 2003). By this mean it is possible to obtain information about the dynamicity of the MT polymer. EB3-GFP was co-transfected with MSS1 or SCR11 in NSC34 cells. Seventy-two hours after transfection, we live-imaged EB3-GFP excursions in



long processes of NSC34 cells and analyzed their velocity by kymograph. Many moving fluorescent dashes were observed in control and spastin-depleted NSC34 cells (Video 1 and 2, respectively). Only a minority (about 8%) of the moving comets were directed towards the cell body, indicating that the NSC34 cells were well differentiated and that the neurites we were studying behaved as bona fide axons (Stepanova *et al.* 2003). We found a significant decrease of the average velocity of the anterograde comets in NSC34 cells in which spastin was knocked down using siRNA, consistent with less MTs undergoing treadmilling and with a more stable MT network (Fig. 1).

#### *Spastin knock down affects axonal growth in primary hippocampal neurons*

The previous experiments suggest that the dynamicity of the MT polymer is affected when the levels of spastin are reduced. To investigate potential outcomes of a more stable MT network for neurite growth and stability in primary neurons, we silenced spastin in mouse hippocampal neurons. The hippocampus is a source of relatively homogeneous neurons following a stereotyped manner of differentiation in vitro, representing an ideal system to observe morphological effects in various experimental conditions (Dotti *et al.* 1988). To directly visualize silenced neurons, we co-transfected the individual siRNAs with a vector encoding for a cytosolic GFP. To minimize the possibility of off-targets effects, experiments were

performed using independent siRNAs and we considered only those phenotypes that were consistently reproduced by using each siRNA (Svoboda 2007).

Hippocampal neurons were transfected immediately after dissociation and analyzed 72 hour later. At this stage, neurons transfected with the control siRNAs had acquired a prominent longer process (the future axon), and several minor processes (later developing into dendrites), showing the characteristic morphology of hippocampal neurons at stage 3-4 of in vitro development (Dotti *et al.* 1988) (Fig. 2A). In contrast, several neurons in which spastin expression was down-regulated displayed an obvious alteration of their morphology (Fig. 2A, B). Frequently, the distinction between a longer major and several minor processes was not readily apparent. In many cases, neurons lacked a prominent major neurite or had two major processes (Fig. 2A). A very small percentage of neurons showed swellings in their axons (5 out of 83 MSS11-treated neurons, 2 out of 33 MSS12-treated neurons, 1 out of 38 MSS13-treated neurons, while no swellings were detected in 108 SCR11-treated neurons and in 103 neurons C-treated neurons), consistent with previously reported findings in spastin knock-out mice (Tarrade *et al.* 2006). We measured the length of the future axons (identified as the longest process of the neuron) in all transfected neurons, independent from their general morphology, and found that spastin depleted-neurons had significantly shorter axons compared to control neurons (Fig. 2B, C). Dendrite number, dendrite length and branching of axons and dendrites were instead not reproducibly

affected (Fig. S2). In conclusion, spastin depletion in primary hippocampal neurons caused a defective development of the axonal processes and affected the general morphology of the neurons.

#### *Effect of spastin overexpression on neurite extension and MT stability*

We then turned to study the effect of increasing spastin levels on neurite growth and stability. Hippocampal neurons were cultured for 1 week and allowed to differentiate long and branched axons before transfection with a construct overexpressing human spastin-GFP under the strong CMV promoter. This construct expresses at high levels both the 68 kDa and the 60 kDa spastin isoforms (not shown). After 24 hours, spastin-transfected neurons displayed extremely short neurites, showing reduced levels of acetylated tubulin, a marker of stable MTs (Fig. 3). No spastin-transfected neurons were found 48 hours after transfection, strongly indicating that overexpression of spastin into already differentiated primary neurons is toxic.

To overcome the drastic phenotype of spastin overexpression in primary neurons, we resorted to immortalized NSC34 cells. We transfected both the wild type spastin-GFP construct and, in parallel, a mutant version of spastin (spastin<sup>K388R</sup>-GFP) that reproduces a mutation found in HSP patients (Fonknechten *et al.* 2000). This mutant binds constitutively to thick MT bundles, behaving as ATP-hydrolysis deficient (Errico *et al.* 2002, Evans *et al.* 2005). The percentage of NSC34 cells expressing wild-type spastin and

elongating neurites (defined as longer than 30  $\mu\text{m}$ ) was only slightly affected 24 hours after transfection, but decreased dramatically after 48 hours (Fig. 4). In contrast, neurite elongation in cells expressing spastin<sup>K388R</sup> was affected in a less pronounced manner, suggesting that the severe effect on neurite elongation observed with the wild-type protein depends on an intact AAA domain (Fig. 4). We ascertained that the fusion with the GFP does not affect these results, by repeating these experiments with a construct containing spastin without any tag (not shown).

In spastin-overexpressing NSC34 cells, as in primary neurons, we found a drastic reduction of the staining for acetylated and detyrosinated tubulin, predominantly associated with stable MTs, while the newly formed tyrosinated MTs were not overtly disrupted (Fig. S3 and Fig. 4 C-H). Consistently, the spastin<sup>K388R</sup> trap mutant stained bundles of acetylated tubulin, but did not colocalize to tyrosinated MTs (Fig. S3 and Fig. 4F-H).

All together, these data indicate that elongation and maintenance of long neurites is severely impaired when spastin is overexpressed at high levels. Moreover, the preferential loss of detyrosinated and acetylated MTs highlights the role of spastin in MT destabilization.

*Mild increase of spastin levels enhances neurite elongation and branching in NSC34 cells*

The previous data were obtained by using constructs that overexpress spastin above physiological levels. To obtain a limited

degree of spastin overexpression, we took advantage of the recent characterization by our group of a cryptic promoter located in the first exon of *SPG4* (Mancuso & Rugarli 2008). The 5' UTR and the region between the first and second ATG of *SPG4* function as a promoter in a variety of cell lines, including NSC34 cells (Mancuso & Rugarli 2008). Based on this data, we developed a dual promoter vector for expressing spastin at low levels. This vector expresses the GFP reporter under the CMV promoter, and spastin under the endogenous cryptic promoter (CMV-EGFP-STOP-5'UTR-spastin, Fig. 5A). This system has the advantage of allowing identification of transfected cells by labeling the whole cytoplasm with GFP (Fig. 5). Since the cryptic promoter did not drive detectable spastin expression in hippocampal neurons, we used this vector for spastin up-regulation in NSC34 cells. This vector expresses low levels of spastin, detectable by immunofluorescence only in cells transfected at high efficiency (Mancuso & Rugarli 2008) (Fig. 5E-G and S4). Spastin showed a diffuse cytoplasm staining pattern with accumulation in punctate structures, consistent with our previous findings (Claudiani *et al.* 2005). We never detected any spastin signal in control cells expressing the CMV-GFP vector at similar high levels (Fig. 5B-D and S4). As a further confirmation of spastin expression, we found that all the cells expressing detectable levels of spastin had a reduced staining for acetylated tubulin (Fig. S4).

NSC34 cells in our culture conditions appear as a mixed population containing a majority of cells with a glial-like shape and a minority of multipolar neuron-like cells with well-developed neurites (Fig. 5B, H).

We analyzed the phenotype of cells in which we could undoubtedly reveal spastin by immunofluorescence and compared it with control cells with similar GFP expression levels. We found that an increased percentage of spastin-expressing cells elongated neurites compared to control cells (Fig. 5K). Furthermore, a consistent fraction of spastin-expressing cells showed an abnormal morphology characterized by the extension of protrusions from the cell body, from the neurites, or from both (Fig. 5L). Exemplary pictures are shown in Figs. 5 and S4. Spastin-expressing cells extended long and tortuous neurites, showing increased branching. Sometimes, enlargements along the axons with the appearance of swellings occurred in correspondence to accumulation of spastin signal (Fig. 5E-G). Lateral extensions protruded also from the cell body of spastin-expressing cells, in some cases resembling the attempt to form a neurite. These data strongly suggest that a limited increase of spastin expression promotes the formation of cell protrusions, neurite extension and branching.

*SPG4 mutant alleles potentially leading to premature termination of translation do not produce truncated spastin isoforms*

The previous data strongly indicate that neurons respond in various ways to variations in spastin levels, consistent with *SPG4* being a dosage-sensitive gene, and with haploinsufficiency as the pathogenic mechanism in the disease. This has been recently questioned by Solowska *et al.* who proposed that expression of abnormal truncated

versions of the spastin long isoform (starting from methionine 1) underlies axonal degeneration in HSP patients (Solowska *et al.* 2008). However, the presence of truncated protein isoforms in cell lines from HSP patients carrying mutations potentially leading to premature protein termination has not been investigated. To this purpose, we selected HSP patients carrying loss-of-function mutations in *SPG4* (see Supplementary Table), and performed western blot analysis using a specific anti-spastin antibody on lymphoblastoid cell lines.

We first analyzed patients from an Italian family in which both a c.1634C>G (p.S545X) mutation and the disease modifier polymorphism c.131C>T (S44L) segregate (Fig. 6A). As previously reported, the patient carrying both the mutation and the polymorphism (EM16-08) is affected by a rapidly progressing form of HSP with infantile onset (see supplementary material and methods) (Chinnery *et al.* 2004, McDermott *et al.* 2006, Svenson *et al.* 2004). Western blot analysis clearly showed that the patients carrying the mutated allele had approximately half the dosage of wild-type protein, independent on whether they also bear the S44L polymorphism (Fig. 6A). Most importantly, we found no evidence for the presence of a truncated spastin isoform (Fig. 6A). We also analyzed *SPG4* transcript levels in patient EM17-08 by real-time PCR, using specific *SPG4* primers located downstream the affected exon. We found that the transcript levels were reduced to approximately 50%, indicating that the c.1634C>G mutation leads to RNA instability by nonsense-mediated decay (Fig. 6B). In addition, we obtained cell

lines from additional three patients with splice site mutations in different regions of the *SPG4* gene (Supplementary Table). Western blot analysis of spastin levels in cell lines from these patients confirmed a reduction of the spastin protein and showed no detectable truncated isoforms (Fig. 6C and S5).

In conclusion, these experiments strongly suggest that the pathogenic mechanism in these patients is haploinsufficiency and rule out the possibility that truncated spastin isoforms are present at detectable level.



## Discussion

MTs are an essential component of the neuronal cytoskeleton. They are implicated in the maintenance of neurite shape, they act as trails for organelle and vesicle transport, and participate in axonal elongation and branching and in turning of the growth cones. Dynamic rearrangements of MTs are crucial for their function. For example, MTs appear to be less stable and less bundled in branching points and growth cones (Dent & Gertler 2003). We show here that neurons are highly susceptible to changes in spastin dosage and respond with an alteration of the cytoskeletal organization and dynamics and abnormal neurite growth.

We show that depletion of spastin in live NSC34 cells associated with reduced rates of movements of EB3-GFP comets. The velocity of movements of the comets might in theory depend both on the movement and on the rate of growth of MTs (Abal *et al.* 2002, Ahmad *et al.* 2006). However, the comet velocity that we detect is not fast enough to suggest transport of the MT polymer. This notwithstanding, we could have missed short MTs moving at high speed, which require acquisition of EB-GFP excursions at least every second (Abal *et al.* 2002). In light of our results, we conclude that spastin has an effect on MT polymerization rate. Intriguingly, depletion of *Drosophila* spastin was previously found to attenuate the turnover at the plus ends of spindle MTs (Zhang *et al.* 2007). It is possible that spastin has a direct effect on MT growth. An alternative and perhaps more likely explanation is that the reduced MT growth

in conditions of spastin down-regulation may be secondary to the presence of longer and older MTs that more easily accumulate post-translational modifications or stabilizing factors rendering them less prone to undergo turnover. Post-translational modifications of tubulin mark subpopulations of MTs thus affecting downstream functions, including polymerization (Hammond *et al.* 2008, Verhey & Gaertig 2007). For example, tyrosinated MTs have recently been shown to play a direct role in recruitment of a subclass of +TIP proteins, molecules that localize to and track with the plus-ends of growing MTs (Peris *et al.* 2006). When spastin levels are reduced, MTs might be enriched in detyrosinated and acetylated tubulin, and recruit EB3-GFP with less efficiency. We and others (Tarrade *et al.* 2006, Yu *et al.* 2008) have not been able to prove that this is the case, but immunofluorescence and western blot analysis may not be sensitive enough to detect subtle changes. In contrast, in a *Drosophila* model, spastin knock-down by RNAi caused defects in synaptic growth and neurotransmission due to an aberrantly stabilized cytoskeleton rich in acetylated MTs (Trotta *et al.* 2004). Conversely, these phenotypes could be rescued by treatment with vinblastine, a MT destabilizing drug (Orso *et al.* 2005). Noteworthy, post-translational modifications of tubulin may play a key and direct role in spastin recognition of MTs for severing. Indeed, in our experiments, spastin overexpression seems to affect preferentially acetylated and detyrosinated versus tyrosinated MTs. This data is consistent with the recent finding that an antibody that recognizes exposed glutamate residues (as it occurs in detyrosinated tubulin) on

the C-terminal tail of tubulin efficiently inhibits MT-severing by *Drosophila* spastin, while an antibody that recognizes  $\alpha$ -tubulin with a C-terminal tyrosine fails to do so, suggesting that spastin may selectively recognize “Glu” tubulin in stable MTs (Roll-Mecak & Vale 2008). All together, reducing or augmenting the activity of a microtubule-severing protein like spastin, by changing its dosage, may have a very complex effect on the MT array that entails the length and the growth of the polymer, the post-translational modifications of the building blocks, and its accessibility to a variety of other stabilizing or destabilizing factors. This has in turn relevant implications for neurite growth.

In hippocampal primary neurons, spastin depletion caused a dramatic alteration of the global morphology of the neurons, which lost their reproducible and stereotyped shape characterized by one axon, a single apical dendrite, and several shorter basilar dendrites. The length of the longest process of each neuron was significantly affected when spastin was knocked down, while dendrite number and length and neurite branching were not altered. Dramatic defects in motor axon outgrowth were also found in the zebrafish, when morpholino antisense oligonucleotides were used to knock-down spastin in the developing embryo (Wood *et al.* 2006). Our result differs from that obtained in rat hippocampal neurons by Yu *et al.*, who detected in spastin-silenced neurons a slight delayed but otherwise normal development of the neurons, associated with a reduction of axonal branches (Yu *et al.* 2008). This discrepancy may

be due to the use of rat versus mouse neurons, to different levels of spastin downregulation, or the siRNAs employed.

Sensitivity of neurons to spastin dosage is also strongly suggested by overexpression experiments. While expression of spastin at high levels provoked a time-dependent neurite shortening in both immortalized and primary neurons, limited increase of spastin levels, by using an endogenous promoter to drive expression, led to the formation of a higher number of long and complex neurites with increased branching. Cells overexpressing spastin, either at high or low levels, always show a dramatic decrease of the staining for acetylated tubulin, a sign of loss of MT stability, probably dependent on the MT-severing activity of the protein. We interpret these results by hypothesizing that excessive MT disruption does not support neurite growth and stability while a limited increase in MT severing might be beneficial by providing the neurites with shorter and motile MTs. Other molecules involved in MT dynamics share similar properties. For instance, both silencing and overexpression of the neuronal specific stathmin family member SCG10 suppresses neurite elongation, while a limited increase in SCG10 levels stimulates neurite growth (Morii *et al.* 2006). A role of spastin in neurite branching and outgrowth is also supported by previous overexpression experiments in rat hippocampal neurons (Yu *et al.* 2008). Furthermore, in *Drosophila* the transcription factor Knot mediates control of the MT-based dendritic arbor outgrowth in class IV neurons by inducing spastin expression (Jinushi-Nakao *et al.* 2007).

A prominent feature of NSC34 cells overexpressing spastin under the endogenous promoter was the extension of lateral protrusions from the cell body and the neurites. Intriguingly, suppression of MT dynamic instability was previously shown to inhibit insertion of vesicles into the plasma membrane of the growth cone, while local disassembly of MTs resulted in addition of new membrane, suggesting that membrane delivery to growing axons is strictly coupled to microtubule dynamics (Zakharenko & Popov 1998). Recent evidence supports a model in which spastin couples microtubule severing to membrane trafficking in completion of cytokinesis by interacting with CHMP1B (Connell *et al.* 2008, Yang *et al.* 2008). It is an intriguing speculation that spastin may link MT dynamics and membrane trafficking in neurite elongation. Future experiments will be required to identify the molecular mechanisms involved.

What is the relevance of our observations for the pathogenesis and treatment of HSP? The large number of mutations identified in the *SPG4* gene clearly shows that loss-of-function alleles are implicated in the vast majority of cases. However, it is possible that truncated polypeptides may be produced by certain alleles, acting in a dominant fashion, as suggested in a recent study (Solowska *et al.* 2008). We found no evidence for the presence of truncated spastin isoforms in patients carrying splice-site or nonsense mutations in *SPG4*, strongly supporting the current view that haploinsufficiency lies at the basis of the disease, at least in the majority of cases. Therapeutic strategies in patients should therefore aim at recovering normal levels of spastin

in neurons. However, our data instruct caution towards simple overexpression strategies and stress the relevance of studying in detail mechanisms of regulation of spastin activity *in vivo*.

### **Acknowledgments**

We authors wish to thank N. Galjart, B.L. Sabatini, and R. Iggo for the generous gift of constructs, and Drs. M. Mancuso, P. Drigo and A. Martinuzzi, for clinical information.

This work was supported by grants from the Italian Telethon Foundation (GGP05057) and the Fondazione Mariani to E.I.R., from the Italian Ministry of Health (RF2007-75) to M.T.B., and ex-art56/2005/1 (to F.T.).

## Figures

*Figure 1. Spastin RNA interference reduces MT dynamics in NSC34 cells*

(A) Still images extracted from time-lapse movies of EB3-GFP comets in neurites from NSC34 cells transfected with the control SCR11 or the spastin specific MSS11 siRNA. Arrowheads mark the initial position of the comets, arrows indicate the actual position of EB3-GFP comets. Scale bar: 10  $\mu$ m. (B) Quantification of the rate of EB3 motility in NSC34 cells transfected with MSS11 compared with control siRNA. This data compare 314 comets from 18 axons of MSS11-treated cells with 263 comets from 12 axons of SCR11 treated cells. Bars represent average values between individual axons  $\pm$  SEM. \*  $p < 0.0001$  with Student's t-test.

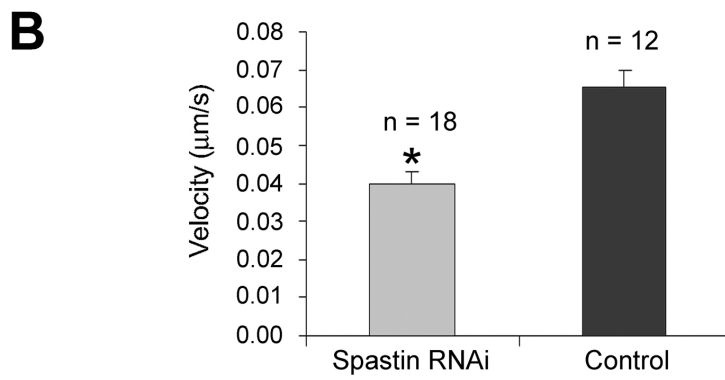
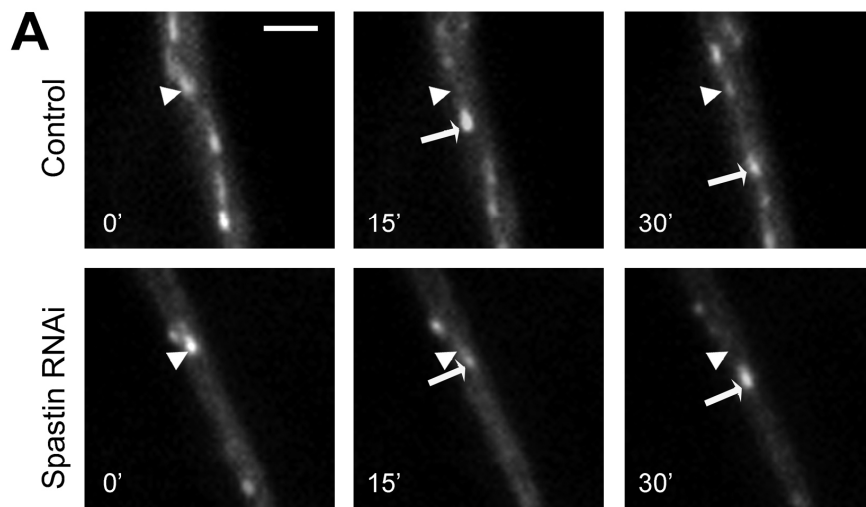




*Figure 2. Silencing of spastin in hippocampal primary neurons affects neurite outgrowth*

(A) Primary hippocampal neurons were electroporated at the time of plating with a vector expressing GFP and spastin-specific siRNAs or control siRNAs and visualized by GFP epifluorescence after 72 hours. Control neurons show the characteristic morphology of hippocampal neurons at stage 3-4 of in vitro development. Decreased levels of spastin alter the general morphology of neurons, affecting both short and long processes. Representative phenotypes are shown. No differences were observed using independent siRNAs. Scale bar: 50  $\mu\text{m}$ . (B) Distribution of neurons in different morphological categories after treatment with spastin specific siRNAs (MSS11 n=83; MSS12 n=33; MSS13 n=37) or control siRNAs (SCR11 n=108, C n=103). Neurons were classified as abnormal when the general morphology of the cell was altered. (C) Spastin RNAi causes a decrease of the length of the long processes. Bar graphs represent average values  $\pm$  SEM. The number of neurons counted in each condition is indicated on top of the bars. Data were collected from independent experiments. \*  $p < 0.00001$  in Student's t-test.

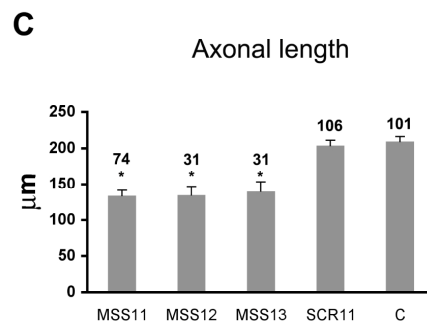
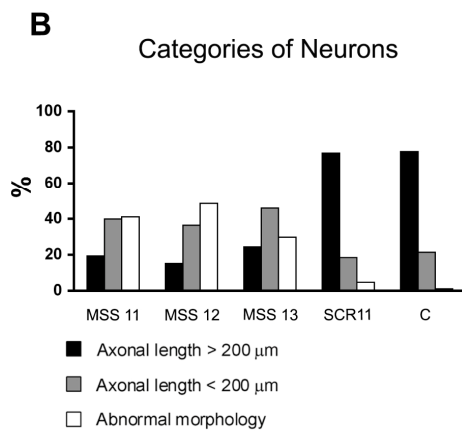
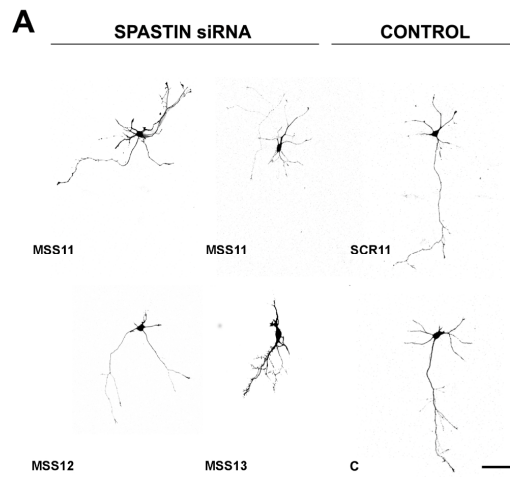


*Figure 3. Spastin overexpression in hippocampal neurons*

Neurons were transfected with lipofectamine after 1 week in culture with a CMV-spastin-GFP construct together with a cytosolic GFP vector (A-C) or with the empty GFP vector alone (D-F). We resorted to co-transfection with GFP to fill the cytoplasm of the neurons and allow easy recognition of their morphology. Neurons were analyzed 24 hours after transfection by double immunofluorescence with anti-GFP and anti-acetylated tubulin antibodies. Spastin overexpressing neurons were recognized because they lose staining for acetylated tubulin (B). Note the dramatic shortening of all their processes. Scale bar is the same in all images and corresponds to 50  $\mu\text{m}$ .

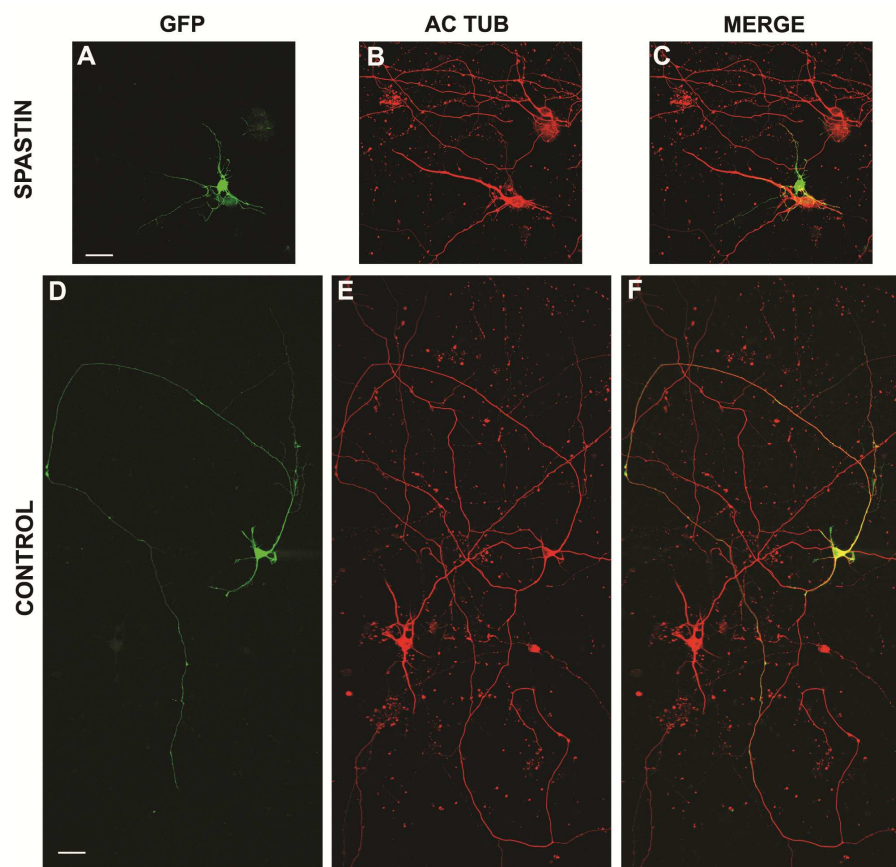


*Figure 4. Spastin overexpression in NSC34 immortalized neurons leads to defects in neurite elongation and maintenance*

NSC34 cells were transiently transfected with empty GFP, Spastin-GFP, and Spastin<sup>K388R</sup>-GFP vectors and the number of cells with neurites longer than 30  $\mu\text{m}$  was scored after 24 (A) or 48 hours (B). At 48 hours a strong reduction in the percentage of spastin-expressing cells with neurites longer than 30  $\mu\text{m}$  was found. Bar graphs represent means of at least 3 independent experiments  $\pm$  SEM. At least 150 transfected cells per experiment per condition were scored (\* $p < 0.01$ ; \*\*  $p < 0.001$  by Student's t-test). (C-H) Immunofluorescence analysis of a representative experiment at 48 hours. The transfected plasmids were revealed by GFP epifluorescence (green), while MTs were stained with anti tyrosinated tubulin antibodies (red). Merged images are also shown. Note that spastin overexpressing cells do not elongate neurites. Scale bar: 50  $\mu\text{m}$ .

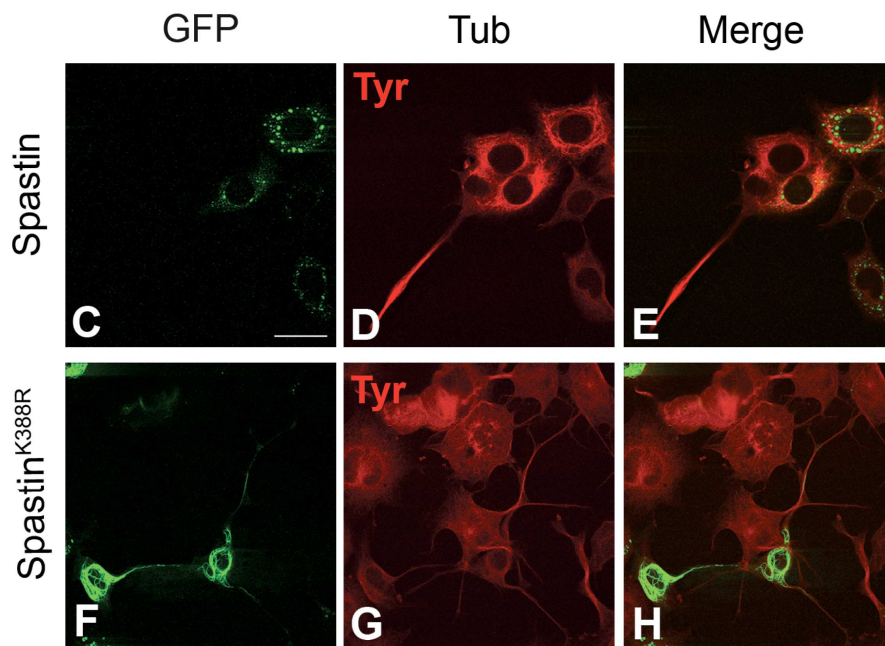
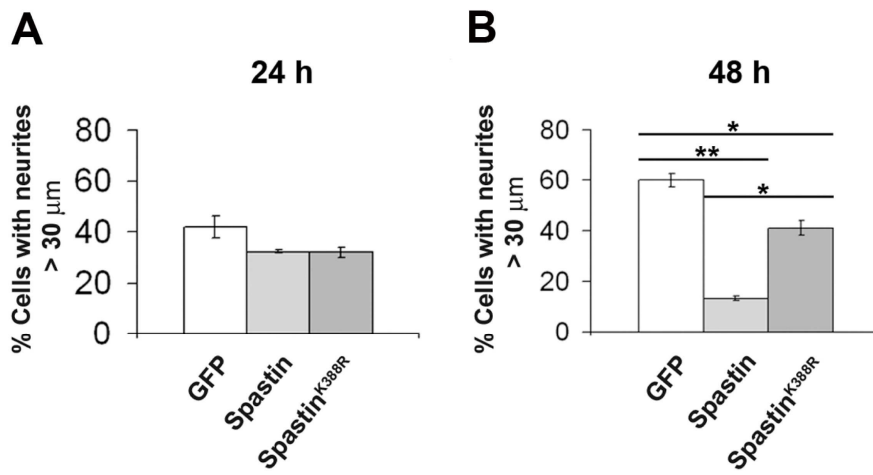


*Figure 5. Spastin upregulation at low levels in NSC34 cells leads to cell protrusions, neurite elongation and branching*

(A) Schematic representation of the dual promoter CMV-EGFP-STOP-5'UTR-spastin. NSC34 cells were transfected with an empty GFP vector (B-D, H) or with the dual promoter construct (E-G, I, J). Cells transfected with CMV-EGFP-STOP-5'UTR-spastin clearly show a modified morphology with the extension of protrusions from the cell body and the neurites. Neurites appeared tortuous and highly branched or showed swellings, often in correspondence to spastin signal (see arrows in E-G). Scale bar: 50  $\mu$ m. (K) An increased number of NSC34 cells extended neurites when spastin is expressed (60 %  $\pm$  9.2 versus 20.2 %  $\pm$  4.8). Bar graphs represent means of 3 independent experiments  $\pm$  SEM. More than 200 transfected cells per condition were scored (\*p < 0.05 by Student's t-test). (L) Quantification of the number of cells with abnormal morphology. Bar graphs represent means of 3 independent experiments  $\pm$  SEM. More than 200 transfected cells per condition were scored (\*p < 0.001 by Student's t-test).

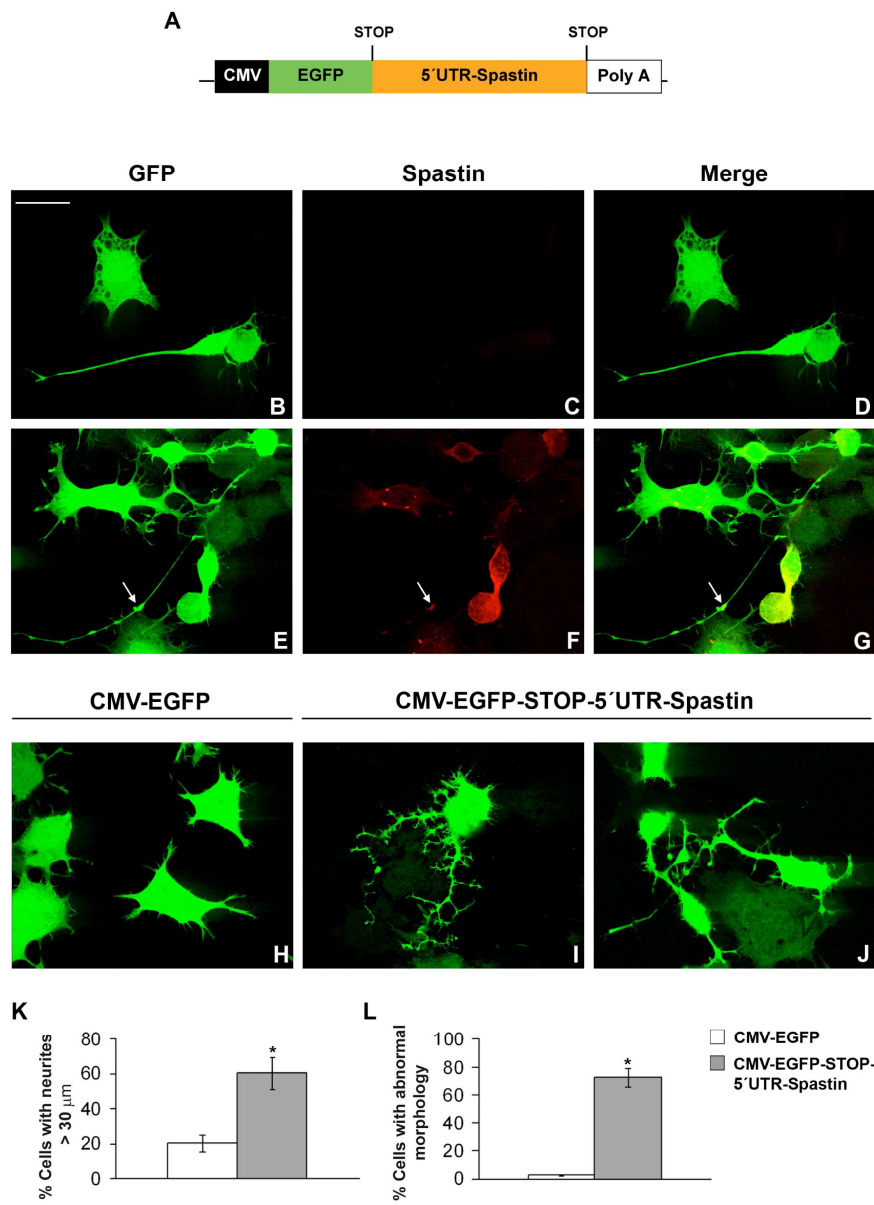
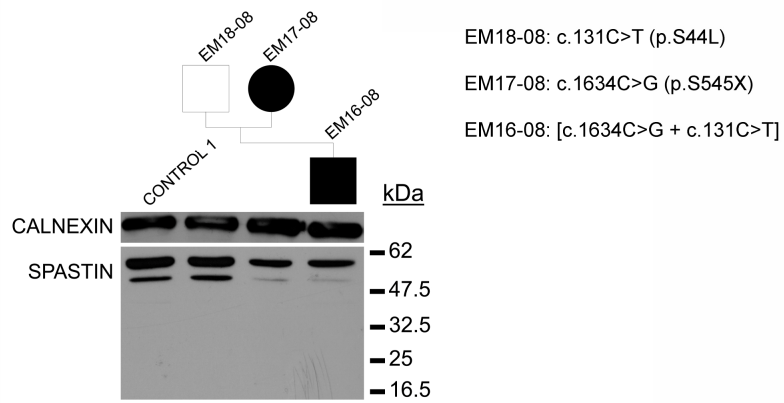




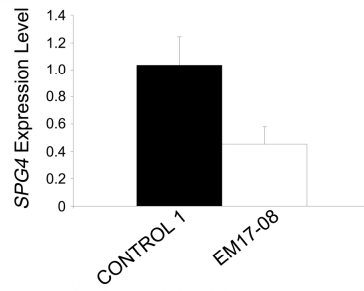
*Figure 6. Lack of truncated abnormal spastin isoform in SPG4 patients*

(A) Western blot analysis of spastin in cell lysates obtained from lymphoblastoid cell lines of individuals from a single family in which both a c.1634C>G (p.S545X) mutation and the disease modifier polymorphism c.131C>T (S44L) segregate. Both patients show reduced levels of spastin compared to the normal control and the individual carrying only the polymorphism. We used an antibody that recognizes amino acids 87 to 354 of spastin (Errico *et al.* 2004). (B) Real-time RT-PCR reveals that the mutation leads to reduction of *SPG4* mRNA levels through nonsense-mediated decay. (C) Western blot analysis of spastin in cell lysates obtained from additional patients carrying *SPG4* mutations. Note that patient EM500-07 bears a c.870 +3 A>G substitution in homozygosity. RT-PCR analysis showed that the mutation is leaky and that approximately 50% of a normal *SPG4* transcript is still present, explaining the apparent sporadic occurrence of the phenotype (not shown). Reduced levels of spastin are seen in all cases compared to the control (note the evident decrement of the smaller spastin isoform deleted of exon 4). No truncated spastin isoforms were detected.

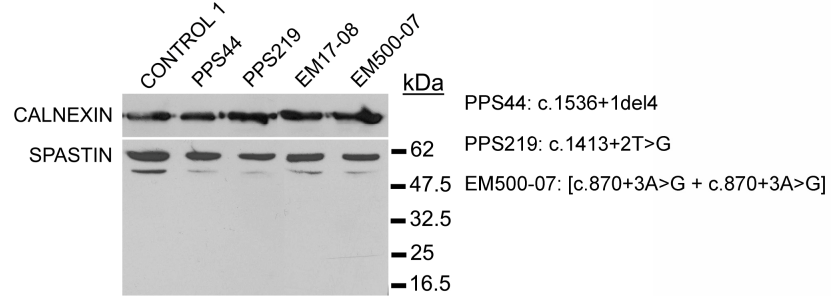
A



B



C



## **Supplementary materials and methods**

### *HSP patients*

All the patients were affected by a pure form of HSP. Disease onset in patient EM16-08 was in the first year of life with difficulties in maintaining upright stance and unsteady gait manifesting one year later. The disease was rapidly progressing and the patient is now wheelchair bound (age 11 years). The mother EM17-08 (41 years old) started showing only mild signs of the disease at the age of 39 years with fatigue during even short walks and sphincter problems which got worse in the last year. She is able to walk without support. Disease onset in patient EM500-07 was in early childhood with bilateral clonus at lower limbs. Disease progression was very slow with walking difficulties appearing only at the age of 39 years. The patient is now 49 years old and is able to walk with aid only. Patient PPS44 belongs to a relatively large family with six members affected in two generations. Disease onset was at the age of 35 years with walking disturbances. She is now 50 years old and still able to walk without support. However, a marked variability in disease onset and progression was observed among the family members carrying the mutation, with some patients manifesting the first symptoms within the first decade and others still asymptomatic at the age of 40. Cognitive impairment was present in one case with onset at 4 years of age. Patient PPS219 had also a positive family history. He presented at the age of 33 years with unbalance and walking difficulties. He is now 61 years old and is able to walk with support

only. There is no cognitive impairment. Disease onset and progression was relatively homogeneous in the family.

### *Constructs*

pMT21-spastin-myc was previously described (Errico *et al.* 2002). The construct spastin (1-225) was obtained by digestion of pMT21-spastin-myc with *XcmI-SalI*, followed by treatment with Klenow, and self-ligation. shMORA and shMORB were kindly provided by R. Iggo and B.L. Sabatini.

### *Real-time PCR*

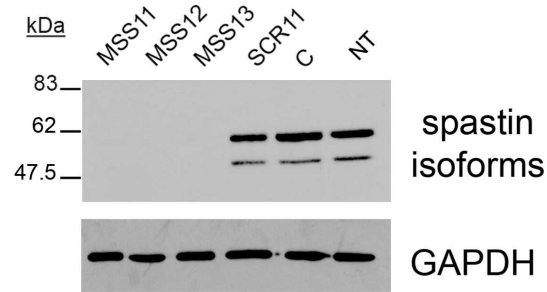
RNA extraction was performed using TRIzol® (Invitrogen), following the manufacturer specifications. cDNA was synthesized using SuperScript™ First-Strand Synthesis System (Invitrogen). Real-time amplification was performed using SYBR® Green PCR Master Mix (Applied Biosystem, Foster City, CA) in an ABI PRISM 7000 Sequence Detection System. cDNA synthesized from 45 ng of RNA was used in each reaction. Primers for  $\alpha$ -actin were used as gene standard reference. Primer sequences for *Spg4* and *Ifit1* are available upon request. Each PCR reaction was performed in triplicate with the following profile: one cycle at 50 °C for 2 min, one cycle at 95 °C for 10 min and then 40 cycles at 95 °C for 15 s and 60 °C for 1 min (two-step protocol).

## Supplementary figures

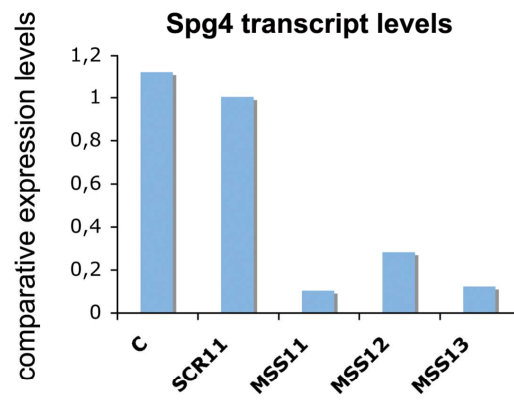
### *S1. Validation of Spg4 gene silencing*

(A) Western blot shows that transfection of three siRNAs specific for spastin (MSS11, MSS12, MSS13) reduces spastin levels compared to untreated control cells (NT), to cells transfected with a generic siRNA control (C) or with a scrambled sequence of MSS11 (SCR11). GAPDH was used as loading control. (B) Real-time RT-PCR shows that *Spg4* transcript is drastically reduced in cells transfected with MSS11, MSS12, MSS13 compared to cells transfected with the control siRNA and a scrambled sequence SCR11. The result of a representative experiments out of five is shown. (C) Expression levels of IFIT1 in NSC34 cells transfected with all the siRNAs used in this study. IFIT1 is a sensitive marker for interferon-stimulated gene activation (Bridge *et al.* 2003). shMORA and shMORB have previously been shown to differentially induce an interferon-responsive gene activation (Bridge *et al.* 2003). shMORA activates the interferon-like response and induced a reduced dendritic complexity when expressed in neurons (Alvarez *et al.* 2006). These constructs were used as positive and negative controls, respectively.

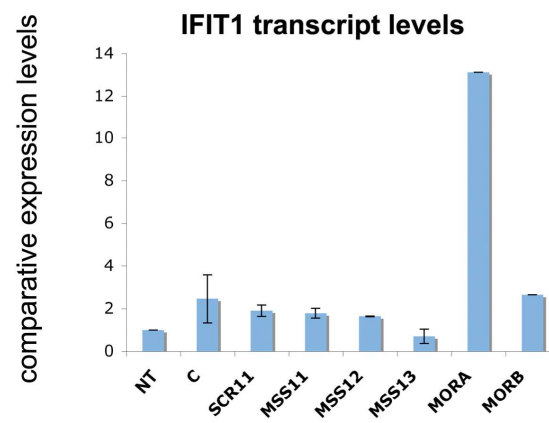
**A**



**B**

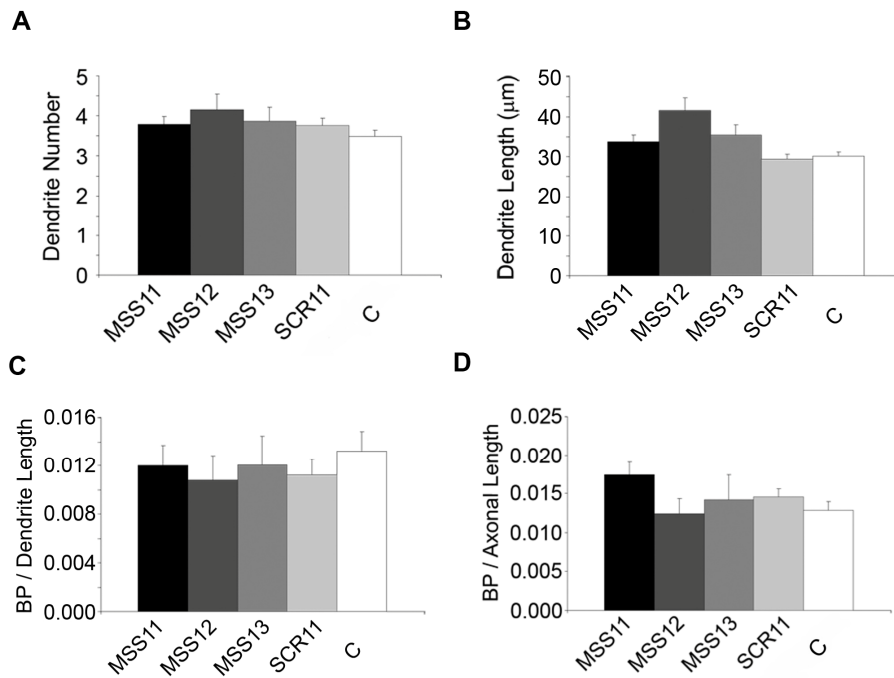


**C**



## S2. Morphometric analyses in spastin-silenced neurons

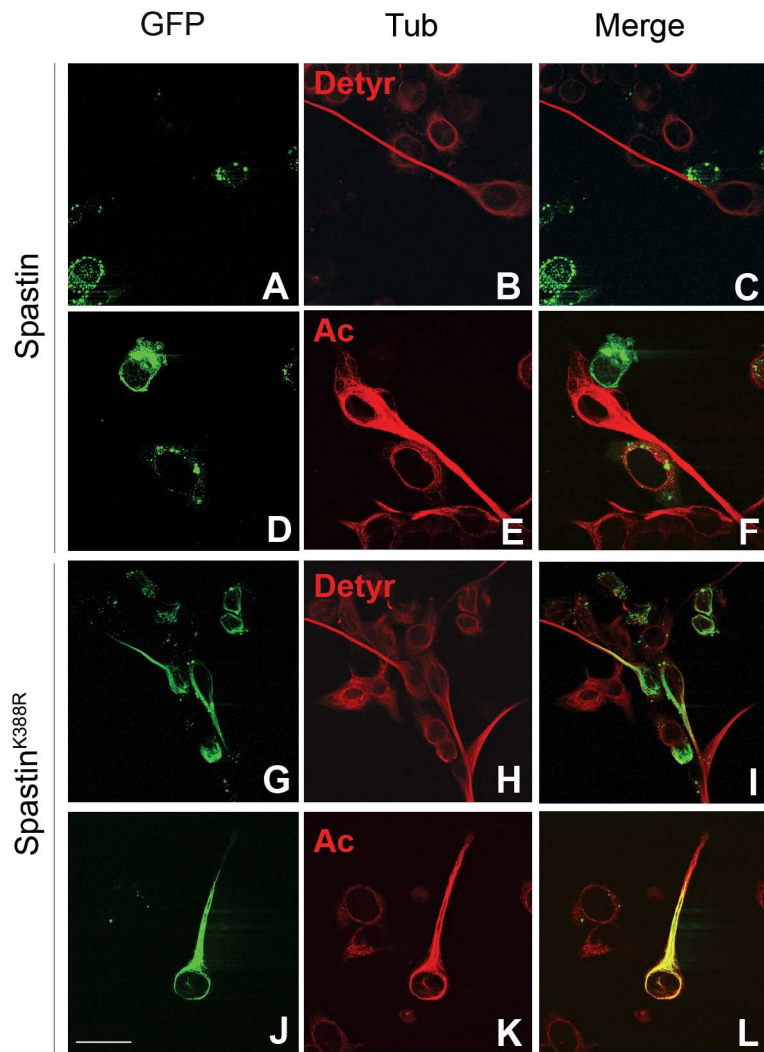
Spastin RNAi does not influence dendrite number (A), dendrite length (B), the number of branching points (BP) per dendrite (C) or per axon (D). Bar graphs represent average values  $\pm$  SEM. The number of neurons counted in each condition is the same as in Figure 2.



### *S3. Spastin overexpression affects acetylated and detyrosinated MTs*

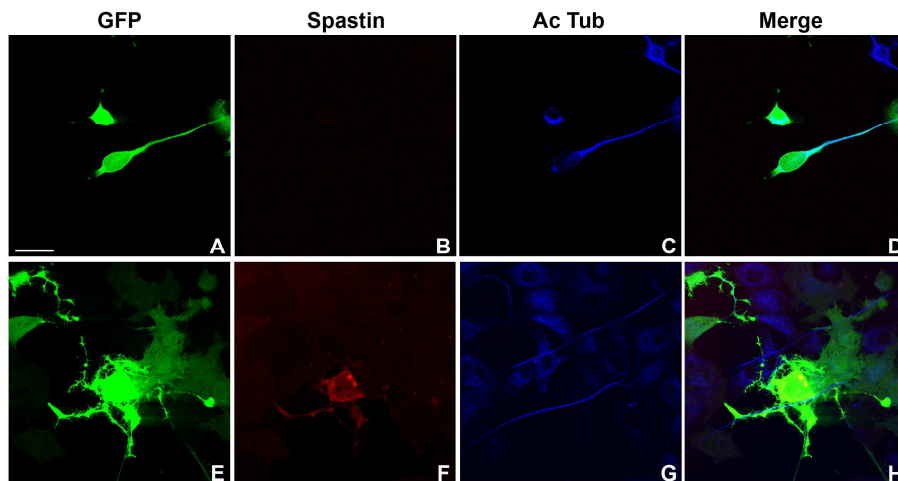
Immunofluorescence analysis after 48 hours of transfection. The transfected plasmids were revealed by GFP epifluorescence (green), while MTs were stained with anti detyrosinated or acetylated tubulin antibodies (red). Merged images are also shown. Overexpression of wild-type spastin causes a drastic reduction in the content of stable MTs stained by detyrosinated and acetylated tubulin antibodies (A-F). Spastin<sup>K388R</sup> decorates bundles of MTs enriched in acetylated tubulin (J-L). Scale bar: 50  $\mu$ m.





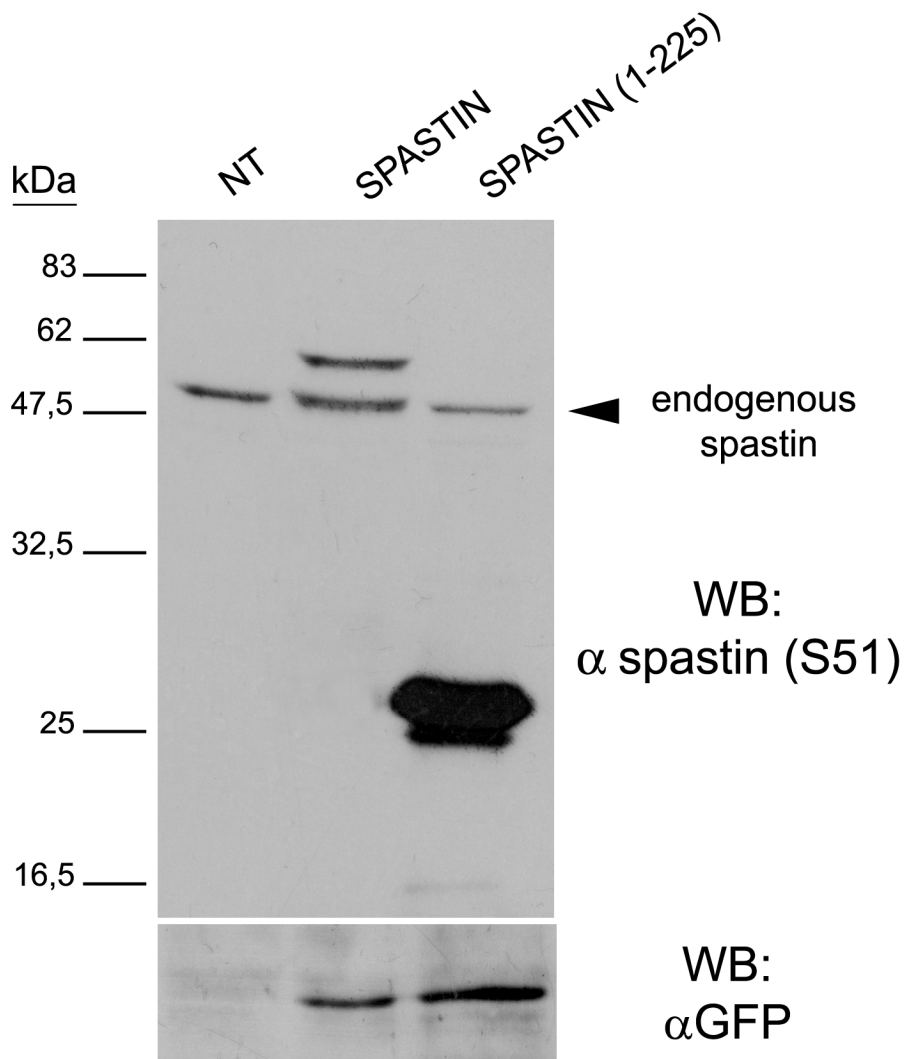
*S4. Expression of spastin under the endogenous promoter leads to decreased levels of acetylated tubulin*

NSC34 cells were transfected with an empty GFP vector (A-D) or with the dual promoter construct (E-H). Cells transfected with CMV-EGFP-STOP-5'UTR-spastin clearly show a modified morphology. These cells express low levels of spastin and show the disappearance of the staining for acetylated tubulin. Scale bar: 50  $\mu$ m.



*S5. Validation of the ability of the spastin antibody to detect truncated spastin isoforms*

Constructs expressing full-length spastin or the truncated version spastin (amino acids 1-225) were transfected in HeLa cells together with an empty GFP vector as transfection control. Spastin (1-225) recapitulates the size of the shorter possible truncated version of spastin in our selection of HSP patients. The antibody S51 recognizes both full-length spastin and the truncated protein in western blot analysis. NT are untransfected cells.



## Video description

### Video 1.

Time-lapse microscopy of a NSC34 cell expressing EB3-GFP. Cells were doubly transfected with EB3-GFP and with the control siRNA SCR11, as described in Materials and methods. The video shows several growing ends of MTs. Images were acquired at 5 s intervals, and the frame display rate is 15 frames/s.

### Video 2.

Time-lapse microscopy of NSC34 cell expressing EB3-GFP. Cells were doubly transfected with EB3-GFP and with the spastin specific siRNA MSS11, as described in Materials and methods. The video shows several growing ends of MTs. Images were acquired at 5 s intervals, and the frame display rate is 15 frames/s.

## Supplementary Table.

### *SPG4 mutations analyzed in this study*

<i>Patient ID</i>	<i>Location</i>	<i>Nucleotide change</i>	<i>Predicted effect on protein</i>	<i>Predicted MW (M1/M87)</i>
EM16-08	Exon 14 / Exon 1*	c.1634C>G/ c.131C>T*	p.S545X/p.S44L*	58/50 kDa
EM17-08	Exon 14	c.1634C>G	p.S545X	
EM500-07	Intron 5	c.870+3A>G (homozygous)	p.E228fsX6	25/15 kDa
PPS219	Intron 11	c.1413 +2 T>G	p.D441fsX6	47.3/38.1 kDa
PPS44	Intron 13	c.1536 +1 del4	p.R498fsX17	53.7/44.5 kDa

\* previously reported polymorphism

## References

- Abal, M., Piel, M., Bouckson-Castaing, V., Mogensen, M., Sibarita, J. B. and Bornens, M. (2002) Microtubule release from the centrosome in migrating cells. *The Journal of cell biology*, **159**, 731-737.
- Ahmad, F. J., He, Y., Myers, K. A., Hasaka, T. P., Francis, F., Black, M. M. and Baas, P. W. (2006) Effects of dynactin disruption and dynein depletion on axonal microtubules. *Traffic (Copenhagen, Denmark)*, **7**, 524-537.
- Alvarez, V. A., Ridenour, D. A. and Sabatini, B. L. (2006) Retraction of synapses and dendritic spines induced by off-target effects of RNA interference. *J Neurosci*, **26**, 7820-7825.
- Baas, P. W., Karabay, A. and Qiang, L. (2005) Microtubules cut and run. *Trends in cell biology*, **15**, 518-524.
- Baas, P. W., Vidya Nadar, C. and Myers, K. A. (2006) Axonal transport of microtubules: the long and short of it. *Traffic (Copenhagen, Denmark)*, **7**, 490-498.
- Cashman, N. R., Durham, H. D., Blusztajn, J. K., Oda, K., Tabira, T., Shaw, I. T., Dahrouge, S. and Antel, J. P. (1992) Neuroblastoma x spinal cord (NSC) hybrid cell lines resemble developing motor neurons. *Dev Dyn*, **194**, 209-221.
- Chinnery, P. F., Keers, S. M., Holden, M. J., Ramesh, V. and Dalton, A. (2004) Infantile hereditary spastic paraparesis due to codominant mutations in the spastin gene. *Neurology*, **63**, 710-712.

- Claudiani, P., Riano, E., Errico, A., Andolfi, G. and Rugarli, E. I. (2005) Spastin subcellular localization is regulated through usage of different translation start sites and active export from the nucleus. *Experimental cell research*, **309**, 358-369.
- Connell, J. W., Lindon, C., Luzio, J. P. and Reid, E. (2008) Spastin couples microtubule severing to membrane traffic in completion of cytokinesis and secretion. *Traffic (Copenhagen, Denmark)*.
- Dent, E. W. and Gertler, F. B. (2003) Cytoskeletal dynamics and transport in growth cone motility and axon guidance. *Neuron*, **40**, 209-227.
- Depienne, C., Stevanin, G., Brice, A. and Durr, A. (2007) Hereditary spastic paraplegias: an update. *Current opinion in neurology*, **20**, 674-680.
- Dotti, C. G., Sullivan, C. A. and Banker, G. A. (1988) The establishment of polarity by hippocampal neurons in culture. *J Neurosci*, **8**, 1454-1468.
- Errico, A., Ballabio, A. and Rugarli, E. I. (2002) Spastin, the protein mutated in autosomal dominant hereditary spastic paraplegia, is involved in microtubule dynamics. *Human molecular genetics*, **11**, 153-163.
- Errico, A., Claudiani, P., D'Addio, M. and Rugarli, E. I. (2004) Spastin interacts with the centrosomal protein NA14, and is enriched in the spindle pole, the midbody and the distal axon. *Human molecular genetics*, **13**, 2121-2132.

- Evans, K. J., Gomes, E. R., Reisenweber, S. M., Gundersen, G. G. and Luring, B. P. (2005) Linking axonal degeneration to microtubule remodeling by Spastin-mediated microtubule severing. *The Journal of cell biology*, **168**, 599-606.
- Fink, J. K. (2006) Hereditary spastic paraplegia. *Curr Neurol Neurosci Rep*, **6**, 65-76.
- Fonknechten, N., Mavel, D., Byrne, P. et al. (2000) Spectrum of SPG4 mutations in autosomal dominant spastic paraplegia. *Hum. Mol. Genet.*, **9**, 637-644.
- Goslin, K. and Banker, G. (1990) Rapid changes in the distribution of GAP-43 correlate with the expression of neuronal polarity during normal development and under experimental conditions. *The Journal of cell biology*, **110**, 1319-1331.
- Hammond, J. W., Cai, D. and Verhey, K. J. (2008) Tubulin modifications and their cellular functions. *Current opinion in cell biology*, **20**, 71-76.
- Hazan, J., Fonknechten, N., Mavel, D. et al. (1999) Spastin, a new AAA protein, is altered in the most frequent form of autosomal dominant spastic paraplegia. *Nature Genet.*, **23**, 296-303.
- Jinushi-Nakao, S., Arvind, R., Amikura, R., Kinameri, E., Liu, A. W. and Moore, A. W. (2007) Knot/Collier and cut control different aspects of dendrite cytoskeleton and synergize to define final arbor shape. *Neuron*, **56**, 963-978.
- Mancuso, G. and Rugarli, E. I. (2008) A cryptic promoter in the first exon of the SPG4 gene directs the synthesis of the 60-kDa spastin isoform. *BMC biology*, **6**, 31.



- McDermott, C. J., Burness, C. E., Kirby, J. et al. (2006) Clinical features of hereditary spastic paraplegia due to spastin mutation. *Neurology*, **67**, 45-51.
- Morii, H., Shiraishi-Yamaguchi, Y. and Mori, N. (2006) SCG10, a microtubule destabilizing factor, stimulates the neurite outgrowth by modulating microtubule dynamics in rat hippocampal primary cultured neurons. *Journal of neurobiology*, **66**, 1101-1114.
- Orso, G., Martinuzzi, A., Rossetto, M. G., Sartori, E., Feany, M. and Daga, A. (2005) Disease-related phenotypes in a Drosophila model of hereditary spastic paraplegia are ameliorated by treatment with vinblastine. *The Journal of clinical investigation*, **115**, 3026-3034.
- Peris, L., They, M., Faure, J. et al. (2006) Tubulin tyrosination is a major factor affecting the recruitment of CAP-Gly proteins at microtubule plus ends. *The Journal of cell biology*, **174**, 839-849.
- Roll-Mecak, A. and Vale, R. D. (2005) The Drosophila homologue of the hereditary spastic paraplegia protein, spastin, severs and disassembles microtubules. *Curr Biol*, **15**, 650-655.
- Roll-Mecak, A. and Vale, R. D. (2008) Structural basis of microtubule severing by the hereditary spastic paraplegia protein spastin. *Nature*, **451**, 363-367.
- Salinas, S., Carazo-Salas, R. E., Proukakis, C., Cooper, J. M., Weston, A. E., Schiavo, G. and Warner, T. T. (2005) Human spastin has

multiple microtubule-related functions. *Journal of neurochemistry*, **95**, 1411-1420.

Solowska, J. M., Morfini, G., Falnikar, A., Himes, B. T., Brady, S. T., Huang, D. and Baas, P. W. (2008) Quantitative and functional analyses of spastin in the nervous system: implications for hereditary spastic paraplegia. *J Neurosci*, **28**, 2147-2157.

Stepanova, T., Slemmer, J., Hoogenraad, C. C. et al. (2003) Visualization of microtubule growth in cultured neurons via the use of EB3-GFP (end-binding protein 3-green fluorescent protein). *J Neurosci*, **23**, 2655-2664.

Svenson, I. K., Kloos, M. T., Gaskell, P. C., Nance, M. A., Garbern, J. Y., Hisanaga, S., Pericak-Vance, M. A., Ashley-Koch, A. E. and Marchuk, D. A. (2004) Intragenic modifiers of hereditary spastic paraplegia due to spastin gene mutations. *Neurogenetics*, **5**, 157-164.

Svoboda, P. (2007) Off-targeting and other non-specific effects of RNAi experiments in mammalian cells. *Current opinion in molecular therapeutics*, **9**, 248-257.

Tarrade, A., Fassier, C., Courageot, S. et al. (2006) A mutation of spastin is responsible for swellings and impairment of transport in a region of axon characterized by changes in microtubule composition. *Human molecular genetics*, **15**, 3544-3558.

Trotta, N., Orso, G., Rossetto, M. G., Daga, A. and Broadie, K. (2004) The hereditary spastic paraplegia gene, spastin, regulates

- microtubule stability to modulate synaptic structure and function. *Curr Biol*, **14**, 1135-1147.
- Verhey, K. J. and Gaertig, J. (2007) The tubulin code. *Cell cycle (Georgetown, Tex)*, **6**, 2152-2160.
- White, S. R., Evans, K. J., Lary, J., Cole, J. L. and Lauring, B. (2007) Recognition of C-terminal amino acids in tubulin by pore loops in Spastin is important for microtubule severing. *The Journal of cell biology*, **176**, 995-1005.
- Wood, J. D., Landers, J. A., Bingley, M., McDermott, C. J., Thomas-McArthur, V., Gleadall, L. J., Shaw, P. J. and Cunliffe, V. T. (2006) The microtubule-severing protein Spastin is essential for axon outgrowth in the zebrafish embryo. *Human molecular genetics*, **15**, 2763-2771.
- Yang, D., Rismanchi, N., Renvoise, B., Lippincott-Schwartz, J., Blackstone, C. and Hurley, J. H. (2008) Structural basis for midbody targeting of spastin by the ESCRT-III protein CHMP1B. *Nature structural & molecular biology*, **15**, 1278-1286.
- Yu, W., Qiang, L., Solowska, J. M., Karabay, A., Korulu, S. and Baas, P. W. (2008) The Microtubule-severing Proteins Spastin and Katanin Participate Differently in the Formation of Axonal Branches. *Molecular biology of the cell*, **19**, 1485-1498.
- Zakharenko, S. and Popov, S. (1998) Dynamics of axonal microtubules regulate the topology of new membrane insertion into the growing neurites. *The Journal of cell biology*, **143**, 1077-1086.

Zhang, D., Rogers, G. C., Buster, D. W. and Sharp, D. J. (2007) Three microtubule severing enzymes contribute to the "Pacman-flux" machinery that moves chromosomes. *The Journal of cell biology*, **177**, 231-242.

### **Supplementary references**

Alvarez, V. A., Ridenour, D. A. and Sabatini, B. L. (2006) Retraction of synapses and dendritic spines induced by off-target effects of RNA interference. *J Neurosci*, **26**, 7820-7825.

Bridge, A. J., Pebernard, S., Ducraux, A., Nicoulaz, A. L. and Iggo, R. (2003) Induction of an interferon response by RNAi vectors in mammalian cells. *Nature genetics*, **34**, 263-264.

Errico, A., Ballabio, A. and Rugarli, E. I. (2002) Spastin, the protein mutated in autosomal dominant hereditary spastic paraplegia, is involved in microtubule dynamics. *Human molecular genetics*, **11**, 153-163.

# Regulation of OPA1 processing and mitochondrial fusion by *m*-AAA protease isoenzymes and OMA1

Sarah Ehses<sup>1</sup>, Ines Raschke<sup>1</sup>, Giuseppe Mancuso<sup>3</sup>, Andrea Bernacchia<sup>3</sup>, Stefan Geimer<sup>5</sup>, Daniel Tondera<sup>6</sup>, Jean-Claude Martinou<sup>6</sup>, Benedikt Westermann<sup>5</sup>, Elena I. Rugarli<sup>3,4</sup> and Thomas Langer<sup>1,2</sup>

<sup>1</sup> Institute for Genetics, Centre for Molecular Medicine (CMMC), Cologne Excellence Cluster on Cellular Stress Responses in Aging-Associated Diseases (CECAD), University of Cologne, Cologne, Germany

<sup>2</sup> Max-Planck-Institute for Biology of Aging, Cologne, Germany

<sup>3</sup> Laboratory of Genetic and Molecular Pathology, Istituto Nazionale Neurologico „C.Besta”, Milano, Italy;

<sup>4</sup> Department of Neuroscience and Medical Biotechnologies, University of Milano-Bicocca, Milan, Italy;

<sup>5</sup> Institute for Cell Biology and Electron Microscopy Laboratory, University of Bayreuth, Bayreuth, Germany; <sup>6</sup> Department of Cell Biology, University of Geneva, Switzerland.

*Published: 2010*

*Journal of Cell Biology Vol. 187 No. 7 1023–1036*

## **Abstract**

Mitochondrial fusion depends on the dynamin-like GTPase OPA1, whose activity is controlled by proteolytic cleavage. Dysfunction of mitochondria induces OPA1 processing and results in mitochondrial fragmentation allowing the selective removal of damaged mitochondria. Here, we demonstrate that two classes of metallopeptidases regulate OPA1 cleavage in the mitochondrial inner membrane: isoenzymes of the ATP-dependent *m*-AAA protease, variable assemblies of the conserved subunits paraplegin, AFG3L1 and AFG3L2, and the ATP-independent peptidase OMA1. Functionally redundant isoenzymes of the *m*-AAA protease ensure the balanced accumulation of long and short isoforms of OPA1 required for mitochondrial fusion. The loss of AFG3L2 in mouse tissues, downregulation of AFG3L1 and AFG3L2 in MEFs, or the expression of a dominant negative AFG3L2 variant in human cells decreases the stability of long OPA1 isoforms and induces OPA1 processing by OMA1. Moreover, cleavage by OMA1 causes the accumulation of short OPA1 variants, if mtDNA is depleted or mitochondrial activities are impaired. Our findings link distinct peptidases to constitutive and induced OPA1 processing and shed new light on the pathogenesis of neurodegenerative disorders associated with mutations in *m*-AAA protease subunits.

## Introduction

Mitochondria are dynamic organelles that undergo continuous remodeling through fusion and fission events. Conserved protein machineries mediate fusion and fission of mitochondrial membranes (Cervený et al., 2007; Hoppins et al., 2007; Westermann, 2008). The dynamin-related GTPase OPA1, which resides in the mitochondrial intermembrane space, is involved in inner membrane fusion, in the regulation of mitochondrial cristae morphology, and in protecting cells from apoptosis (Frezza et al., 2006; Griparic et al., 2004; Lenaers et al., 2009; Meeusen et al., 2006; Olichon et al., 2003). Mutations in OPA1 cause dominant optic atrophy, a progressive neurological disease characterized by degeneration of the retinal ganglion cells and atrophy of the optic nerve (Amati-Bonneau et al., 2009). Mitochondria contain various OPA1 isoforms that arise from alternative splicing and proteolytic processing events at two sites, S1 and S2, generating shorter isoforms (Delettre et al., 2001; Ishihara et al., 2006).

A combination of long and short OPA1 isoforms is required for mitochondrial fusion (Song et al., 2007), pointing to a crucial regulatory role of OPA1 processing. Roughly equimolar concentrations of long and short isoforms of OPA1 are formed under normal conditions. However, low mitochondrial ATP levels, the dissipation of the membrane potential across the inner membrane ( $\Delta\Psi_m$ ), or apoptotic stimuli induce OPA1 cleavage resulting in the loss of long isoforms (Baricault et al., 2007; Duvezin-Caubet et al., 2006;

Ishihara et al., 2006). Various proteases in the inner membrane have been linked to the processing of OPA1. The *i*-AAA protease YME1L1 regulates OPA1 cleavage at S2, which is only present in a subset of OPA1 variants (Griparic et al., 2007; Song et al., 2007). Debate exists about the protease cleaving OPA1 at S1, as both the rhomboid protease PARL and the *m*-AAA protease, an oligomeric ATP-dependent metallopeptidase in the inner membrane, have been proposed to be involved in OPA1 processing (Cipolat et al., 2006; Ishihara et al., 2006). However, normal OPA1 processing in murine embryonic fibroblasts (MEFs) lacking PARL or the *m*-AAA protease subunit paraplegin raised doubts about the role of either protease for OPA1 processing *in vivo* (Duvezin-Caubet et al., 2007).

Notably, human and murine mitochondria possess different *m*-AAA protease isoenzymes, which differ in their subunit composition but exert at least partially redundant activities (Koppen et al., 2007). Three homologous subunits are expressed in the mouse, AFG3L1, AFG3L2, and paraplegin. While paraplegin was exclusively detected in heterooligomeric complexes with AFG3L1 and AFG3L2, homooligomeric complexes composed of AFG3L1 or AFG3L2 do exist. Functionally redundant isoenzymes might therefore substitute for the loss of paraplegin and maintain OPA1 processing in the absence of paraplegin. Complementation studies in yeast indeed demonstrated functional conservation of different mammalian *m*-AAA protease isoenzymes and revealed their ability to cleave OPA1 expressed heterologously in yeast (Duvezin-Caubet et al., 2007). This notwithstanding they have been linked to different



neurodegenerative diseases in human: mutations in *Spg7* encoding paraplegin cause a recessive form of hereditary spastic paraplegia (HSP), while heterozygous mutations in *Afg3l2* are responsible for a dominant form of spinocerebellar ataxia, SCA28 (Cagnoli et al., 2008; DiBella et al., 2008). It is presently unclear whether this reflects functional differences of *m*-AAA isoenzymes or results from a tissue-specific expression of *m*-AAA protease subunits (Koppen et al., 2007). Here, we have assessed the function of different *m*-AAA isoenzymes *in vivo* using RNA interference and demonstrate that OPA1 processing and mitochondrial fusion depends on AFG3L1 and AFG3L2. Moreover, we identify a novel peptidase in the inner membrane, OMA1, which mediates OPA1 processing if *m*-AAA proteases are absent or mitochondrial activities are impaired.

## Results

### *AFG3L1 and AFG3L2 are required for mitochondrial fusion*

We used RNA interference in MEFs to downregulate *m*-AAA protease subunits individually or in combination. Immunoblotting revealed effective depletion of AFG3L1, AFG3L2, and paraplegin (Fig. 1A). Mitochondrial morphology was monitored by fluorescence microscopy in cells cotransfected with a mitochondrially targeted DsRed variant. Neither paraplegin-depleted mitochondria nor mitochondria from *Spg7*<sup>-/-</sup> MEFs showed morphological abnormalities (not shown and Suppl. Fig. S1). Similarly, mitochondria of cells transfected with either *Afg3l1* or *Afg3l2* specific siRNA appeared largely normal in morphology (Fig. 1B, C). However, concomitant downregulation of both subunits caused fragmentation of the mitochondrial network in ~80% of the cells (Fig. 1B, C). Examination of these cells by electron microscopy revealed a severe disturbance of the mitochondrial ultrastructure (Fig. 1D). Lamellar cristae were either completely absent or severely reduced in number in cells lacking AFG3L1 and AFG3L2, whereas the structure of cristae was not significantly affected upon downregulation of AFG3L1 or AFG3L2 (Fig. 1D). These findings reveal overlapping activities of AFG3L1 and AFG3L2 and demonstrate an essential role of the *m*-AAA protease for the ultrastructure of mitochondria.

An impaired fusion or increased fission may cause fragmentation of the mitochondrial network in the absence of AFG3L1 and AFG3L2. To distinguish between these possibilities, we transfected interfered

cells with a dominant-negative variant of the fission component DRP1, DRP1<sup>K38A</sup>. In agreement with previous observations (James et al., 2003; Smirnova et al., 1998), expression of DRP1<sup>K38A</sup> impaired fission and resulted in the elongation of mitochondrial tubules due to ongoing fusion (Fig. 2A, B). In contrast, cells lacking AFG3L1 and AFG3L2 maintained punctiform mitochondria upon expression of DRP1<sup>K38A</sup>, strongly suggesting that the organelles are unable to fuse. As independent evidence, we found that cells interfered for *Afg3l2* and *Afg3l1* did not form a highly interconnected network when exposed to low concentrations of cycloheximide (CHX) (Fig. 2C, D) indicating that they have lost the ability to undergo stress-induced mitochondrial hyperfusion (SIMH), an adaptive response against stress (Tondera et al., 2009). We therefore conclude that the fusion of mitochondrial membranes depends on AFG3L1 and AFG3L2.

#### *The m-AAA protease controls the stability of L-OPA1*

OPA1 regulates both mitochondrial fusion and cristae morphogenesis (Lenaers et al., 2009). MEFs express mainly two alternative transcripts of OPA1, variants 1 and 7, which are cleaved resulting in the accumulation of five OPA1 forms: two long (a, b) and three short isoforms (c-e) (Duvezin-Caubet et al., 2007; Ishihara et al., 2006). Downregulation of individual subunits of the *m*-AAA protease isoenzymes did not reproducibly affect the processing of OPA1 (Fig. 3A). However, the concomitant loss of AFG3L1 and AFG3L2 affected significantly the accumulation of OPA1 variants (Fig. 3A): the long

OPA1 isoforms were no longer detected while short forms, mainly e, accumulated (Fig. 3A). This shift was not significantly enhanced in *Spg7<sup>-/-</sup>* cells (Fig. 3A). These results substantiate the overlapping activities of AFG3L1 and AFG3L2 and point to an impaired OPA1 processing in *m*-AAA protease-depleted MEFs.

Both long and short OPA1 isoforms are necessary to support mitochondrial fusion (Song et al., 2007). The loss of long OPA1 isoforms can therefore account for the fragmentation of the mitochondrial network upon depletion of AFG3L1 and AFG3L2. To test this hypothesis, we assessed mitochondrial morphology after coexpression of *Afg3l1* and *Afg3l2* siRNAs with a Flag-tagged version of OPA1 splicing variant 1 (v1), in which the amino acid residues flanking the processing site had been deleted (v1 $\Delta$ S1) (Ishihara et al., 2006). Mitochondrial morphology was also analyzed in AFG3L1- and AFG3L2-depleted MEFs expressing S-OPA1, a hybrid protein composed of a short form of OPA1 fused to the mitochondrial target sequence of AIF (Ishihara et al., 2006). We observed a partial but statistically significant restoration of a tubular network in *m*-AAA protease-deficient cells upon expression of v1 $\Delta$ S1 but not of S-OPA1 (Fig. 3B), suggesting that the *m*-AAA protease regulates mitochondrial fusion via OPA1.

These findings for the first time link the function of AFG3L1 and AFG3L2 to the biogenesis of OPA1. Surprisingly, depletion of AFG3L1 and AFG3L2 caused a loss rather than a stabilization of long OPA1 isoforms. We therefore monitored directly the efficiency of OPA1 processing in the absence of *m*-AAA protease subunits by expressing

Flag-tagged v1 or v1ΔS1 in MEFs (Ishihara et al., 2006). Downregulation of AFG3L1 and AFG3L2 promoted processing of v1 and led to the loss of long OPA1 forms (Fig. 3C). v1ΔS1 was present at severely decreased levels in cells lacking both *m*-AAA protease subunits suggesting degradation of the OPA1 variant (Fig. 3C). Indeed, if protein synthesis was inhibited by CHX, v1ΔS1 was stable upon further incubation of control cells (Fig. 3D). In contrast, v1ΔS1 level decreased in the absence of AFG3L1 and AFG3L2 (Fig. 3D), explaining the only partial restoration of the tubular mitochondrial network upon expression of this variant in AFG3L1/AFG3L2-depleted cells (Fig. 3B). We conclude from these experiments that turnover as well as cleavage of OPA1 at S1 is enhanced upon downregulation of *m*-AAA protease subunits.

#### *Respiratory activity of m-AAA protease deficient mitochondria*

Disruption of the mitochondrial membrane potential and decreased ATP levels within mitochondria have been shown to induce processing of OPA1 (Baricault et al., 2007; Duvezin-Caubet et al., 2006). Respiratory chain deficiencies have recently been reported in brain mitochondria of *Afg3l2*<sup>-/-</sup> mice (Maltecca et al., 2008). We therefore assessed the formation of the mitochondrial membrane potential in cells depleted of *m*-AAA protease subunits using the membrane-potential dependent fluorescent dye JC-1 (Fig. 3E). Whereas fluorescence dropped upon dissipation of the membrane potential by carbonyl cyanide *m*-chlorophenyl hydrazone (CCCP), the

membrane potential was maintained upon depletion of *m*-AAA protease subunits (Fig. 3E). Similarly, TMRE measurements in *Afg3l2*<sup>-/-</sup> MEFs grown on glucose or galactose did not reveal an impaired membrane potential (Suppl. Fig. S2).

In subsequent experiments, we measured oxygen consumption in MEFs lacking *m*-AAA protease subunits to evaluate phosphorylating respiration with endogenous substrates. Downregulation of AFG3L1 and AFG3L2 did not significantly affect oxygen consumption, irrespective of the presence of paraplegin (Fig. 3F). However, respiration was significantly increased upon inhibition of the mitochondrial F<sub>1</sub>F<sub>0</sub>-ATP synthase with oligomycin, suggesting a higher proton leakage under conditions of membrane hyperpolarization (Fig. 3F). In *m*-AAA protease-depleted cells we also observed a small but significant decrease of the maximum respiratory capacity, which was measured under uncoupled conditions (Fig. 3F). Accordingly, the ratio of uncoupled respiration and oligomycin-inhibited respiration, that is the respiratory control ratio (RCR), was reduced to about 50% when AFG3L1 and AFG3L2 were downregulated (Fig. 3F). The loss of paraplegin did not further decrease the RCR (Fig. 3F). These results indicate that the capacity of the oxidative phosphorylation system to supply ATP under conditions of high energy demand is limited in the absence of the *m*-AAA protease. Under normal conditions, however, respiration was not impaired upon downregulation of *m*-AAA protease subunits, suggesting that AFG3L1 and AFG3L2 affect directly mitochondrial fusion.

### *A dominant negative mutant of AFG3L2*

To substantiate the role of the *m*-AAA protease for OPA1 processing, we generated mutant variants of AFG3L2, in which glutamate 408 within the Walker B motif of the AAA domain or glutamate 575 within the proteolytic site were replaced by glutamine (WB, E408Q; PS, E575Q). While glutamate 575 is essential for proteolytic activity, glutamate 408 is conserved within AAA+ ATPases and is required to activate a water molecule for nucleophilic attack on bound ATP. AAA+ ATPases harboring a corresponding mutation in the Walker B motif lack ATPase activity and trap ATP (Dalal et al., 2004; Weibezahn et al., 2003, Augustin et al., 2009). We established stable HEK293 cell lines allowing the tetracycline-inducible expression of C-terminally tagged AFG3L2 variants. In contrast to mouse fibroblasts, human cells express only two *m*-AAA protease subunits, AFG3L2 and paraplegin (Kremmidiotis et al., 2001). Induction of AFG3L2 expression in the presence of tetracycline resulted in an approximately 2-fold overexpression of AFG3L2 (Fig. 4B). While overexpression of AFG3L2 or AFG3L2<sup>E575Q</sup> (PS) did not affect cell growth, cells expressing AFG3L2<sup>E408Q</sup> (WB) showed a prominent reduction of their growth rate (Fig. 4A) indicating that AFG3L2<sup>E408Q</sup> (WB) but not AFG3L2<sup>E575Q</sup> (PS) exerts a dominant negative effect on other *m*-AAA protease subunits. Long OPA1 isoforms were destabilized in the presence of AFG3L2<sup>E408Q</sup> (WB), while they accumulated at normal levels upon expression of AFG3L2 or AFG3L2<sup>E575Q</sup> (PS) (Fig. 4B). Consistently, the analysis of mitochondrial morphology in these cell lines revealed fragmentation

of the mitochondrial network in the majority of cells expressing AFG3L2<sup>E408Q</sup> (WB) (Fig. 4C, D). In contrast, expression of AFG3L2 of AFG3L2<sup>E575Q</sup> (PS) did not affect the morphology of mitochondria (Fig. 4C, D). Expression of the dominant negative AFG3L2 variant did not dissipate the mitochondrial membrane potential in HEK293 cells (Fig. 4E), nor was the oxygen consumption of HEK293 cells impaired (Fig. 4F). However, similar to *m*-AAA protease-deficient MEFs, we observed a reduced RCR in cells expressing AFG3L2<sup>E408Q</sup> (WB) (Fig. 4F), suggesting an impaired energy metabolism under conditions of high energy demand.

We conclude from these experiments that expression of a dominant negative variant of AFG3L2 and depletion of *m*-AAA protease subunits by RNA interference affects similarly mitochondrial morphology and OPA1 processing.

#### *OMA1 mediates OPA1 processing in the absence of m-AAA proteases*

Our results suggest that an unidentified protease mediates processing and degradation of the long OPA1 isoforms in *m*-AAA protease-deficient cells. Notably, lack of paraplegin (Fig. 3A), PARL or HtrA2/Omi did not stabilize L-OPA1 in the absence of AFG3L1 and AFG3L2 (Suppl. Fig. S3A). Furthermore, concomitant downregulation of AFG3L1 and AFG3L2 with YME1L1 or LON did not rescue long OPA1 isoforms (Suppl. Fig. S3B). To restrict the number of possible proteases involved in this process, we incubated AFG3L1/AFG3L2-deficient MEFs expressing v1 with different protease inhibitors and



monitored the accumulation of Flag-tagged v1 and endogenous OPA1 by immunoblotting (Fig. 5A). The stability of OPA1 was not affected upon incubating cells with pepstatin A, E-64d, or the broad-spectrum serine protease inhibitor Pefabloc (Fig. 5A). On the other hand, *o*-phenantroline (*o*-phe), a membrane-permeable metalloprotease inhibitor, stabilized v1 resulting in the accumulation of the long as well as the precursor form of OPA1 (Fig. 5A). This is consistent with previous experiments on CCCP-induced OPA1 processing (Ishihara et al., 2006). Similarly, the proteasome inhibitor MG132 stabilized v1 in AFG3L1/AFG3L2-depleted cells (Fig. 5A). OPA1 levels in mitochondria thus depend critically on the activity of 26S proteasomes and an unknown metallopeptidase. It is conceivable that inhibition of the general mitochondrial processing peptidase causes the accumulation of the precursor form of OPA1 within mitochondria in the presence of *o*-phe. Similarly, 26S proteasomes may degrade newly synthesized OPA1 in the cytosol prior to import into mitochondria, rather than mediating the turnover of preexisting mitochondrial OPA1. In agreement with this hypothesis, MG132 did not stabilize v1 $\Delta$ S1 in the absence of AFG3L1 and AFG3L2 when cytosolic protein synthesis was inhibited by CHX (Suppl. Fig. S3C). The inhibitor studies thus did not allow us to identify protease(s) controlling the stability of L-OPA1 within mitochondria.

We have previously identified Oma1 in the inner membrane of yeast mitochondria as a metallopeptidase, whose activity overlaps with the *m*-AAA protease (Oma1 for overlapping activity with m-AAA protease 1) (Käser et al., 2003). Oma1 is conserved in evolution with

homologous proteases present in vertebrates. Human OMA1, however, has been localized to the ER membrane (Bao et al., 2003). To re-examine the subcellular localization of OMA1, we expressed an OMA1-variant harboring a C-terminal GFP-domain in MEFs (Fig. 5B). OMA1-GFP was exclusively localized to mitochondria and not detected in the ER membrane (Fig. 5B). Similarly, a tubular mitochondrial network was visible in immunofluorescence studies after transient expression of an OMA1-variant harboring a C-terminal Flag-tag (data not shown). We conclude that OMA1, as yeast *Oma1*, is localized in mitochondria.

To examine whether OMA1 affects OPA1 processing in the mitochondrial inner membrane, we used three different oligonucleotides directed against *Oma1* for RNA interference. qRT-PCR experiments revealed efficient downregulation of *Oma1* transcripts by >80% (Suppl. Fig. S4A). Depletion of OMA1 slightly reduced the level of OPA1 isoforms c and e, which are generated by S1 cleavage and accumulate at low levels under these conditions in MEFs (Fig. 5C). However, we observed a significant stabilization of L-OPA1 in AFG3L1/AFG3L2-deficient MEFs upon downregulation of OMA1, whereas transfection of the cells with scrambled oligonucleotides had no effect (Fig. 5C).

We monitored OPA1 processing directly after transient expression of the Flag-tagged OPA1 variant v1 in MEFs (Fig. 5D). In the presence of AFG3L1 and AFG3L2, Flag-tagged L-OPA1 accumulated in OMA1-depleted cells (Fig. 5D) indicating that OMA1 is able to cleave overexpressed OPA1. In the absence of AFG3L1 and AFG3L2, on the

other hand, downregulation of OMA1 stabilized L-OPA1 demonstrating that OMA1 mediates turnover and increased OPA1 processing in the absence of the *m*-AAA protease (Fig. 5D).

OPA1 isoforms accumulated virtually as in wild type cells in MEFs depleted of both OMA1 and the *m*-AAA protease. We therefore examined the morphology of the mitochondrial network after expression of a mitochondrially targeted dsRed variant in these cells (Fig. 5E and F). Depletion of OMA1 did not significantly affect mitochondrial morphology in the presence of the *m*-AAA protease, but restored the tubular network in AFG3L1/AFG3L2-deficient MEFs (Fig. 5E and F). Electron micrographs revealed a normal, lamellar cristae morphology of mitochondria lacking both the *m*-AAA protease and OMA1 (Fig. 5E). These findings substantiate our conclusion that the *m*-AAA protease regulates mitochondrial fusion via OPA1 and demonstrate that OMA1 is epistatic to the *m*-AAA protease.

To further define the functional interrelationship of OMA1 and the *m*-AAA protease, we assessed the assembly of *m*-AAA proteases in OMA1-depleted mitochondria by blue-native gel electrophoresis (Suppl. Fig. S4B). Downregulation of OMA1 did not affect the formation of the proteolytic complexes containing AFG3L2 and/or AFG3L1. Moreover, depletion of OMA1 did not interfere with the maturation of AFG3L1 or AFG3L2 (Fig. 5C), which occurs autocatalytically upon import into mitochondria (Koppen et al., 2009). Similarly, processing of an OMA1 variant carrying a C-terminal myc-tag was not impaired in mitochondria depleted of AFG3L1 and AFG3L2 (Suppl. Fig. S4C).

### *Tissue-specific destabilization of L-OPA1 in Afg3l2<sup>-/-</sup> mice*

Mutations in the *m*-AAA protease subunits paraplegin and AFG3L2 cause neurodegeneration in human, but molecular details of the pathogenesis are currently not understood. Our experiments revealed an at least partially redundant function of AFG3L1 and AFG3L2 for mitochondrial fusion in MEFs (Fig. 1). However, as AFG3L1 is a pseudogene in human (Kremmidiotis et al., 2001) and expressed at low levels in the mouse brain (Koppen et al., 2007; Martinelli et al., 2009), it is conceivable that the regulation of OPA1 processing by the *m*-AAA protease is of potential pathogenic relevance. To examine whether the loss of AFG3L2 impairs OPA1 cleavage *in vivo*, we monitored OPA1 processing in mitochondria isolated from tissues of a recently established *Afg3l2<sup>-/-</sup>* mouse line (Maltecca et al., 2008). The abundance of individual OPA1 isoforms varies in different tissues, as previously described (Fig. 6A) (Akepati et al., 2008). In the absence of AFG3L2, L-OPA1 isoforms accumulated at strongly reduced levels in brain, heart and kidney, demonstrating that the stability of L-OPA1 depends on AFG3L2 *in vivo*. Notably, deletion of *Afg3l2* hardly affected OPA1 isoforms in the liver (Fig. 6A), consistent with a compensatory effect of AFG3L1, which is expressed at higher levels relative to AFG3L2 in liver (Koppen et al., 2007).

To analyze whether depletion of OMA1 can suppress deleterious effects of the loss of the *Afg3l2* gene, we monitored OPA1 processing and mitochondrial morphology in *Afg3l2<sup>-/-</sup>* MEFs (Fig. 6B-D). Deletion of *Afg3l2* affected only slightly cleavage of OPA1 in MEFs grown on

glucose-containing medium, most likely due to the presence of AFG3L1 in these cells (Fig. 6B). However, L-OPA1 was absent in *Afg3l2*<sup>-/-</sup> MEFs grown in the presence of galactose, i.e. conditions with an increased demand for mitochondrial respiratory function (Fig. 6B). This was accompanied by a fragmentation of the mitochondrial network in the majority of these cells (Fig. 6C and D). Depletion of OMA1 in immortalized *Afg3l2*<sup>-/-</sup> MEFs, cultured either in glucose- or galactose-containing medium, stabilized L-OPA1 providing further evidence that OMA1 mediates OPA1 processing if the function of the *m*-AAA protease is impaired (Fig. 6E).

#### *Mitochondrial dysfunction induces OPA1 processing by OMA1*

We next examined whether OMA1 cleaves OPA1 also under other cellular conditions known to induce OPA1 processing. Current models suggest that a dysfunction of mitochondria accompanied by decreased mitochondrial ATP levels stimulates OPA1 processing and results in mitochondrial fragmentation (Baricault et al., 2007; Duvezin-Caubet et al., 2006). We therefore compared the accumulation of OPA1 isoforms in a human osteosarcoma cell line containing (WT) or lacking mitochondrial DNA (mtDNA<sup>0</sup>) (Fig. 7A). While long and short OPA1 isoforms accumulated in these cells in the presence of mtDNA, short isoforms accumulated in mtDNA<sup>0</sup> cells (Fig. 7A). Strikingly, long OPA1 isoforms were detected after RNAi-mediated downregulation of OMA1, suggesting that the loss of mtDNA induces OPA1 cleavage by OMA1.

OPA1 is converted into short isoforms upon dissipation of  $\Delta\Psi_m$  with the uncoupler CCCP or upon inhibition of the  $F_1F_0$ -ATP synthase with oligomycin (Fig. 7B and C) (Duvezin-Caubet et al., 2006; Ishihara et al., 2006). Downregulation of OMA1 prior to addition of CCCP or oligomycin significantly stabilized long OPA1 isoforms indicating that OPA1 processing is mediated by OMA1 under both conditions (Fig. 7B and C). In conclusion, these experiments identify OMA1 as the protease responsible for the inducible cleavage of OPA1 at processing site S1.

## Discussion

Mutations in *m*-AAA protease subunits cause neurodegeneration but pathogenic mechanisms remain enigmatic. Our results identify the *m*-AAA protease as a novel regulator of mitochondrial membrane fusion and cristae morphology, suggesting that *m*-AAA protease associated diseases may represent a group of neurological disorders caused by deficiencies in mitochondrial dynamics. Murine AFG3L1- and AFG3L2-containing *m*-AAA protease isoenzymes exert at least partially overlapping activities during membrane fusion. The relative expression of AFG3L1 and AFG3L2 in different tissues will therefore determine whether or not a functional impairment of one *m*-AAA protease subunit affects the morphology of the mitochondrial network. Notably, the *m*-AAA protease subunit predominantly expressed in the mouse brain is AFG3L2, while AFG3L1 is only present at lower levels (Koppen et al., 2007; Martinelli et al., 2009). This explains severe neurological defects (Maltecca et al., 2008) and cerebellar degeneration in mice with reduced levels of AFG3L2-containing *m*-AAA isoenzymes (Martinelli et al., 2009), reminiscent of patients with heterozygous mutations in human *AFG3L2* (Cagnoli et al., 2008; DiBella et al., 2008).

Whereas mitochondrial fusion depends on the presence of either AFG3L1 or AFG3L2, the third *m*-AAA protease subunit paraplegin is not required to maintain a reticulated mitochondrial network. Deletion of *Spg7* encoding paraplegin did not affect mitochondrial morphology in MEFs. Moreover, phenotypes observed upon

downregulation of AFG3L1 and AFG3L2 were not worsened in paraplegin-deficient cells. It should be noted, however, that an efficient depletion of AFG3L1 and AFG3L2 inactivates paraplegin that only exists in heterooligomeric complexes with AFG3L1 and AFG3L2 (Koppen et al., 2007). Thus, it is conceivable that paraplegin-containing isoenzymes may control mitochondrial morphology in cells expressing limiting levels of AFG3L1 and AFG3L2. This may explain the cell-type specific axonal degeneration associated with mutations in paraplegin both in mouse and human (Casari et al., 1998; Ferreira et al., 2004).

The *m*-AAA protease controls mitochondrial fusion via OPA1 (Fig. 8). The loss of AFG3L2 in various tissues of the mouse, downregulation of AFG3L1 and AFG3L2 in MEFs, or the expression of a dominant negative AFG3L2 variant in human cells decreases OPA1 stability and results in an increased processing and turnover of long OPA1 isoforms. This causes fragmentation of the tubular mitochondrial network which is at least partially restored upon expression of an OPA1 variant lacking the cleavage site S1. Our experiments thus link for the first time the function of AFG3L1 and AFG3L2 to OPA1 *in vivo*. Strikingly, inactivation or loss of the *m*-AAA protease does not result in the accumulation of long OPA1 isoforms, as predicted by experiments in yeast (Duvezin-Caubet et al., 2007), but decreases their stability. The accelerated cleavage of OPA1 in the absence of the *m*-AAA protease is mediated by OMA1, a new member of a conserved and widespread family of membrane-bound M48 metalloproteases. We have previously identified yeast Oma1 in the



mitochondrial inner membrane as a peptidase which can substitute for the function of the *m*-AAA protease during degradation of a misfolded membrane protein (Oma1 for overlapping activity with m-AAA protease) (Käser et al., 2003). Similarly, synthetic growth defects have been observed when mutations in the bacterial AAA protease FtsH were combined with mutations in HtpX, a distant homologue of OMA1, indicating overlapping proteolytic activities (Shimohata et al., 2002). In agreement with these findings, we demonstrate here that mammalian OMA1, similar to the *m*-AAA protease, can cleave OPA1. The substrate specificity of OMA1 is distinct from yeast Oma1 which cleaves neither OPA1 when expressed in yeast nor the yeast OPA1-homologue Mgm1 (Duvezin-Caubet et al., 2007). Differences in substrate recognition by OMA1-like peptidases may therefore explain why the loss of the *m*-AAA protease is not accompanied by increased OPA1 processing in yeast. Interestingly, mitochondrial rhomboid proteases – though highly conserved – also differ in their ability to cleave OPA1. Both yeast Pcp1 and its mammalian homologue PARL mediate processing of Mgm1 but neither of them cleave OPA1 when expressed in yeast (Duvezin-Caubet et al., 2007).

The regulation of OPA1 stability and processing at site S1 by two peptidases raises the question which peptidase mediates constitutive and stress-induced OPA1 cleavage. Our experiments reveal that OMA1 promotes OPA1 processing if mitochondrial activities are impaired (Fig. 8). The loss of mtDNA, dissipation of  $\Delta\Psi_m$ , or a decrease of mitochondrial ATP levels induces OPA1 processing by OMA1. The molecular mechanism of OMA1 activation under stress

conditions remains to be determined. Mitochondrial dysfunction may alter the accessibility of the S1 cleavage site in OPA1 allowing stress-induced cleavage by OMA1. Alternatively, stress conditions may increase the proteolytic activity of OMA1 itself. It is also possible that stress conditions lower mitochondrial ATP levels and thereby *m*-AAA protease activity, resulting in the accumulation of an activator of OMA1.

In contrast to the stress-induced OPA1 cleavage, constitutive cleavage of OPA1 during mitochondrial biogenesis affects only a subset of the newly imported OPA1 molecules and results in an approximately equimolar accumulation of long and short isoforms. As both forms are required for mitochondrial fusion (Song et al., 2007), their balanced formation is critical for the maintenance of the mitochondrial network. While our experiments identify OMA1 as the peptidase responsible for stress-induced OPA1 cleavage, two possibilities must be considered for constitutive OPA1 processing.

According to the first scenario, OMA1 is responsible for both constitutive and induced OPA1 cleavage. The *m*-AAA protease, on the other hand, is required to stabilize long OPA1 isoforms and inhibit OMA1 activity under normal conditions, possibly exerting functions beyond a role as a processing enzyme. These may include the ATP-dependent membrane dislocation of OPA1 preceding its proteolytic cleavage. A similar non-proteolytic activity has been assigned to the *m*-AAA protease during the biogenesis of yeast cytochrome *c* peroxidase (Tatsuta et al., 2007). In yeast, the ATP-dependent mitochondrial import motor was proposed to regulate Mgm1

processing by the rhomboid protease in response to mitochondrial ATP levels in a process termed alternative topogenesis (Herlan et al., 2004). Constitutive OPA1 processing might be regulated in a similar manner. Notably, membrane dislocation could be also affected by an altered phospholipid composition of mitochondrial membranes, which has recently been observed in yeast mitochondria lacking the *m*-AAA protease (Osman et al., 2009). Several observations indeed suggest that OMA1 can cleave OPA1 in the presence of the *m*-AAA protease. Depletion of OMA1 in human osteosarcoma cells or in MEFs cultured in galactose-containing medium leads to the disappearance of OPA1 isoforms c and e, indicating that OMA1 can affect constitutive OPA1 processing at S1. Moreover, OMA1 is required for S1 cleavage of OPA1 overexpressed in MEFs. However, an OMA1-like peptidase appears to be absent in *C. elegans* and *D. melanogaster* although mitochondrial morphology depends on OPA1 in both organisms. In addition, neither downregulation nor overexpression of OMA1 did affect mitochondrial morphology in MEFs suggesting that OMA1 is dispensable for the balanced formation of long and short OPA1 isoforms.

According to the second scenario, constitutive and stress-induced OPA1 processing are mediated by two distinct peptidases, which differ in their enzymatic properties: the ATP-dependent *m*-AAA protease ensures the balanced accumulation of long and short isoforms under constitutive conditions, while OMA1 acting in an ATP-independent manner completely converts long OPA1 isoforms into short forms under stress conditions. In agreement with a role of the

*m*-AAA protease as a processing enzyme under normal conditions, reconstitution experiments in yeast demonstrate that AFG3L1 and AFG3L2 can cleave OPA1 in a heterologous environment (Duvezin-Caubet et al., 2007). Moreover, paraplegin binds OPA1 when overexpressed and stimulates OPA1 processing (Ishihara et al., 2006). OPA1 processing by ATP-dependent and ATP-independent peptidases under different physiological conditions would resolve the apparent caveat of previous studies suggesting that processing of OPA1 may involve the *m*-AAA protease but is accelerated at decreased mitochondrial ATP levels. It offers also an attractive possibility for regulation: low ATP levels may impair membrane dislocation of OPA1 possibly mediated by the *m*-AAA protease and thereby make OPA1 accessible for OMA1 cleavage under stress conditions. Clearly, further experiments are required to define the relative contribution of the *m*-AAA protease and OMA1 to constitutive OPA1 cleavage, which may also depend on relative expression levels in different tissues and cell types. Regardless, the identification of proteases involved in OPA1 processing now allows assessing the relevance of an impaired OPA1 cleavage and mitochondrial fragmentation for the maintenance of cellular functions and for various disease states.

## Material and methods

### *Generation of immortalized MEFs lines.*

All animal procedures were performed according to protocols approved by the Institutional Animal Care and Use Committee. Generation of *Spg7*<sup>-/-</sup> mice (Ferreirinha et al., 2004) and *Afg3l2*<sup>Emv66/Emv66</sup> genetic characterization (Maltecca et al., 2008) were previously described. Primary MEFs were established from E14.5 *Spg7*<sup>-/-</sup> or E13.5 *Afg3l2*<sup>Emv66/Emv66</sup> and littermate wild type embryos and immortalized by SV40 transformation. MEFs were cultured in DMEM containing 4.5 g/L of glucose and supplemented with 10% FCS. When specified, MEFs were cultured in DMEM with 6 mM galactose. The human osteosarcoma-derived cell line 143B and its p<sup>0</sup> derivative were grown in medium supplemented with 50 µg/ml uridine.

### *Downregulation of m-AAA protease subunits and OMA1*

RNAi-mediated knockdown of paraplegin, AFG3L1, AFG3L2 and OMA1 was performed using specific Stealth™ RNAi and the nontargeting Stealth™ RNAi Negative Control (Invitrogen). The sequences are

5'-GCGCGUCAUUGCUGGUACUGCUAAA-3' for Paraplegin,

5'-CCUGCCUCCGUACGCUCUAUCAUA-3' for AFG3L2,

5'-GCGAAACC-AUGGUGGAGAAGCCAUA-3' for AFG3L1,

5'-GGAUACAGUCAAGUUGCAGAGUA-3',

5'-AGUUCUCAGAGAGUCUUCAUGGCUA-3',

5'-GCUUCUUGGUCUGAGUGC-AUUUGGA-3' for murine OMA1.

For human OMA1, stealth siRNAs with the sequences

5'-TGGACTACTGCTTGCTGCAAAGGCT-3' and

5'-TGGCAGCAAATGGAGTTCGTTGA-TA-3' were used.

10-20 nM of each siRNA were transfected twice with Lipofectamine™ (Invitrogen). Downregulation was monitored by immunoblot analysis of cell lysates generated after two days if not indicated otherwise.

#### *Expression of AFG3L2 variants and OMA1*

Human *Afg3l2* was cloned into pcDNA5/FRT/TO and mutations were introduced into the Walker B motif (E408Q) or the proteolytic center (E575Q). Stable transformants in FlpIn T-REx 293 cells were obtained by cotransfection with the plasmid pOG44 allowing expression of Flp-recombinase (Invitrogen). Expression of fusion proteins harbouring a C-terminal hexahistidine epitope tag was induced with 1 µg/ml tetracycline. After 24 hrs, we analyzed cell lysates by immunoblotting and assessed mitochondrial morphology. The coding region of murine *Oma1* (NM\_025909) was cloned into the EcoRI/BamHI sites of the vector pEGFP-N2 in frame with GFP.

#### *Assessment of cell growth*

5×10<sup>3</sup> FlpIn T-REx 293 expressing AFG3L2 variants were seeded in medium with or without 1 µg/ml tetracycline. To assess the number of living cells in culture, we used the One Solution Cell Proliferation

Assay (Promega) and monitored the conversion of a tetrazolium compound to formazan determining the absorbance at 490 nm.

#### *Fluorescence microscopy*

Mitochondrial morphology was examined after expression of mito-DsRed using a DeltaVision microscope (Applied Precision) (Merkwirth et al., 2008). Fluorescence images were acquired using a Cool Snap HQ/ICX285 camera (Sony) and a PlanApo N 60x/1.42 oil objective (Olympus). Image stacks were deconvoluted with the SoftWorx Imaging suite (Applied precision). Image files were further processed with the CORELDRAW™ 11 Graphics Suite software. For co-localization of OMA1-GFP and mitochondria, we stained cells with Mitotracker Red CMXRos (Invitrogen) and used a Nikon Eclipse E600 microscope and a Nikon Plan Apo 60XA/1.40 oil objective. Images were acquired with Bio-Rad Radiance 2100 confocal microscope. For detection of the ER, cells were stained with an antiserum directed against calnexin examined using a Nikon Eclipse TE2000-S + BD CARV II imaging station, and a Nikon Plan Apo VC 100X/1.40 oil objective and images acquired using a QuantEM 512 SC camera and deconvoluted with the Metamorph software.

#### *Transmission electron microscopy*

MEFs were plated on glass coverslips, transfected with siRNA and after 48 hrs flat-embedded (Merkwirth et al., 2008). Ultrathin sections (60-70 nm) were cut and mounted on pioloform-coated

copper grids (Plano). Sections were stained with lead citrate and uranyl acetate and viewed with a JEOL JEM-2100 transmission electron microscope (JEOL Ltd., Tokyo, Japan) operated at 80 kV. Micrographs were taken using a Gatan Erlangshen ES500W CCD camera (Gatan Inc.).

#### *Polarographic measurements*

Respiration of intact cells was measured at 37°C with a Clark-type electrode oxygraph (Hansatech Inc.).  $2.5 \times 10^6$  cells were assayed in 250 mM saccharose, 20 mM HEPES pH 7.4, 10 mM  $\text{KH}_2\text{PO}_4$ , 4 mM  $\text{MgCl}_2$ , 1 mM EDTA, 5 mM glucose, 2 mM pyruvate and 4 mM glutamate. After recording endogenous respiration, ATP synthase was inhibited with 2  $\mu\text{M}$  oligomycin followed by uncoupling of oxidative phosphorylation using CCCP with concentrations of 250-750 nM. Cellular respiration was inhibited with 2 mM KCN and was corrected to KCN-insensitive respiration.

#### *Inhibitor studies*

To induce SIMH, MEFs were exposed to 1  $\mu\text{M}$  CHX for 3 hrs. 2-3 days after transfection with siRNAs and plasmids MEFs were incubated for 5 hrs with the following protease inhibitors: 5  $\mu\text{M}$  MG132, 0.5 mM  $\sigma$ -phe, 50  $\mu\text{M}$  pepstatin A, 0.5 mM Pefabloc SC and 50  $\mu\text{M}$  E-64d. To induce OPA1 cleavage, MEFs were treated either with 2  $\mu\text{M}$  oligomycin 60 hours after transfection, or with 20  $\mu\text{M}$  CCCP 48 hours after transfection.



### *Antibodies*

Polyclonal antibodies directed against murine *m*-AAA protease subunits were described previously (Koppen et al., 2007). An antiserum recognizing murine LON was kindly provided by Dr. C. Suzuki. The following commercially available antibodies were used:  $\alpha$ -OPA1 (Molecular Probes),  $\alpha$ -Flag M2 (Sigma),  $\alpha$ -SLP2 (Genway Biotech Inc.),  $\alpha$ -calnexin (Stressgen) and  $\alpha$ -CII (Molecular Probes).

### *Online Supplemental Material*

Five supplemental figures are available online. Fig. S1 shows the mitochondrial morphology in paraplegin-deficient MEFs. Fig. S2 demonstrates the maintenance of the mitochondrial membrane potential in *Afg3l2*<sup>-/-</sup> mitochondria using TMRE fluorescence. Fig. S3 shows the stability of OPA1 in AFG3L1/AFG3L2-deficient cells lacking various mitochondrial proteases, and the effect of an inhibition of cytosolic protein synthesis on OPA1 isoforms accumulating in *m*-AAA protease deficient MEFs in the presence of MG132. Fig. S4 shows the quantification of OMA1 mRNA levels in MEFs after downregulation of OMA1 by RNAi, demonstrates the assembly of AFG3L2 and AFG3L1 in *m*-AAA protease complexes in OMA1-deficient mitochondria by BN-PAGE analysis, and reveals normal processing of OMA1 in *m*-AAA protease-deficient mitochondria. Fig. S5 shows the accumulation of AFG3L1 and AFG3L2 in OMA1-deficient MEFs.

## **Acknowledgements**

We thank Dr. G. Cox for providing the *Afg3l2*<sup>Emv66</sup> mouse line, Dr. K. Mihara for OPA1 expression plasmids, Drs. J. Downward, B. de Strooper, and R. Wiesner for cell lines, Dr. C. Suzuki for LON-specific antibodies, and Dr. T. Tatsuta for discussion. This work was supported by grants of the Deutsche Forschungsgemeinschaft, the German-Israeli-Project (DIP grant F.5.1) and the European Research Council to T.L., and the MDA, UMDF, and CARIPO foundations to E.I.R.

## **Abbreviations**

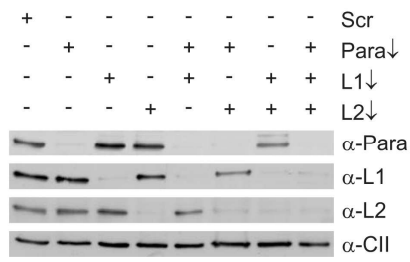
CCCP, carbonyl cyanide *m*-chlorophenyl hydrazone; CHX, cycloheximide; MEF, mouse embryonic fibroblast; *o*-phe, *o*-phenantroline; RCR, respiratory control ratio; SIMH, stress-induced mitochondrial hyperfusion, ER, endoplasmic reticulum.

## Figure Legends

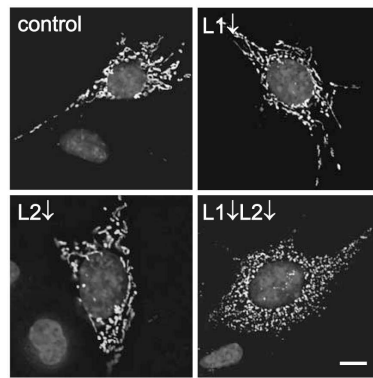
*Figure 1. Fragmentation of mitochondria in MEFs depleted of AFG3L1 and AFG3L2.*

(A) Immunoblot analysis of MEFs transfected with siRNAs directed against AFG3L1, AFG3L2 and paraplegin, or scrambled siRNA (Scr) using specific antisera recognizing paraplegin (Para), AFG3L1 (L1), AFG3L2 (L2) and the 70 kDa subunit of complex II (CII). (B, C) Mitochondrial morphology in AFG3L1- and AFG3L2-deficient MEFs was visualized by expression of mito-DsRed and nuclear DNA was stained with DAPI. >150 MEFs were scored in each experiment. Columns represent means  $\pm$  SD of three independent experiments (\*\*,  $p < 0.01$ ). Bar, 10  $\mu$ m. (D) Mitochondrial ultrastructure in MEFs transfected with scrambled, AFG3L1-, or AFG3L2-specific siRNAs or siRNAs against AFG3L1 and AFG3L2. Representative transmission electron micrographs of mitochondria are shown. Bar, 0.2  $\mu$ m.

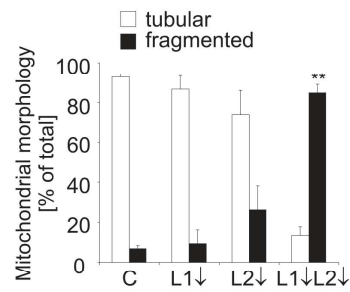
**A**



**B**



**C**



**D**

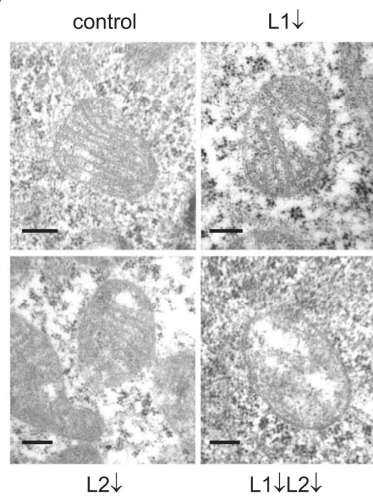
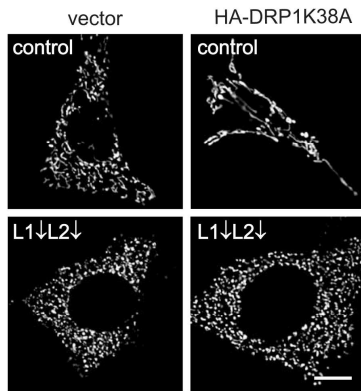


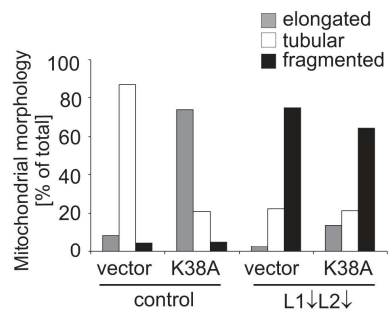
*Figure 2. AFG3L1 and AFG3L2 are required for mitochondrial fusion.*

**(A, B)** Inhibition of fission does not restore a tubular network in the absence of AFG3L1 and AFG3L2. Dominant negative DRP1<sup>K38A</sup>-HA and mito-DsRed were expressed in *m*-AAA protease-deficient MEFs and mitochondrial morphology was assessed after 24 hrs. >200 cells were scored per experiment. **(C, D)** Stress-induced mitochondrial hyperfusion (SIMH) depends on AFG3L1 and AFG3L2. After depletion of AFG3L1 and AFG3L2, MEFs were incubated for three (C, D) and six (D) hrs in the presence of 1  $\mu$ M cycloheximide (+CHX) as indicated. > 150 cells were scored for each experiment. Columns represent means  $\pm$  SD of three independent experiments (\*\*,  $p < 0.01$ ). Bar, 10  $\mu$ m.

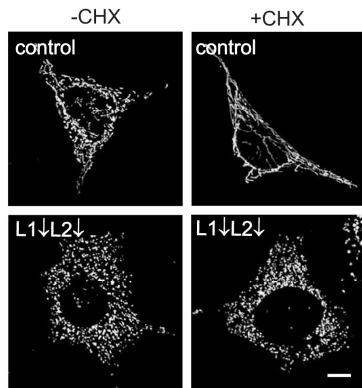
**A**



**B**



**C**



**D**

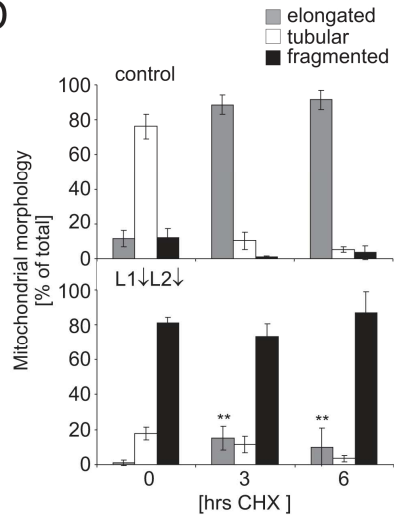


*Figure 3. Destabilization of long OPA1 isoforms in the absence of the m-AAA protease.*

**(A)** Immunoblot analysis of *Spg7*<sup>+/+</sup> and *Spg7*<sup>-/-</sup>-MEFs depleted of AFG3L1 and AFG3L2 as indicated. Cells lysates were analyzed with antibodies directed against OPA1, AFG3L1 (L1), AFG3L2 (L2) and, for control, the 70 kDa subunit of complex II (CII). OPA1 isoforms are marked with a-e. **(B)** Mitochondrial morphology in AFG3L1-/AFG3L2-deficient MEFs expressing OPA1 variants. Prior to depletion of AFG3L1 and AFG3L2, MEFs were transfected with plasmids encoding Flag-tagged OPA1 variants v1ΔS1 or S-OPA1. >150 cells were scored. Bars represent means ± SD of three independent experiments. \*, p<0.05. **(C)** Immunoblot analysis of AFG3L1/AFG3L2-deficient MEFs expressing Flag-tagged OPA1 splice variants 1 (v1) and 1ΔS1 (v1ΔS1). Cell lysates were analyzed three days after siRNA transfection by SDS-PAGE and immunoblotting using anti-Flag and anti-CII antibodies. **(D)** Degradation of v1ΔS1 in AFG3L1-/AFG3L2-depleted MEFs. Two days after siRNA transfection, cells were incubated for 6 hrs with CHX (100 µg/ml) and analyzed as described in (C). **(E)** Mitochondrial membrane potential in MEFs depleted of *m-AAA* protease subunits was analyzed with the fluorescent dye JC-1 and flow cytometry at 590 nm. Dissipation of the membrane potential with CCCP was used as control. Relative intensities to cells transfected with scrambled RNAi (C) are shown. Data represent means ± SD of three independent experiments. \*\*, p<0.01. **(F)** Oxygen consumption in *Spg7*<sup>+/+</sup>- and *Spg7*<sup>-/-</sup>-MEFs depleted of AFG3L1/AFG3L2 was measured under

routine conditions and in the presence of oligomycin (OLG) and CCCP. RCR, respiratory control ratio. Bars represent means  $\pm$  SD of three independent experiments. \*,  $p < 0.05$ , \*\*,  $p < 0.01$ ; \*\*\*,  $p < 0.001$ .

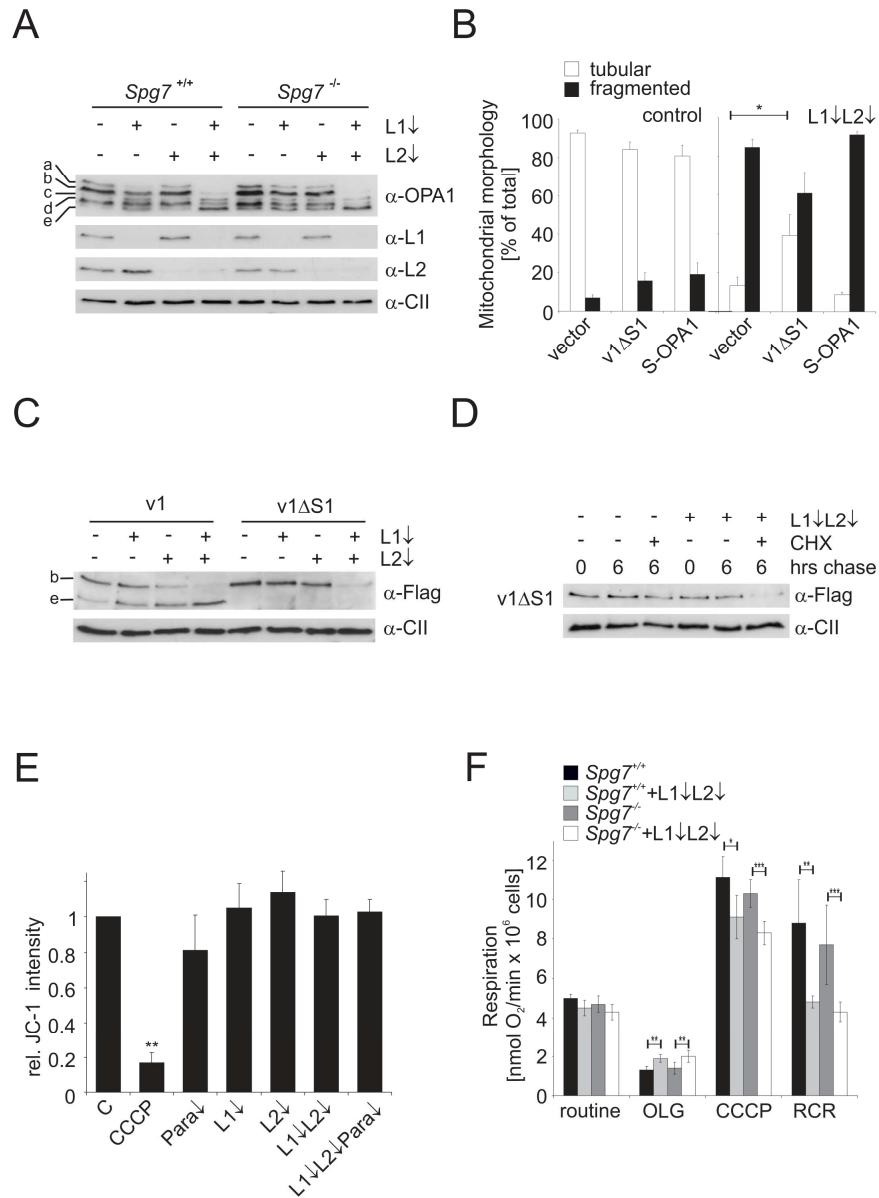
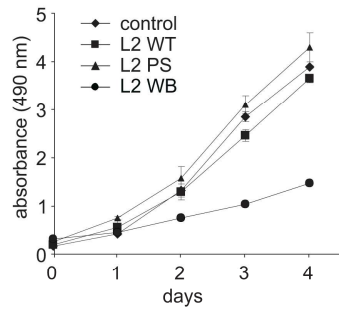




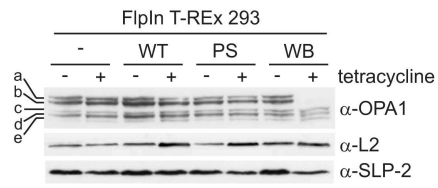
*Figure 4. Expression of dominant negative AFG3L2<sup>E408Q</sup> inhibits cell proliferation and impairs mitochondrial morphology and OPA1 processing.*

**(A)** Growth of cells expressing AFG3L2 (L2 WT), AFG3L2<sup>E575Q</sup> (L2 PS) or AFG3L2<sup>E408Q</sup> (L2 WB). Graphs represent means  $\pm$  SD of three independent experiments. **(B)** Immunoblot analysis of FlpIn T-REx 293 cells expressing AFG3L2 variants. Cell lysates were analyzed 24 hrs after addition of tetracycline using antibodies directed against OPA1, AFG3L2 and SLP-2. **(C, D)** Mitochondrial morphology in cells expressing AFG3L2 variants. >100 cells were scored. Bar, 10  $\mu$ m. WT, AFG3L2; PS, AFG3L2<sup>E575Q</sup>; WB, AFG3L2<sup>E408Q</sup>. **(E)** Membrane potential in cells expressing AFG3L2 (WT) or AFG3L2<sup>E408Q</sup> (WB). **(F)** Oxygen consumption in cells expressing AFG3L2 (WT) or AFG3L2<sup>E408Q</sup> (WB) measured as in Fig. 3F. \*\*\*,  $p < 0.001$ .

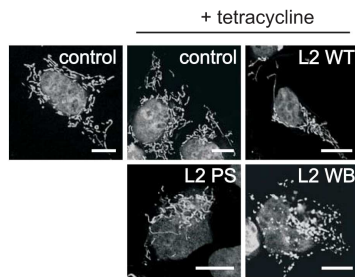
**A**



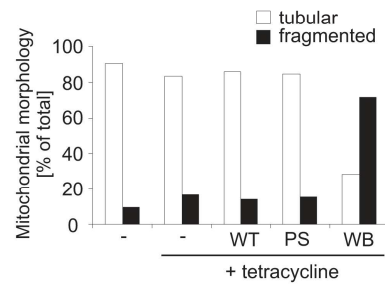
**B**



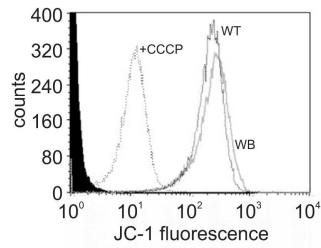
**C**



**D**



**E**



**F**

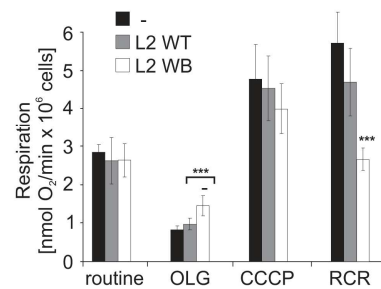


*Figure 5. OMA1 degrades OPA1 in AFG3L1/AFG3L2-deficient MEFs.*

**(A)** Stability of OPA1 and OPA1 variant 1 in the presence of different protease inhibitors. Flag-tagged OPA1 variant 1 was expressed in MEFs which were subsequently depleted of AFG3L1 and AFG3L2. After 48 hrs, MEFs were incubated for 5 hrs with Pepstatin A, E-64d, Pefabloc SC, *o*-phe, or MG132 and cell lysates were analyzed by immunoblotting with  $\alpha$ -Flag,  $\alpha$ -OPA1 and  $\alpha$ -CII. p, OPA1 precursor; b, long OPA1 isoform; e, short OPA1 isoform. **(B)** Localization of OMA1 to mitochondria. Fluorescence microscopy of MEFs expressing murine OMA1 harboring a C-terminal GFP tag. Mitochondria were stained with Mitotracker Red CMXRos, while the endoplasmic reticulum was detected using an antiserum directed against calnexin. Bar, 10  $\mu$ m. **(C)** Immunoblot analysis of MEFs transfected with siRNAs directed against AFG3L1, AFG3L2 and OMA1, or scrambled siRNA (Scr) using specific antisera recognizing OPA1, AFG3L1 (L1), AFG3L2 (L2) and the 70 kDa subunit of complex II (CII). Three different siRNAs directed against OMA1 were used. **(D)** Immunoblot analysis of MEFs transfected with siRNAs directed against AFG3L1/AFG3L2 and OMA1 and Flag-tagged OPA1 splice variant 1 (v1). Cell lysates were analyzed three days after transfection by SDS-PAGE and immunoblotting using  $\alpha$ -Flag,  $\alpha$ -AFG3L1,  $\alpha$ -AFG3L2,  $\alpha$ -OPA1 and  $\alpha$ -CII antibodies. **(E)** Mitochondrial morphology in MEFs transfected with AFG3L1/AFG3L2- and OMA1-siRNA was visualized by expression of mito-DsRed (left panel). Mitochondrial ultrastructure was analyzed by electron microscopy. **(F)** Quantification of mitochondrial

morphology. >150 MEFs were scored in each immunofluorescence experiment. Columns represent means  $\pm$  SD of three independent experiments. \*\*,  $p < 0.01$ . Bar, 10  $\mu$ m.

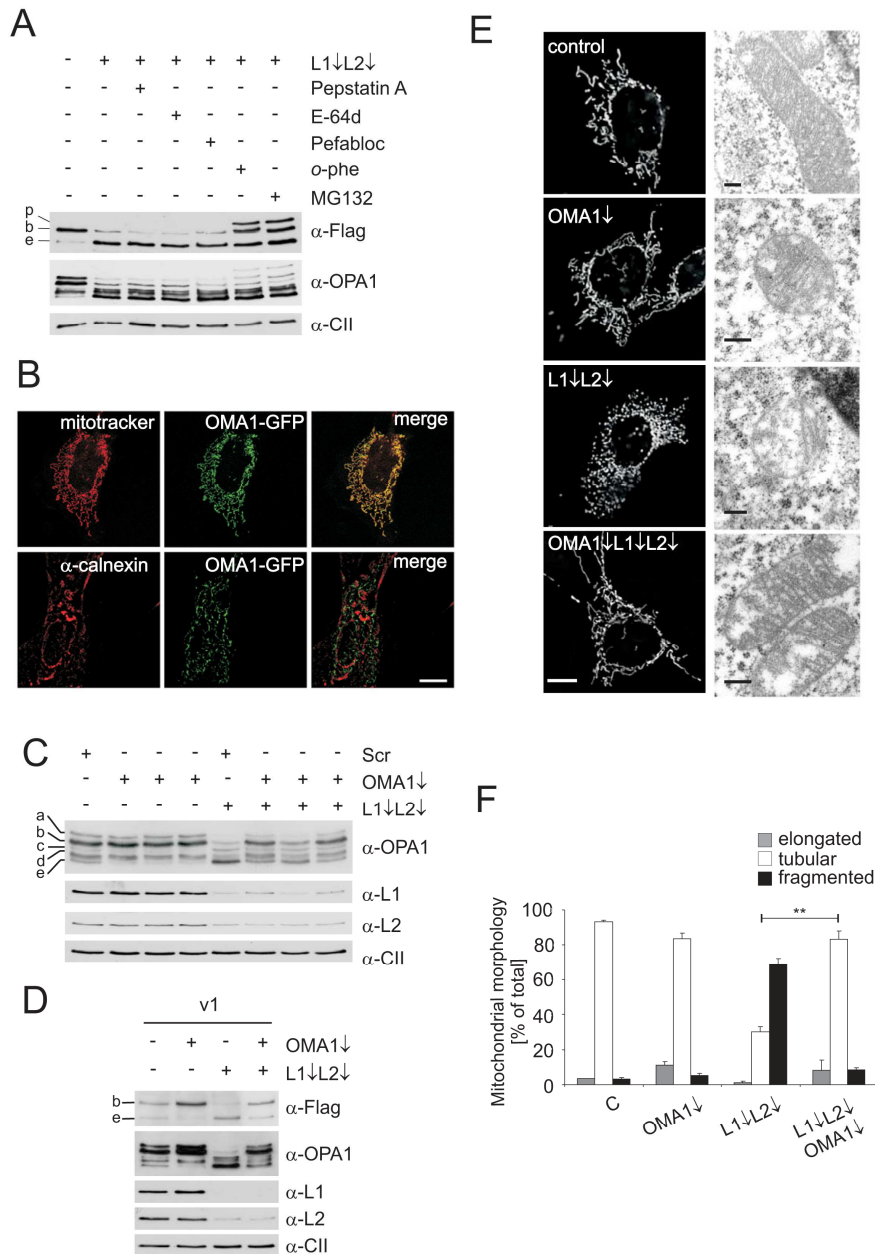


*Figure 6. Impaired OPA1 processing in Afg3l2<sup>-/-</sup> mice.*

**(A)** Immunoblot analysis of mitochondria isolated from brain, liver, heart, and kidney of wild type ( $L2^{+/+}$ ) or  $Afg3l2^{-/-}$  ( $L2^{-/-}$ ) mice using antisera directed against OPA1 and the 70 kDa subunit of complex II (CII). **(B)** Immunoblot analysis of OPA1 in wild type ( $L2^{+/+}$ ) or  $Afg3l2^{-/-}$  ( $L2^{-/-}$ ) primary MEFs grown in the presence of glucose or galactose. **(C, D)** Mitochondrial morphology in wild type ( $L2^{+/+}$ ) or  $Afg3l2^{-/-}$  ( $L2^{-/-}$ ) cells was visualized by expression of a mitochondrially targeted GFP. >100 cells were scored. Columns represent means  $\pm$  SD of three independent experiments. Bar, 10  $\mu$ m. **(E, F)** Stabilization of long OPA1 isoforms in  $Afg3l2^{-/-}$  ( $L2^{-/-}$ ) MEFs grown in glucose or galactose upon downregulation of OMA1. Immunoblot analysis was performed using specific antisera recognizing OPA1 and CII. Scr, scrambled RNAi.

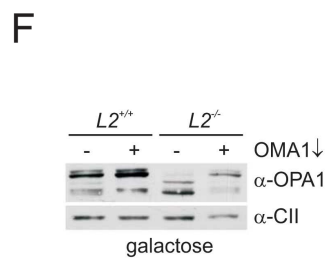
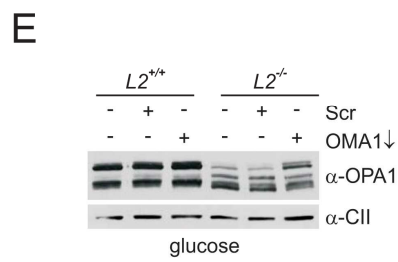
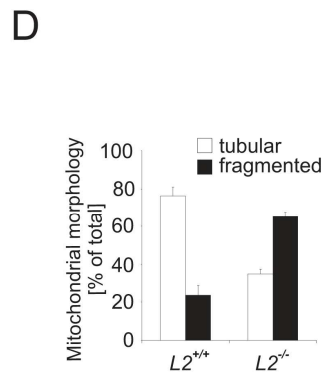
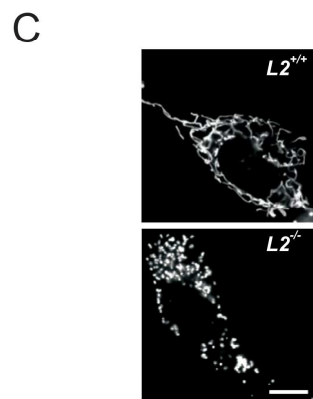
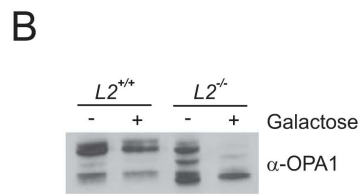
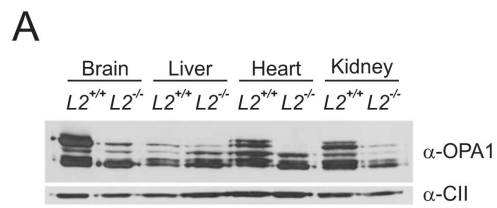
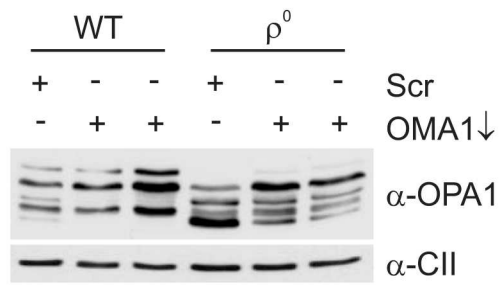


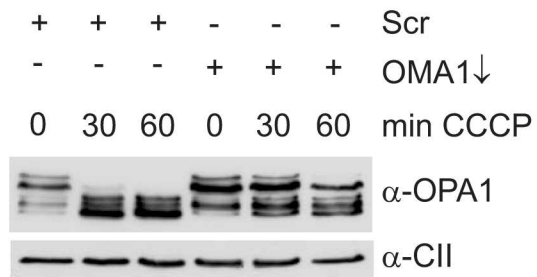
*Figure 7. Mitochondrial dysfunction induces OPA1 processing by OMA1.*

**(A)** OMA1 stabilizes long OPA1 isoforms in the absence of mtDNA. Immunoblot analysis of human osteosarcoma cells (143B) using specific antisera recognizing OPA1 and the 70 kDa subunit of complex II (CII). Cells lacking mtDNA ( $\rho^0$ ) were transfected with OMA1-specific or scrambled (Scr) siRNA and compared to parental cells containing mtDNA (WT). Cell lysates were analyzed 72 hrs after transfection. **(B, C)** Stabilization of long OPA1 isoforms against **(B)** CCCP- and **(C)** oligomycin (OLG)-induced processing in OMA1-depleted MEFs. MEFs transfected with OMA1-specific or scrambled (Scr) siRNA were incubated after 48 hrs with 20  $\mu$ M CCCP or after 60 hours with 2  $\mu$ M oligomycin for the indicated time periods. Cell lysates were analyzed by SDS-PAGE and immunoblotted with antibodies directed against OPA1 and CII.

**A**



**B**



**C**

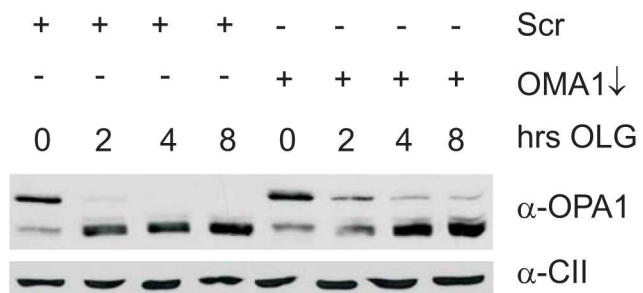
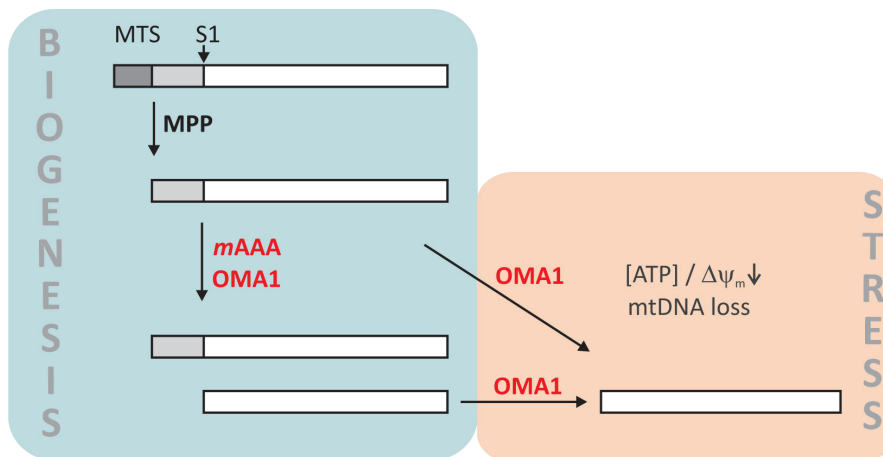




Figure 8. Two peptidases regulate OPA1 cleavage at S1.

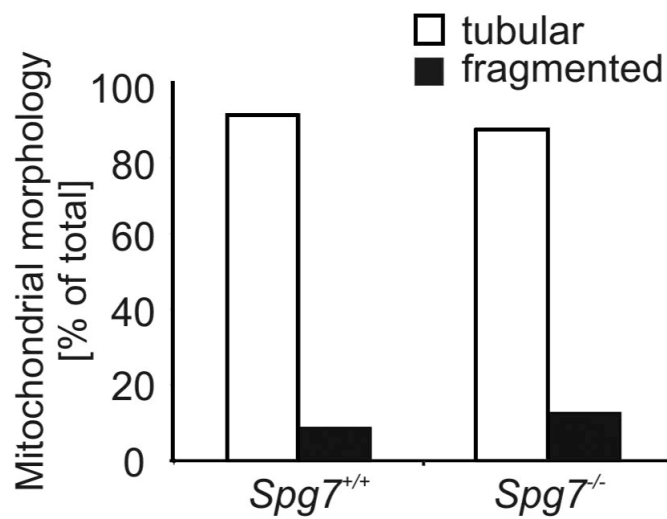
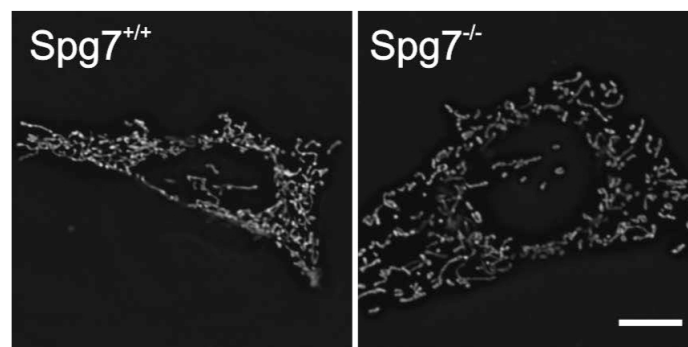
Newly imported OPA1 molecules are processed by the mitochondrial processing peptidase (MPP) in the matrix space (Ishihara et al., 2006). The stability of long OPA1 isoforms depends on *m*-AAA protease isoenzymes containing AFG3L1 and AFG3L2, which ensure the balanced formation of long and short OPA1 isoforms upon S1 cleavage and maintain mitochondrial fusion. The *m*-AAA protease itself may act as a processing peptidase for OPA1 or promote constitutive cleavage by OMA1. At decreased mitochondrial ATP levels, after dissipation of  $\Delta\Psi_m$ , or in the absence of mtDNA OMA1 promotes stress-induced OPA1 processing resulting in the complete conversion of long OPA1 isoforms to short variants. Constitutive cleavage of OPA1 at site 2 is not shown.



## Supplemental Figure Legends

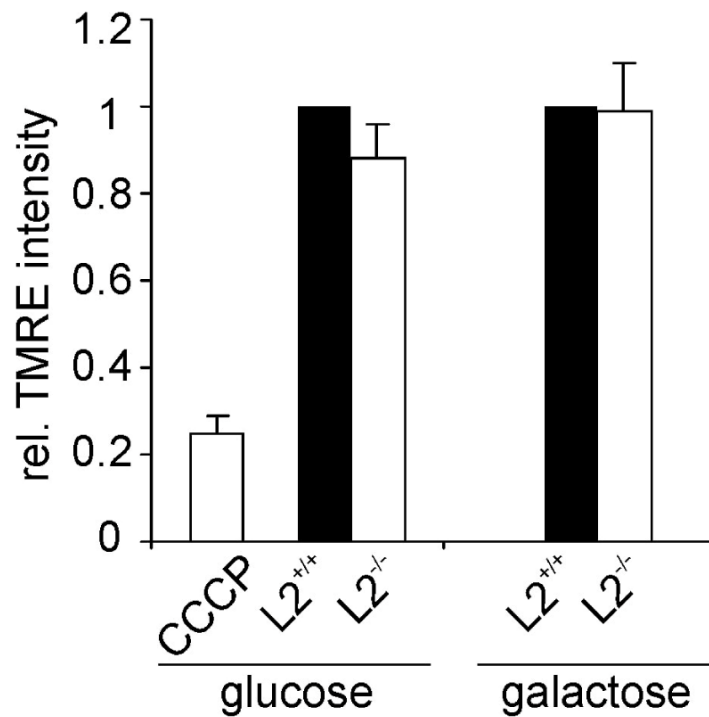
### Supplemental Figure S1.

Mitochondrial morphology in paraplegin-deficient MEFs. Mitochondria were visualized in *Spg7*<sup>+/+</sup> and *Spg7*<sup>-/-</sup> MEFs after transient transfection with mito-dsRed. >150 cells were scored and classified into classes containing tubular or fragmented mitochondria. Bar, 10  $\mu$ m.



Supplemental Figure S2.

Maintenance of the mitochondrial membrane potential in *Afg3l2*<sup>-/-</sup> mitochondria. Mitochondria were isolated from wild type (*L2*<sup>+/+</sup>) and *Afg3l2*<sup>-/-</sup> (*L2*<sup>-/-</sup>) MEFs cultured on glucose- or galactose-containing medium and stained with the fluorescent dye TMRE. Fluorescence intensity in wild type mitochondria was set to 1. For control, the membrane potential was dissipated by adding CCCP (2  $\mu$ M) when indicated. Data represent means  $\pm$  SD of at least four independent experiments.



*Supplemental Figure S3.*

**(A-B)** OPA1 stability in AFG3L1/AFG3L2-deficient cells lacking mitochondrial proteases. AFG3L1 and AFG3L2 were downregulated in *Par1*<sup>-/-</sup>-MEFs and *HtrA2*<sup>-/-</sup>-MEFs (A). MEFs were transfected with specific siRNA against YME1L1, LON, AFG3L1/AFG3L2 or scrambled siRNA as indicated (B). Cell lysates were analyzed by immunoblotting with the following antibodies:  $\alpha$ -YME1L1 (ProteinTech Group, Inc.),  $\alpha$ -LON,  $\alpha$ -OPA1 and  $\alpha$ -CII. \* unspecific crossreaction. **(C)** Inhibition of cytosolic protein synthesis alleviates the accumulation of OPA1 isoforms in *m*-AAA protease deficient MEFs in the presence of MG132. Cells depleted of AFG3L1 and AFG3L2 were transfected with the Flag-tagged OPA1 variant v1 $\Delta$ S1. After 48 hrs cells, cells were incubated in the presence of MG132 (5  $\mu$ M) for 30 min before CHX (100  $\mu$ g/ml) was added. After a further incubation for 4.5 hrs cell extracts were analyzed by SDS-PAGE and immunoblotting using antibodies directed against the Flag-epitope and, for control, and the 70 kDa subunit of complex II (CII). p, OPA1 precursor; b, long OPA1 isoform.

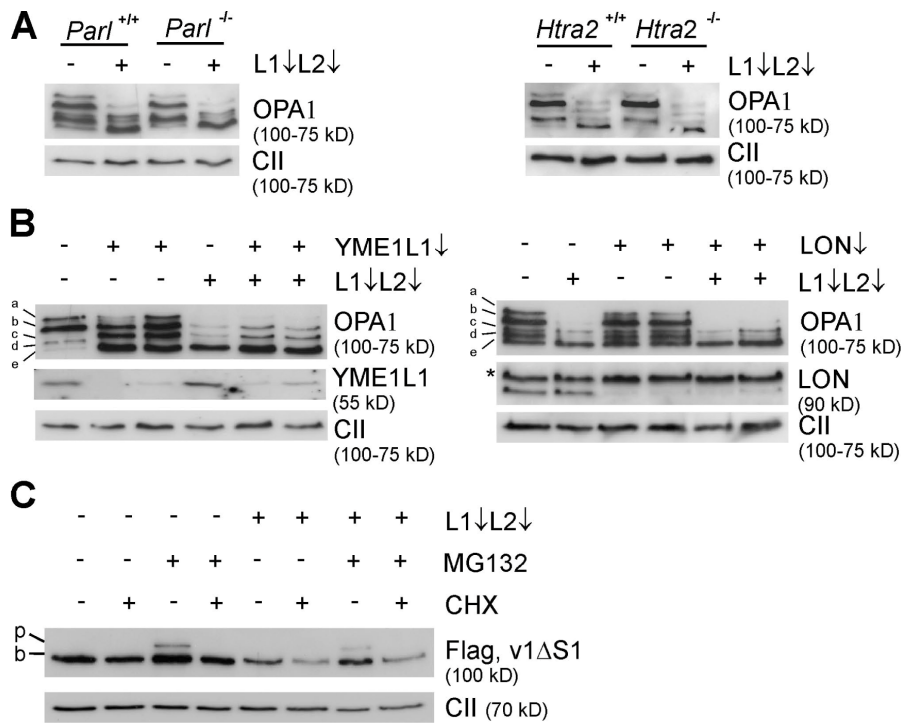


*Figure S4.*

Functional interplay of OMA1 and *m*-AAA protease complexes. **(A)** OMA1 mRNA levels in MEFs after down-regulation of OMA1. MEFs were transfected with three different OMA1 siRNAs, and mRNA levels were determined by quantitative real-time PCR with the Roche Light Cycler system using the primers 5'-AGTGGATACAGTCAAAGTTGCAG-3' and 5'-GTTTGAGAGCCTGTGGTATGAG-3'. OMA1 mRNA expression levels were normalized to GAPDH mRNA determined with the primers 5'-TCCACCACCACCTGTTGCTGTA-3' and 5'-ACCACAGTCCATGCCATCAC-3' and are shown relative to WT levels in untreated cells. **(B)** Assembly of AFG3L2 (L2) and AFG3L1 (L1) in *m*-AAA protease complexes in OMA1-deficient mitochondria. Mitochondria were isolated from MEFs grown in glucose-containing medium, which had been transfected with scrambled (scr) or OMA1-specific siRNA. After solubilization of mitochondrial membranes in 10 g digitonin/g, extracts were analyzed by blue-native gel electrophoresis (3–13% [wt/vol]) and analyzed by immunoblotting using antisera directed against AFG3L1 and -2, consecutively, and HSP60 and subunit 1 of complex IV (CIV; Invitrogen) for control. 649-kD thyroglobulin and 440-kD ferritin were used as molecular standards. The asterisk refers to a cross-reacting band. **(C)** Accumulation of OMA1 in *m*-AAA protease-deficient mitochondria. OMA1 carrying a C-terminal myc epitope was expressed from pcDNA3 under the control of the cytomegalovirus promoter and transiently expressed in MEFs. Cells

were transfected with scrambled or AFG3L1- and/or AFG3L2-specific siRNAs as indicated. Cell extracts were analyzed by SDS-PAGE and immunoblotting using antisera directed against AFG3L1 and -2, the myc epitope, and, as a loading control, SLP-2.

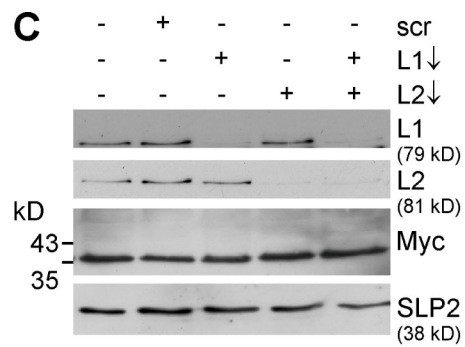
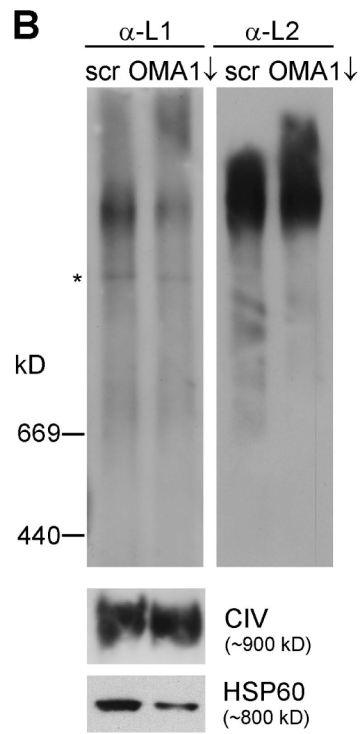
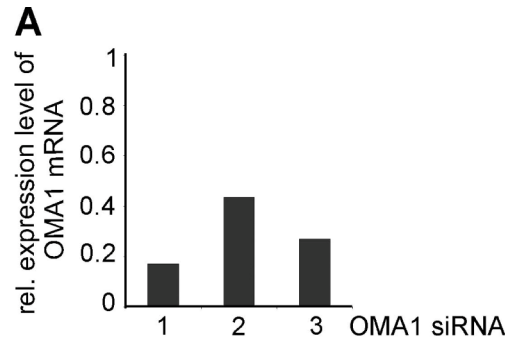
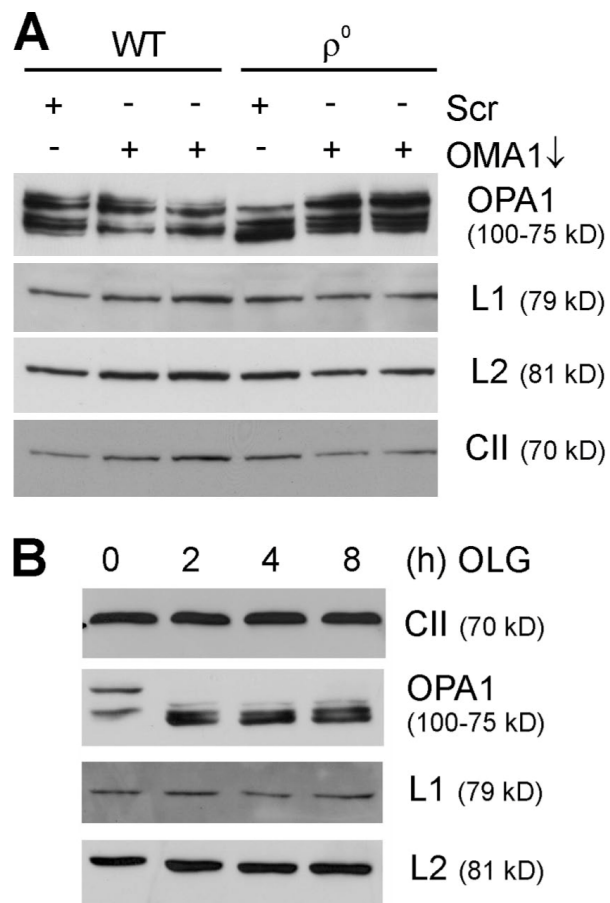




Figure S5.

Down-regulation of OMA1 does not affect the accumulation of AFG3L1 and -2 in mitochondria. (A) Mitochondria were isolated from WT MEFs and of MEFs lacking mtDNA ( $\rho^0$ ). (B) WT mitochondria were treated with 2  $\mu$ M oligomycin (OLG) for the indicated time periods. Mitochondrial extracts were analyzed by SDS-PAGE and immunoblotting using antisera directed against AFG3L1 (L1), AFG3L2 (L2), OPA1, and, as a loading control, the 70-kD subunit of complex II (CII).



## References

- Akepati, V.R., E.C. Muller, A. Otto, H.M. Strauss, M. Portwich, and C. Alexander. 2008. Characterization of OPA1 isoforms isolated from mouse tissues. *J. Neurochem.* 106:372-383.
- Amati-Bonneau, P., D. Milea, D. Bonneau, A. Chevrollier, M. Ferre, V. Guillet, N. Gueguen, D. Loiseau, M.A. Crescenzo, C. Verny, V. Procaccio, G. Lenaers, and P. Reynier. 2009. OPA1-associated disorders: Phenotypes and pathophysiology. *Int. J. Biochem. Cell Biol.* in press.
- Augustin, S., Gerdes, F., Lee, S., Tsai, F.T.F., Langer, T., and Tatsuta, T. (2009). An intersubunit signalling network coordinates ATP-hydrolysis by *m*-AAA proteases. *Mol. Cell.* 10: 457-468.
- Bao, Y.C., H. Tsuruga, M. Hirai, K. Yasuda, N. Yokoi, T. Kitamura, and H. Kumagai. 2003. Identification of a human cDNA sequence which encodes a novel membrane-associated protein containing a zinc metalloprotease motif. *DNA Res.* 10:123-128.
- Baricault, L., B. Segui, L. Guegand, A. Olichon, A. Valette, F. Larminat, and G. Lenaers. 2007. OPA1 cleavage depends on decreased mitochondrial ATP level and bivalent metals. *Exp. Cell Res.* 313:3800-3808.
- Cagnoli, C., G. Stevanin, A. Durr, P. Ribai, S. Forlani, A. Brussino, P. Pappi, L. Pugliese, M. Barberis, R.L. Margolis, S.E. Holmes, S. Padovan, N. Migone, D. Di Bella, F. Taroni, A. Brice, and A. Brusco. 2008. Mutations in AFG3L2 gene (SCA28) in autosomal

dominant cerebellar ataxias. *In* Annual meeting of the American Society of Human Genetics, Philadelphia, Pennsylvania.

- Casari, G., M. De-Fusco, S. Ciarmatori, M. Zeviani, M. Mora, P. Fernandez, G. DeMichele, A. Filla, S. Coccozza, R. Marconi, A. Durr, B. Fontaine, and A. Ballabio. 1998. Spastic paraplegia and OXPHOS impairment caused by mutations in paraplegin, a nuclear-encoded mitochondrial metalloprotease. *Cell*. 93:973-983.
- Cervený, K.L., Y. Tamura, Z. Zhang, R.E. Jensen, and H. Sesaki. 2007. Regulation of mitochondrial fusion and division. *Trends Cell Biol*. 17:563-569.
- Cipolat, S., T. Rudka, D. Hartmann, V. Costa, L. Serneels, K. Craessaerts, K. Metzger, C. Frezza, W. Annaert, L. D'Adamio, C. Derks, T. Dejaegere, L. Pellegrini, R. D'Hooge, L. Scorrano, and B. De Strooper. 2006. Mitochondrial rhomboid PARL regulates cytochrome c release during apoptosis via OPA1-dependent cristae remodeling. *Cell*. 126:163-175.
- Dalal, S., M.F. Rosser, D.M. Cyr, and P.I. Hanson. 2004. Distinct roles for the AAA ATPases NSF and p97 in the secretory pathway. *Mol. Biol. Cell*. 15:637-648.
- Delettre, C., J.M. Griffoin, J. Kaplan, H. Dollfus, B. Lorenz, L. Faivre, G. Lenaers, P. Belenguer, and C.P. Hamel. 2001. Mutation spectrum and splicing variants in the *OPA1* gene. *Hum. Genet*. 109:584-591.
- DiBella, D., F. Lazzaro, A. Brusco, G. Battaglia, P. A., A. Finardi, V. Fracasso, M. Plumari, C. Cagnoli, F. Tempia, A. Brussino, C.

Gellera, C. Mariotti, P. Plevani, S. DiDonato, T. Langer, M. Muzi-Falconi, and F. Taroni. 2008. AFG3L2 mutations cause autosomal dominant ataxia SCA28 and reveal an essential role of the m-AAA AFG3L2 homocomplex in the cerebellum. *In* Annual meeting of the American Society of Human Genetics, Philadelphia, Pennsylvania.

Duvezin-Caubet, S., R. Jagasia, J. Wagener, S. Hofmann, A. Trifunovic, A. Hansson, A. Chomyn, M.F. Bauer, G. Attardi, N.G. Larsson, W. Neupert, and A.S. Reichert. 2006. Proteolytic processing of OPA1 links mitochondrial dysfunction to alterations in mitochondrial morphology. *J. Biol. Chem.* 281:37972-37979.

Duvezin-Caubet, S., M. Koppen, J. Wagener, M. Zick, L. Israel, A. Bernacchia, R. Jagasia, E.I. Rugarli, A. Imhof, W. Neupert, T. Langer, and A.S. Reichert. 2007. OPA1 processing reconstituted in yeast depends on the subunit composition of the m-AAA protease in mitochondria. *Mol. Biol. Cell.* 18:3582-3590.

Ferreirinha, F., A. Quattrini, M. Priozi, V. Valsecchi, G. Dina, V. Broccoli, A. Auricchio, F. Piemonte, G. Tozzi, L. Gaeta, G. Casari, A. Ballabio, and E.I. Rugarli. 2004. Axonal degeneration in paraplegin-deficient mice is associated with abnormal mitochondria and impairment of axonal transport. *J. Clin. Invest.* 113:231-242.

Frezza, C., S. Cipolat, O. Martins de Brito, M. Micaroni, G.V. Beznoussenko, T. Rudka, D. Bartoli, R.S. Polishuck, N.N. Danial, B. De Strooper, and L. Scorrano. 2006. OPA1 controls apoptotic

cristae remodeling independently from mitochondrial fusion.  
*Cell*. 126:177-189.

Griparic, L., T. Kanazawa, and A.M. van der Bliek. 2007. Regulation of the mitochondrial dynamin-like protein Opa1 by proteolytic cleavage. *J. Cell Biol.* 178:757-764.

Griparic, L., N.N. van der Wel, I.J. Orozco, P.J. Peters, and A.M. van der Bliek. 2004. Loss of the intermembrane space protein Mgm1/OPA1 induces swelling and localized constrictions along the lengths of mitochondria. *J. Biol. Chem.* 279:18792-18798.

Herlan, M., C. Bornhovd, K. Hell, W. Neupert, and A.S. Reichert. 2004. Alternative topogenesis of Mgm1 and mitochondrial morphology depend on ATP and a functional import motor. *J. Cell Biol.* 165:167-173.

Hoppins, S., L. Lackner, and J. Nunnari. 2007. The machines that divide and fuse mitochondria. *Annu. Rev. Biochem.* 76:751-780.

Ishihara, N., Y. Fujita, T. Oka, and K. Mihara. 2006. Regulation of mitochondrial morphology through proteolytic cleavage of OPA1. *EMBO J.* 25:2966-2977.

James, D.I., P.A. Parone, Y. Mattenberger, and J.C. Martinou. 2003. hFis1, a novel component of the mammalian mitochondrial fission machinery. *J. Biol. Chem.* 278:36373-36379.

Käser, M., M. Kambacheld, B. Kisters-Woike, and T. Langer. 2003. Oma1, a novel membrane-bound metallopeptidase in mitochondria with activities overlapping with the *m*-AAA protease. *J. Biol. Chem.* 278:46414-46423.

- Koppen, M., M.D. Metodiev, G. Casari, E.I. Rugarli, and T. Langer. 2007. Variable and Tissue-Specific Subunit Composition of Mitochondrial *m*-AAA Protease Complexes Linked to Hereditary Spastic Paraplegia. *Mol. Cell. Biol.* 27:758-767.
- Koppen, M., Bonn, F., Ehses, S., and Langer, T. (2009). Autocatalytic processing of *m*-AAA protease subunits in mitochondria. *Mol. Biol. Cell.* in press.
- Kremmidiotis, G., A.E. Gardner, C. Settasatian, A. Savoia, G.R. Sutherland, and D.F. Callen. 2001. Molecular and functional analyses of the human and mouse genes encoding AFG3L1, a mitochondrial metalloprotease homologous to the human spastic paraplegia protein. *Genomics.* 76:58-65.
- Lenaers, G., P. Reynier, G. Elachouri, C. Soukkarieh, A. Olichon, P. Belenguer, L. Baricault, B. Ducommun, C. Hamel, and C. Delettre. 2009. OPA1 functions in mitochondria and dysfunctions in optic nerve. *Int. J. Biochem. Cell Biol.* in press.
- Maltecca, F., A. Aghaie, D.G. Schroeder, L. Cassina, B.A. Taylor, S.J. Phillips, M. Malaguti, S. Previtali, J.L. Guenet, A. Quattrini, G.A. Cox, and G. Casari. 2008. The mitochondrial protease AFG3L2 is essential for axonal development. *J. Neurosci.* 28:2827-2836.
- Martinelli, P., V. La Mattina, A. Bernacchia, R. Magnoni, F. Cerri, G. Cox, A. Quattrini, G. Casari, and E.I. Rugarli. 2009. Genetic interaction between the *m*-AAA protease isoenzymes reveals novel roles in cerebellar degeneration. *Hum Mol Genet.* 18:2001-2013.

- Meeusen, S., R. DeVay, J. Block, A. Cassidy-Stone, S. Wayson, J.M. McCaffery, and J. Nunnari. 2006. Mitochondrial inner-membrane fusion and crista maintenance requires the dynamin-related GTPase Mgm1. *Cell*. 127:383-395.
- Merkwirth, C., S. Dargazanli, T. Tatsuta, S. Geimer, B. Lower, F.T. Wunderlich, J.C. von Kleist-Retzow, A. Waisman, B. Westermann, and T. Langer. 2008. Prohibitins control cell proliferation and apoptosis by regulating OPA1-dependent cristae morphogenesis in mitochondria. *Genes Dev*. 22:476-488.
- Olichon, A., L. Baricault, N. Gas, E. Guillou, A. Valette, P. Belenguer, and G. Lenaers. 2003. Loss of OPA1 perturbs the mitochondrial inner membrane structure and integrity, leading to cytochrome c release and apoptosis. *J. Biol. Chem*. 278:7743-7746.
- Osman, C., M. Haag, C. Potting, J. Rodenfels, P.V. Dip, F.T. Wieland, B. Brugger, B. Westermann, and T. Langer. 2009. The genetic interactome of prohibitins: coordinated control of cardiolipin and phosphatidylethanolamine by conserved regulators in mitochondria. *J. Cell Biol*. 184:583-596.
- Shimohata, N., S. Chiba, N. Saikawa, K. Ito, and Y. Akiyama. 2002. The Cpx stress response system of Escherichia coli senses plasma membrane proteins and controls HtpX, a membrane protease with a cytosolic active site. *Genes Cells*. 7:653-662.
- Smirnova, E., D.L. Shurland, S.N. Ryazantsev, and A.M. van der Bliek. 1998. A human dynamin-related protein controls the distribution of mitochondria. *J. Cell Biol*. 143:351-358.

- Song, Z., H. Chen, M. Fiket, C. Alexander, and D.C. Chan. 2007. OPA1 processing controls mitochondrial fusion and is regulated by mRNA splicing, membrane potential, and Yme1L. *J. Cell Biol.* 178:749-755.
- Tatsuta, T., S. Augustin, M. Nolden, B. Friedrichs, and T. Langer. 2007. *m*-AAA protease-driven membrane dislocation allows intramembrane cleavage by rhomboid in mitochondria. *EMBO J.* 26:325-335.
- Tondera, D., S. Grandemange, A. Jourdain, M. Karbowski, Y. Mattenberger, S. Herzig, S. Da Cruz, P. Clerc, I. Raschke, C. Merkwirth, S. Ehses, F. Krause, D.C. Chan, C. Alexander, C. Bauer, R. Youle, T. Langer, and J.C. Martinou. 2009. SLP-2 is required for stress-induced mitochondrial hyperfusion. *EMBO J.* 28:1589-1600.
- Weibezahn, J., C. Schlieker, B. Bukau, and A. Mogk. 2003. Characterization of a trap mutant of the AAA+ chaperone ClpB. *J. Biol. Chem.* 278:32608-32617.
- Westermann, B. 2008. Molecular machinery of mitochondrial fusion and fission. *J. Biol. Chem.* 283:13501-13505.



**Alternative splicing of Spg7, a gene involved in Hereditary Spastic Paraplegia, encodes a variant of Paraplegin targeted to the Endoplasmic Reticulum.**

G. Mancuso<sup>1,2</sup>, P. Crivello<sup>2</sup> and E. I. Rugarli<sup>1,2,3</sup>

<sup>1</sup> Biocenter, University of Cologne, Cologne, Germany

<sup>2</sup> Laboratory of Genetic and Molecular Pathology, Istituto Nazionale Neurologico „C.Besta”, Milano, Italy;

<sup>3</sup> Department of Neuroscience and Medical Biotechnologies, University of Milano-Bicocca, Milan, Italy;

*Submitted*

## Abstract

Hereditary spastic Paraplegia (HSP) is a group of heterogeneous genetic diseases characterized by weakness and spasticity of the lower limbs due to distal axonal degeneration of corticospinal axons. 4% of recessive familial cases and 12% of sporadic cases of HSP are caused by mutation in the SPG7 gene. Paraplegin, the product of SPG7, is part of the *m*-AAA protease, a hexameric complex that resides inside the mitochondrial inner membrane. This complex performs quality control system by degrading in a selective manner non-assembled and damaged polypeptides. Moreover, the *m*-AAA protease is also responsible for maturation of specific substrates. We show here the existence of a novel isoform of Paraplegin (Paraplegin2) encoded by alternative splicing of *Spg7*. Paraplegin2 lacks the mitochondrial targeting sequence, but is identical to mature Paraplegin in mitochondria. Due to the presence of two transmembrane domains in the N-terminal region, Paraplegin 2 is anchored to the endoplasmic reticulum (ER) membrane and exposes its catalytic domain inside the lumen. In addition, we show that Paraplegin2 forms a high molecular weight complex in brain microsomes. Finally, we show that Paraplegin2 interacts with Seipin, an ER protein involved in lipid droplets formation and mutated in an autosomal dominant form of HSP. This interaction, the existence of several other ER proteins involved in HSP, and the fact that this alternative splicing is conserved in humans hint to a possible new role of SPG7 in the pathogenesis of the disease.

## Introduction

Hereditary Spastic Paraplegia (HSP) is a group of diseases characterized by progressive spasticity and weakness of the lower limbs due to the relentless retrograde degeneration of cortical motor neuron axons [1]. The age of onset is variable, from early childhood to 70 years of age [2]. HSPs are genetically heterogeneous: they can be inherited as autosomal dominant, autosomal recessive or X-linked forms and many proteins, with very different function and subcellular localization, have been associated with this group of diseases [3]. Recently the functional characterization of several HSP proteins like REEP1, Spastin, Atlastin [4, 5], NIPA1 [5, 6] and Seipin [7] has linked this disease to alteration of the endoplasmic reticulum (ER) morphogenesis and to ER stress. Another group of HSP genes encodes for mitochondrial proteins, like Paraplegin [8] and HSP60 [9]. The pathogenetic mechanism that connects alterations in different subcellular organelles to the same axonal degeneration process is still not clear.

Paraplegin is the product of the SPG7 gene, mutations in which cause 4% of recessive familial cases of HSP[10] and 12% of sporadic cases [11]. This protein is part of the *m*-AAA protease, a key component of a quality control system that conducts the surveillance of proteins of the inner membrane of mitochondria by degrading in a selective manner non-assembled and damaged polypeptides. The first characterization of this protease was performed in *S. Cerevisiae* and described the *m*-AAA as a hetero-oligomeric complex composed by

highly homologous subunits (Yta10p and Yta12p) [12]. In mammals three different components are known as part of *m*-AAA complex: Paraplegin [8], AFG3L2 [13] and AFG3L1, even if the last one is only present as a pseudogene in humans [14]. Yeast and mammalian subunits of the *m*-AAA protease contain an N-terminal mitochondrial targeting sequence (MTS), two transmembrane domains, a AAA domain (ATPase Associated with various cellular Activities) and a C-terminal metal-dependent proteolytic domain. The AAA domain defines the superfamily of AAA+ proteins, a group of ATPases characterized by a conserved region of 220-250 amino acids called AAA cassette [15]. The protease owes its name to the presence of this domain and to the topology of the proteolytic domain that is exposed towards the matrix space of mitochondria. The *m*-AAA complex actively extracts transmembrane segments and pull solvent-exposed domains across the membrane before exerting proteolytic activity [16, 17]. In addition, a more recent function attributed to yeast *m*-AAA protease involves its ability to mediate proteolytic maturation of specific proteins like the mitochondrial ribosomal component MrpL32 [18], opening a complete new perspective on the role of this complex in cell metabolism.

In contrast to yeast, where the *m*-AAA protease is only present as a hetero-oligomeric complex, in mammals AFG3L2 and AFG3L1 can also assemble into homo-oligomeric complexes. This homo-assembling ability was never reported for Paraplegin [18, 19]. Notably, both homo- and hetero-oligomeric complexes are able to process the ribosomal subunit MrpL32 and to mediate degradation of non-native

membrane proteins in a reconstituted yeast system, demonstrating functional complementation. Even if these experiments highlight a functional redundancy among the complexes, it is important to underline that the *m*-AAA subunits are differently expressed in tissues and that these differences in expression levels could lead to tissue-specific functions [19, 20]. An *Spg7*<sup>-/-</sup> mouse model was previously generated by deletion of the first two exons of the gene by homologous recombination. These mice show motor impairments at the rotarod test at 4.5 months and abnormal movements of the hindlimbs due to late-onset retrograde axonal degeneration in long descending motor spinal tracts, long ascending sensory spinal tracts and peripheral and optic nerves, resembling the HSP phenotype. Moreover, ultrastructural analysis reveal the presence of structural abnormal mitochondria in spinal cord axons, alterations that become more pronounced with aging [21]. Intramuscular delivering of SPG7 gene through AAV vectors in knock-out mice stop the progression of neuropathological change and rescues mitochondrial morphology [22].

In this work, we identified a novel splicing isoform for Paraplegin that starts from an upstream alternative first exon and splice directly on exon 2 or 3. This protein isoform does not possess a MTS and localizes to the ER, where it exposes its catalytic domain inside the lumen. Furthermore we show that this Paraplegin isoform can interact with Seipin, when both proteins are overexpressed. The presence of this protein in mouse tissues opens up to new roles of Paraplegin in HSP pathogenesis.

## Results:

### *1. An alternative Paraplegin isoform localizes to the Endoplasmic Reticulum.*

The *Spg7* gene is located on chromosome 8 and composed by 17 exons. Bioinformatic tools allowed us to find an alternative first exon for this gene (exon 1b) located around 2,5 Kb upstream of the previously described exon 1 (from now, exon 1a). A complete cDNA starting from exon 1b (BC055488) was cloned from retina library. Moreover, six different Expressed Sequence Tags (ESTs) starting from this alternative exon and splicing directly on exon 2 or 3 are present in the UCSC database: BG261783, BI732145, BG293510, CO425637, BU504990 and BG293225 (Figure 1, A). These ESTs also derive from eye and retina libraries, but were obtained from different developmental stages.

As a first step we analyzed the expression of these alternative splicing isoforms using a RT-PCR approach (Figure 1, B). Our results suggest that the alternative splicing occurs in all the analyzed tissues, even if the ratio between the splicing ex1b-2 and ex1b-3 seems to present a some tissue variability. Notably the eye presents a strong amplification signal for both the alternative splicing variants.

Paraplegin is encoded starting from the AUG present on exon 1a. The first and the second exons are responsible for the synthesis of the MTS of the protein. After import, MTS is cleaved away by the action of Mitochondrial Processing Peptidase (MPP) and of the *m*-AAA itself, leading to a mature protein that starts from Methionine 106 [23].

Remarkably, the first in-frame AUG found in the alternative splicing isoforms resides on exon 3 and encodes for the Methionine 106 of the mitochondrial protein, the first N-terminal amino acid after protein maturation, indicating that the protein encoded by the alternative mRNA is identical to the mature mitochondrial paraplegin. We therefore predicted that the alternative protein loses its mitochondrial localization, without alteration in the protein structure. From now, we will refer to this alternative protein as Paraplegin2.

To analyze the localization of Paraplegin2 in living cells, we transfected Mouse Embryonic Fibroblasts (MEFs) with the BC055488 clone and we performed an immunofluorescence assay using a specific  $\alpha$ -Paraplegin antibody (V61) [21], comparing the results with the one obtained by Paraplegin overexpression (Figure 2, A-F). As expected, the signal for Paraplegin completely overlaps with the mitochondrial marker (Figure 2, A-C) while the one for Paraplegin2 do not, assuming a more reticular pattern (Figure 2, D-F).

Like Paraplegin, also Paraplegin2 presents two transmembrane domains located in the N-terminal of the protein. For this reason, we decided to check the possibility that the protein resides inside membranes of the secretory pathways. We transfected the BC055488 clone and labelled both Endoplasmic Reticulum (ER) and Golgi apparatus using two specific markers (Figure 2, G-L). We found a complete co-localization between ER protein Calnexin and Paraplegin2 signals, indicating that overexpressed Paraplegin2

localizes to the ER. Notably, we can also detect a partial co-localization with the Golgi apparatus protein GM130.

## *2. The catalytic domain of Paraplegin2 is exposed inside ER lumen.*

In mitochondria Paraplegin is inserted into the inner membrane and exposes its catalytic domain in the mitochondrial matrix. This topology plays a crucial role on the function of the protein, determining accessibility only to a specific subset of targets and substrates [16-18]. To investigate the topology of Paraplegin2, we performed a live imaging Fluorescence Protease Protection (FPP) assay on MEF cells [24]. In this assay Proteinase K is used to disrupt GFP signal obtained from proteins that are not protected by organelle membranes. We transfected cells using four clones encoding different green fluorescent proteins (GFPs): a GFP resides to cytosol and nuclei, an ER-GFP in which the GFP is fused with a transmembrane domain that links the protein to the external surface of ER membrane [25], a KDEL-GFP which is retained inside ER lumen and a Para2-GFP in which the GFP is fused in frame to the C-terminal of our Paraplegin2 protein. This assay reveals that Para2-GFP fluorescent signal is protected from Proteinase K action and behaves like KDEL-GFP, suggesting that Paraplegin2 exposes its catalytic domain inside ER lumen (Figure 3, A). In addition of fluorescence pattern analysis, we also performed a quantification of GFP fluorescence intensity before and after Proteinase K addition,



corroborating our results in a quantitative matter (Supplementary Figure 1).

To confirm these findings, we performed an SDS-page protection assay. As expected, we see a shift in the gel motility of Para2-GFP after the treatment with the Proteinase K, due to degradation of not-protected N-terminal portion of the protein. Moreover, the signal completely disappears when Triton X-100 is added demonstrating the protective action of ER membrane on Para2-GFP C-terminal portion (Figure 3 B).

These findings suggest that Paraplegin2 resides into the ER membrane and expose its catalytic domain inside ER-lumen (Figure 3, C).

### *3. Paraplegin2 needs a partner to form an high molecular weight complex*

Mitochondrial Paraplegin is part of a high molecular weight complex called *m*-AAA protease. Like most AAA+ proteins, Paraplegin needs to form an hexamer to be active and hydrolyze ATP [26]. Differently from AFG3L2 and AFG3L1, Paraplegin seems to be unable to homo-oligomerize into a functional *m*-AAA protease complex [18, 19]. As far as we know, no alternative isoform for AFG3L2 and AFG3L1 are predicted to be found outside mitochondria. To address whether Paraplegin2 is part of a high molecular weight complex we performed a gel filtration assay transfecting Paraplegin2 cDNA into COS7 cells. As control, mitochondrial Paraplegin cDNA was also transfected.

Transfection of both Paraplegin and Paraplegin2 alone do not lead to the formation of high molecular weight complexes (Figure 4, A), suggesting that the presence or the amount of an interacting partner is limiting in these conditions. We therefore repeat the experiment in same conditions, but co-expressing AFG3L2 and we show the formation of the *m*-AAA complex for mitochondrial Paraplegin (Figure 4, B), but still the absence of a complex formed by Paraplegin2. These data suggest that Para2 is unable to form a homo-oligomeric complex in the ER without the presence or the right amount of a specific interacting partner (Figure 4, B).

*4. Paraplegin2 is endogenously synthesized in mouse brain and forms an high molecular weight complex.*

As suggested by previous experiments, overexpression is not the right condition to use for functional studies on Paraplegin2, so we decided to look for endogenous protein.

For this purpose, we isolated mitochondrial and microsomal fractions from mouse brain using different centrifugation steps and we probed this samples with V61 antibody (Figure 5, A). In the microsomal fraction the antibody recognizes a protein that has the expected molecular weight and co-migrates with mature Paraplegin. Notably, no microsomal signals were detected for AFG3L2 nor 70 kDa subunit of Complex II, demonstrating that our fraction is free from mitochondrial contaminations (Figure 5, A).

To assess if on physiological condition Paraplegin2 is able to form a high molecular weight complex, we use the same purified fractions to perform another gel filtration assay. The results showed the presence of a high molecular weight complex in the mitochondrial fraction, formed by Paraplegin, but also a complex in the microsomal fraction corresponding to the molecular weight of the band that V61 antibody reveals on SDS-page (Figure 5, B).

We can conclude that Paraplegin2 is endogenously synthesized in mouse brain even if it appears less abundant than Paraplegin. Moreover, this protein forms an high molecular weight complex under physiological conditions.

##### *5. Paraplegin2 interacts with Seipin, an ER protein involved in HSP.*

Recently, several genes involved in ER morphogenesis and stress have been linked to HSPs [4-7]. BSCL2 is one of these genes and it encodes for Seipin. A particular subset of mutations in this protein, targeting two different glycosylation sites (N88S and S90L), leads to accumulation of misfolded Seipin in the ER and cause cell death through Unfolded Protein Response (UPR) and ER stress pathway [27]. In mitochondria, Paraplegin plays a key role in misfolded protein degradation and protein quality control, so we decided to check if Paraplegin2 could have the same function in the ER and we postulated it may recognize Seipin as a substrate.

First of all we confirmed that both proteins localize to the ER in transfected COS7 cells using an immunofluorescence assay (Figure 6, A).

To clarify if they are not only localized in the same organelle, but also able to interact with each other, we performed an immunoprecipitation assay on COS7 cells overexpressing Paraplegin2 and a N-terminal myc tagged Seipin (myc-Seipin). First sets of immunoprecipitations were performed pulling down Seipin with  $\alpha$ -myc antibody and revealing with  $\alpha$ -Paraplegin2 V61. This experiment clearly reveals that in this conditions the two protein can be co-immunoprecipitated (Figure 6, B). Similarly,  $\alpha$ - Paraplegin V61 is able to pull down myc-Seipin (Figure 6, C). Finally, we performed a third set of immunoprecipitation adding to the experiment the mutated form of Seipin (N88S). Interestingly Paraplegin2 myc-Seipin interaction results to be not affected by mutation in Seipin glycosylation site (N88S) (Figure 6, D). Moreover, this interaction is specific for Paraplegin2 and cannot be reproduced using Paraplegin (Figure 6, D).

These last findings suggest that Paraplegin2 and Seipin interact upon overexpression, opening to new possibilities for the role of SPG7 in HSP pathogenesis.

## **Materials and methods:**

### *1. RT-PCR and cloning.*

Amplification of the alternative splicing isoform of Spg7 was obtained by RT-PCR using these oligos:

Ex1-bis 5'-GAGGAAGCCAGCCACGAGGTG-3',

Ex4 5'-GAGGGAGTTCAGCAGGCTCATG-3'.

RNA was isolated from mouse tissue using TRIzol Kit (Invitrogen) and retro translated into cDNA using SuperScript kit (Invitrogen). For GAPDH amplification we used these oligos:

FW 5'-ATGGAAATCCCATCACCATCTT-3',

REV 5'-CGCCCCACTTGATTTTGG-3'.

BC055488 clone was ordered from imaGenes (IRAKp961N10120Q).

Generation of Para2-GFP construct was made by amplification of Paraplegin2 cDNA from BC055488 clone using these oligos:

FW 5'-TTCTCGAGAACACCTCAAGGATGAAGCAG-3',

REV 5'-TTGGATCCCGGGAGCCGGAGCCTCCTC-3'.

The amplified cDNA was then cloned 5' and in-frame to the GFP cDNA of pEGFP n°2 vector (Clontech). MYC-Seipin vectors, wild-type and mutants, were kindly gifts of professor C. Blackstone.

### *2. Immunofluorescence analysis and live imaging microscopy.*

MEF and COS7 cells were cultured on DMEM with 10% Fetalclone III serum (Hyclone) and transiently transfected for 24 hours using Lipofectamine2000 (Invitrogen). Immunofluorescence assays were performed as previously reported [28]. Confocal microscopy was

performed with a Bio-Rad (Hercules, CA, USA) Radiance 2100 confocal microscope at 1024 x 1024-pixel resolution. To perform live imaging FPP assay cultures were transferred to a live cell imaging workstation composed of an inverted microscope (Nikon Eclipse TE2000-S + BD CARV II, Nikon, Melville, NY, USA), a heated (37°C) chamber and a Nikon Plan Apo VC 100X/1.40 oil objective. Images were collected every 5 seconds for 10 minutes using a cooled camera (QUANTEM 512 SC) driven by METAMORPH software (Molecular Devices Ltd, Downingtown, PA, USA). The same software was used for fluorescence quantification measurements.

*3. SDS-page protection assay, subcellular fractionation and gel filtration assay.*

For SDS-page protection assay COS7 cells were transiently transfected with Para2-GFP construct using Lipofectamine2000 and collected after 24 hours. Cells were resuspended into a specific buffer (10 mM Tris-HCl pH=7.4, 10 mM NaCl, 1,5 mM MgCl<sub>2</sub>, 10% w/v Sucrose) and disrupted using a 29g needle. Debris were discarded by centrifugation at 3000g for 3 minutes. The sample was then divided into three aliquots: proteinase K was added to final concentration of 50 µg/ml in two of the three fractions and Triton X-100 was added to a final concentration of 1% into one of these two. All the aliquots were incubated for 15 minutes at 25° C, then the reactions were stopped by adding 2 mM PMSF and all the proteins were loaded on an SDS-page gel and blotted on PVDF membrane (Amersham).

For mitochondria and microsomes purification, mouse brains were homogenized (10 strokes) in 10 volumes/g of wet tissue isolation buffer (220 mM D-Mannitol, 70 mM Sucrose, 20 mM Hepes, 1 mM EDTA and 0,1 % w/v BSA, pH=7.2) using a glass/Teflon pestle. The crude homogenate was sequentially centrifuged at 500g and 1000g for 10' and then supernatant was centrifuged again at 8000g for 10' for mitochondria precipitation. The supernatant fraction obtained from this step was cleaned by two 10' centrifugations at 20000g before performing microsomal precipitation at 150000g for 2 hours. The crude mitochondrial fraction obtained from the first 8000g centrifugation was then resuspended in 6 volumes/g of wet tissue of isolation buffer and purified again with the same 500g, 1000g and 8000g centrifugation steps. Both mitochondrial and microsomal fractions were resuspended in RIPA buffer (50 mM Tris-HCl, 1% w/v NP-40, 0,25% w/v Sodium Deoxicolate, 150 mM NaCl and 1 mM EDTA, pH=7,4) for SDS-page experiments and in GF buffer (30 mM Tris-HCl pH=7,4, 10 mM Mg-acetate, 150 mM K-acetate pH=7,4, 1mM PMSF and 5 mM ATP) for gel filtration assays. Gel filtration analysis were performed as previously reported [19].

#### *4. Immunoprecipitation assay*

For immunoprecipitation assays COS7 cells were transiently transfected using Lipofectamine2000 (Invitrogen) and collected after 24 hours using a scraper. Cell lysis were performed in Triton Buffer (1X PBS, 10% v/v Glycerol, 1mM ATP, 4mM Mg-acetate, 0,5 mM

PMSF, 0,5% v/v Triton X-100). Immunoprecipitations were performed using Protein G sepharose (GE Healthcare) and following manufacturer specifications.

### *5. Antibodies*

V61 rabbit polyclonal antibody [21] was used for Paraplegin and Paraplegin2 staining and immunoprecipitations,  $\alpha$ -AFG3L2 anti peptide polyclonal rabbit antibody [29] was used for AFG3L2, mouse monoclonal  $\alpha$ -70 kDa subunit (Invitrogen) was used for Complex II, rabbit polyclonal Calnexin antibody (Stressgen) was used for Calnexin and ER staining, mouse GM130 antibody (BD transduction laboratories) was used for Golgi staining, polyclonal rabbit  $\alpha$ -GFP antibody (ABcam) was used for GFP and rabbit polyclonal  $\alpha$ -MYC antibody (Sigma) was used for Seipin staining and IPs.



## Discussion:

In this study we discovered a novel isoform of Paraplegin (Paraplegin2) encoded by an alternative splicing of the *Spg7* gene. This protein localizes to the ER where it exposes its ATPase and proteolytic domains inside the lumen.

Several evidences suggest the physiological relevance of Paraplegin2. Firstly, several ESTs and a complete cDNA have been sequenced from different mouse libraries. Moreover, we could amplify *Spg7* mRNA containing exon 1b in all the mouse tissues we analyzed, revealing only differences in the ratio between the isoform with or without exon 2. Since RT-PCR is not a quantitative assay it is difficult to compare the expression levels of the alternative *Spg7* transcripts in different tissues. However, the expression profile of the ESTs suggests an enrichment of Paraplegin 2 in the retina. Secondly, Paraplegin2 is encoded starting from the Methionine 106. This residue corresponds to the N-terminal residue in mature Paraplegin after the MPP/*m*-AAA double cleavage [23], strongly suggesting that the functionality of Paraplegin2 might be preserved. Finally, we showed evidences that Paraplegin2 is endogenously synthesized in mouse brain. This protein accumulates in the microsomal fraction and perfectly co-migrates with Paraplegin on SDS-page.

All AAA+ proteins form functional haxameric complexes after homo-oligomerization or hetero-oligomerization with a highly homologous protein [26]. In mitochondria, Paraplegin hetero-oligomerizes with AFG3L2 and/or AFG3L1 to form the *m*-AAA protease, but it is unable

to homo-oligomerize into a stable complex [18, 19]. We proved that Paraplegin2 behaves in the same way. As a consequence of this, a high molecular weight complex for Paraplegin2 is only visible when the endogenous protein is analyzed, indicating that both the presence and the right levels of a partner are needed to obtain the oligomerization. However, no evidences of alternative ER isoforms of AFG3L2 or AFG3L1 were found and so the identity of the Paraplegin2 partner is still unclear. A candidate for this role could be YME1L1, the gene that encodes for the subunit of the *i*-AAA protease. The role of this complex in mitochondria is closely related with the *m*-AAA protease and YME1L1 presents high sequence and structural homology with Paraplegin, AFG3L1, and AFG3L2 [30, 31]. In databases several ESTs for YME1L1 have been reported in which the first canonical exon is replaced by an alternative one. The protein encoded by these mRNAs has a different N-terminal portion and is predicted to lose its mitochondrial localization. Further studies are needed to clarify if alternative YME1L1 can be the Paraplegin2 partner in the ER. Notably, the two proteins present opposite orientation in the mitochondrial inner membrane, but the N-terminal region of YME1L1 encoded by alternative splicing mRNA is predicted to be very different from the mitochondrial mature one, possibly leading to a change in protein topology.

These data open up to a possible a novel function for Paraplegin2 inside the ER. In mitochondria, Paraplegin and the *m*-AAA protease play a key role in misfolded protein degradation and substrate maturation, so we hypothesize that Paraplegin2 acts in a similar way.

Up to now is not so clear how ER misfolded integral membrane proteins that lack prominent soluble domains are recognized for degradation. In some cases these substrates are recognized directly by E3 ubiquitin ligases [32-34], but the presence of an additional system cannot be excluded. Unfortunately, missing information about Paraplegin2 partner hampers to use an overexpression approach for studying in more details the function of the protein. These aspects could be instead investigated by down-regulation or dominant negative mutant overexpression strategies. Moreover, the interaction of Paraplegin2 and Seipin suggests the possibility that the Paraplegin2 complex might be needed during Seipin folding and assembly [35] or might be required for Seipin N-terminal processing [7], even if we couldn't reproduce these cleavage conditions in our experimental conditions (data not shown). Seipin is the product of the BSCL2 gene and has been shown to be involved in lipid droplet formation [36]. Future studies will be needed to address a possible function of Paraplegin2 in concert with Seipin in this pathway. Finally, Spg7 cause 4% of recessive familial cases of HSP [10] and 12% of sporadic cases [11], so we have to consider possible implications of Paraplegin2 in the pathogenesis of the disease. An alternative splicing of SPG7 is in fact reported also for humans, where two different exons alternative to the canonical one were found. Also in these cases, the protein encoded by these alternative transcripts are predicted to lose the mitochondrial localization. Further analyses are needed to confirm these predictions experimentally, but if a human Paraplegin2 exists we cannot exclude that it plays a role in the

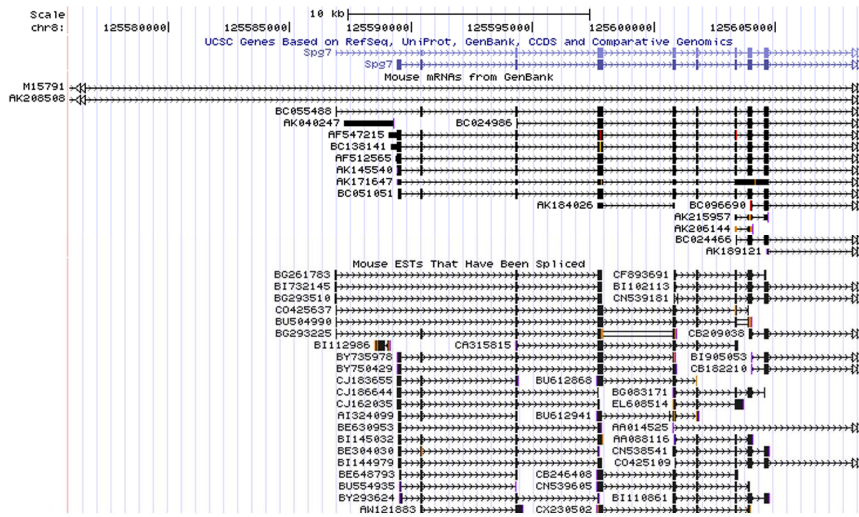
pathogenesis of HSP. A great proportion of SPG7 mutations in fact occurs inside the AAA+ and the proteolytic domains, potentially disrupting the function of both Paraplegin and Paraplegin2. From this point of view, the *Spg7* knock-out mouse previously generated in our laboratories could be a mitochondrial-specific null model. This mouse was generated by deletions of the first two exons of *Spg7* [21], but retains exon 1b and due to the exon 1b-3 splicing can still synthesize Paraplegin2 (data not shown). Even if the mitochondrial dysfunctions caused by the complete loss of Paraplegin are well reassumed in the knock-out model [21], we cannot exclude that the presence of Paraplegin2 leads to a milder or incomplete phenotype. Recently, Seipin and Nipa1 proteins have been linked to HSP through ER stress pathways due to misfolded or aberrant accumulation of mutated polypeptides [6, 27]. Moreover, at least four others HSP associated proteins, including Spastin (encoded by *SPG4*), Atlastin1 (encoded by *SPG3A*), Receptor Expression Enhancing Protein 1 (REEP1; encoded by *SPG31*) and Strumpellin (encoded by *SPG8*), are involved in ER membrane shaping and modeling events. This is an important subgroup, as mutations in the genes encoding these proteins cause up to 60% of HSP cases in North America and northern Europe [37]. These findings suggest that alteration of ER morphogenesis plays a crucial role in HSP pathogenesis and highlight the possibility that also Paraplegin2 may contribute to these pathways.

## Figure legends:

### *Figure 1:*

(A) A print-out of UCSC genome browser shows the existence of a complete *Spg7* cDNA (BC055488) and six different ESTs starting from an upstream alternative exon (Exon 1b). These ESTs present either ex1b-2 or ex1b-3 splicing and derives all from eye and retina libraries obtained at different developmental stages. (B) An RT-PCR experiment was performed on several mouse tissue cDNA using a specific couple of oligos that anneals respectively on exon 1b and on exon 4. The amplification products can be detected as a 200bp long or a 300bp long DNA fragment, depending if the splicing occurs on exon 2 or on exon 3. As control, the same experiment was performed using a couple of oligos specific for an housekeeping gene (GAPDH).

A



B

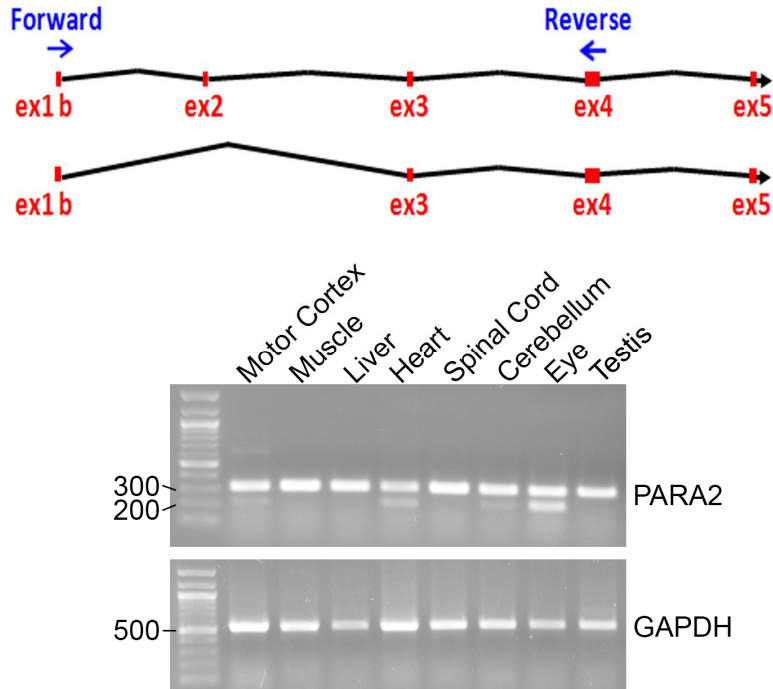


*Figure 2:*

**(A-C)** Immunofluorescence analysis on Paraplegin2 localization in MEF cells performed using a confocal microscope. The signal obtained by staining MEFS cells overexpressing Paraplegin with the  $\alpha$ -Paraplegin V61 antibody completely overlaps with the signal given by overexpression of mitochondrial-GFP. **(D-F)** As expected, Paraplegin2 loses the mitochondrial localization. **(G-L)** To further investigate the Paraplegin2 localization, we stained BC055488 overexpressing MEFS with GM130, a marker for Golgi, and with Calnexin, a marker for Endoplasmic Reticulum, revealing that Para2 localizes to the ER.

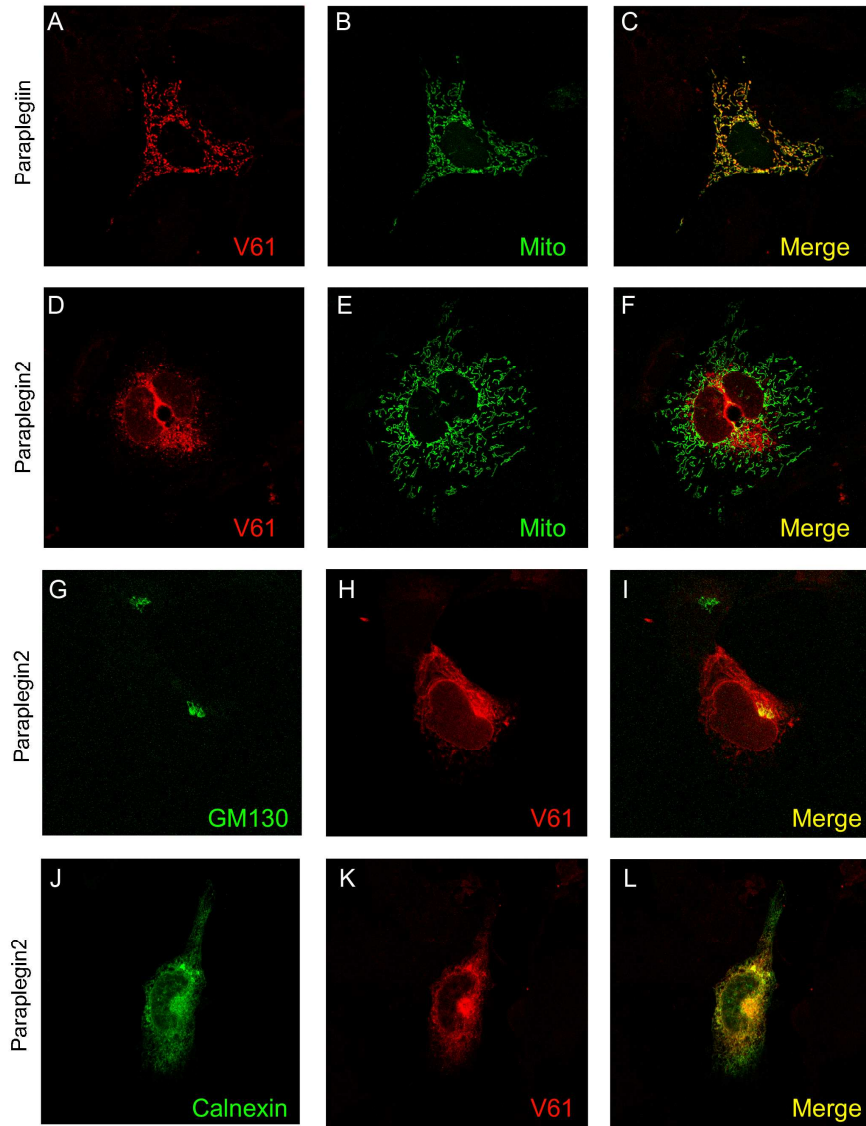




*Figure 3:*

**(A)** FPP assay on MEFs transfected with different GFPs. In the first lane we show the action of permeabilization with digitonin (10  $\mu$ M) on the cytosolic soluble fraction of GFP (lane 1). We perform the protection analysis adding 50  $\mu$ g/ml proteinase K and collecting new pictures after 3 minutes of treatment. Proteinase K action clearly disrupts the fluorescence pattern of cytosolic-exposed ER-GFP (lane 2), but can't act on both KDEL-GFP and Para2-GFP fluorescence pattern due to ER membrane protection (lane 3 and 4). **(B)** An SDS-page protection assay was then performed on COS7 cells transiently transfected with Para2-GFP construct. Para2-GFP was analyzed by incubation with  $\alpha$ -GFP antibody. Incubation with an N-terminal Calnexin antibody was performed as control. The asterisk marks an aspecific band revealed by  $\alpha$ -GFP antibody. The shift on Para2-GFP motility after Proteinase K treatment (Arrows) and the disappearing of the signal in presence of Triton X-100 demonstrate that Para2 exposes its catalytic domain inside ER-lumen **(C)**.

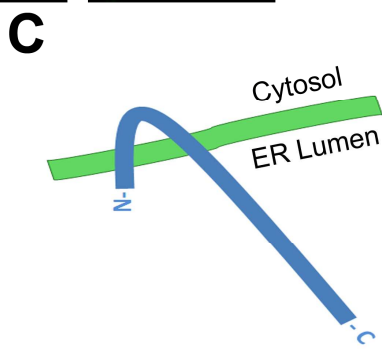
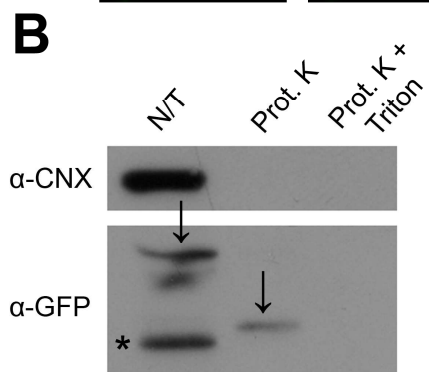
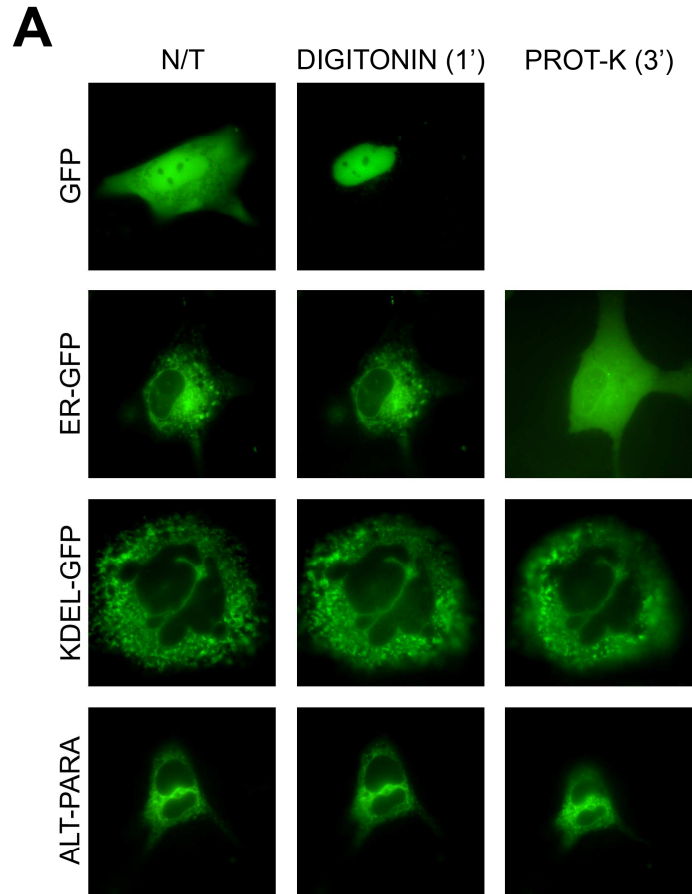


*Figure 4:*

**(A)** Gel Filtration analysis of Paraplegin and Paraplegin2 high molecular weight complexes. Extracts obtained from 10 cm plates of confluent COS7 cells transfected with Paraplegin and Paraplegin2 cDNAs were fractionated by Superose 6 sizing chromatography. Eluate fractions were TCA precipitated and analyzed by SDS-PAGE and immunoblotting using V61  $\alpha$ -Paraplegin polyclonal antibodies. Overexpression of Paraplegin and Paraplegin2 alone can't lead to the formation of an high molecular weight complex. **(B)** When AFG3L2 is co-expressed, the formation of a high molecular weight complex becomes possible for Paraplegin (\*), but not for Paraplegin2, suggesting that also in the ER a partner is needed. The following marker proteins were used for calibration: 1, Tyroglobulin (660 kDa); 2, Ferritin (440 kDa); 3, Alcohol Dehydrogenase (150 kDa); 4, Carbonic anhydrase (29 kDa).

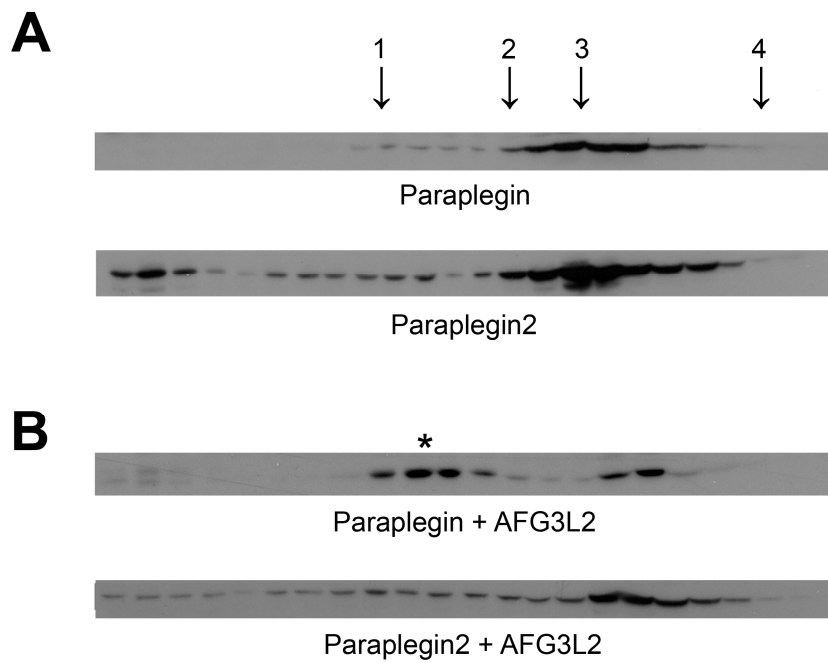
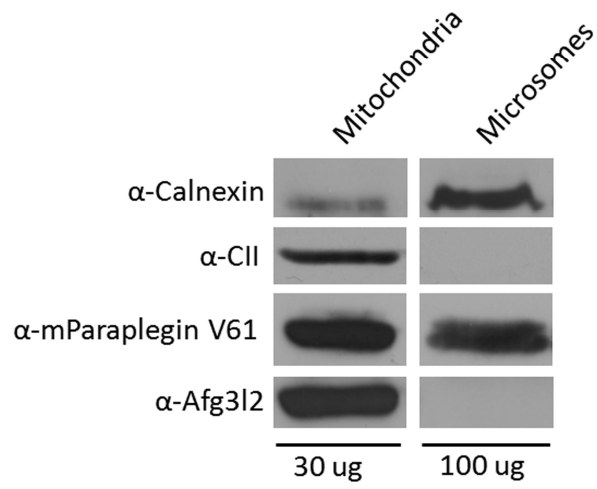


*Figure 5:*

**(A)** Western blot analysis of mitochondrial and microsomal fractions obtained from adult mouse brains. Enrichment of mitochondria and microsomes in the fraction were evaluated by using two specific markers: Calnexin for microsomes and 70 kDa subunit of Complex II for mitochondria. This experiment shows the presence of a protein with the same molecular weight of Paraplegin inside the microsomal fraction, recognized by V61 Paraplegin antibody. **(B)** Gel Filtration analysis of endogenous Paraplegin and Paraplegin2 high molecular weight complexes was then performed. Protein obtained from mitochondrial and microsomal purified fractions were fractionated by Superose 6 sizing chromatography. Eluate fractions were TCA precipitated and analyzed by SDS-PAGE and immunoblotting using V61  $\alpha$ -paraplegin polyclonal antibodies. The experiment shows the presence of an high molecular weight complex (\*) both in mitochondria and microsomes. The following marker proteins were used for calibration: 1, Tyroglobulin (660 kDa); 2, Ferritin (440 kDa); 3, Alcohol Dehydrogenase (150 kDa); 4, Carbonic Anhydrase (29 kDa).

**A**



**B**

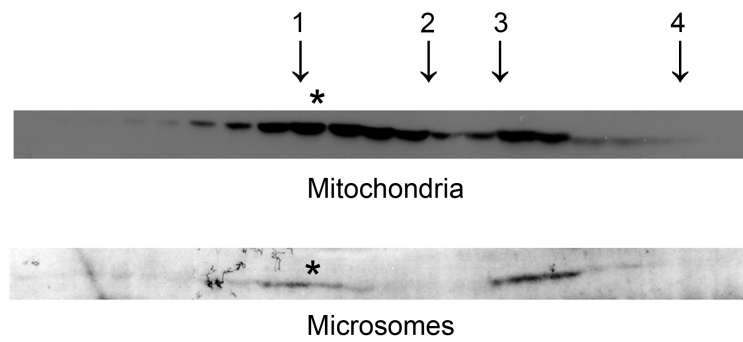
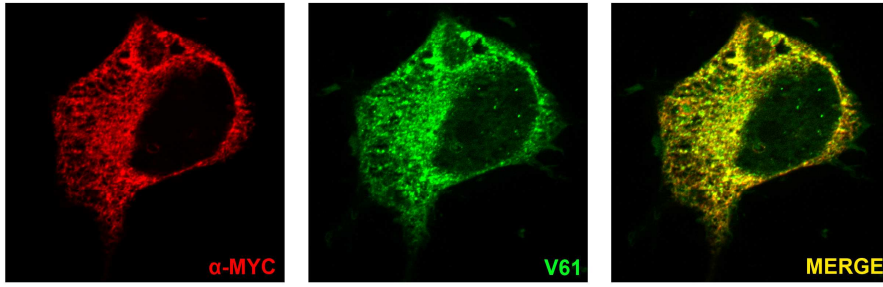


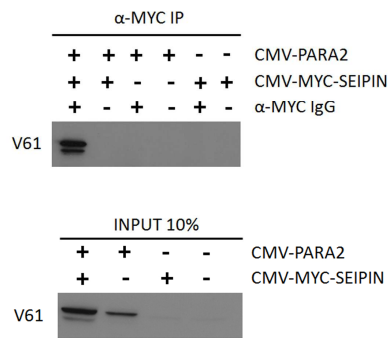
*Figure 6:*

**(A)** Immunofluorescence assay on COS7 cells overexpressing Paraplegin2 and myc-Seipin shows perfect colocalization between the two proteins. **(B-C)** We used the same overexpression system to co-immunoprecipitate myc-Seipin and Paraplegin2 and we obtained positive results pulling down myc-Seipin and revealing for Paraplegin2, but also pulling down Paraplegin2 and revealing for myc-Seipin. **(D)** As expected, this interaction is specific for Paraplegin2 and cannot be obtained using Paraplegin. Moreover, HSP linked mutation in glycosylation sites of myc-Seipin (N88S) do not affect the co-immunoprecipitation.

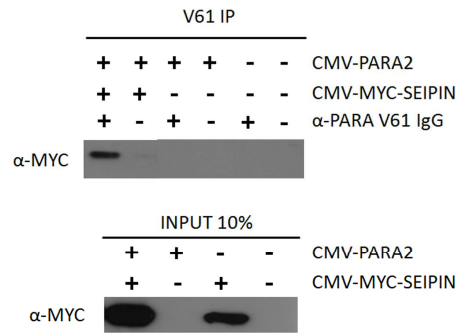
**A**



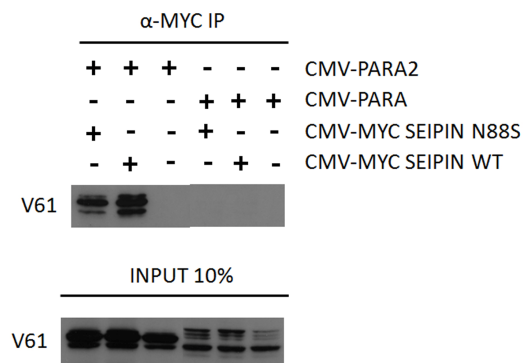
**B**



**C**



**D**

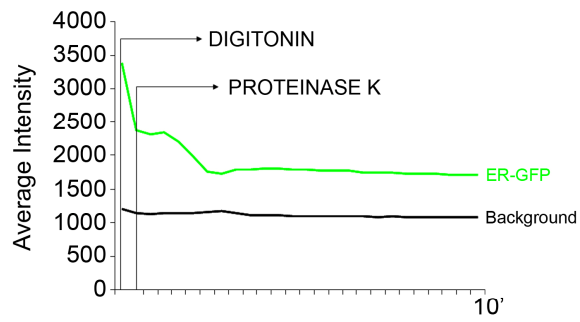




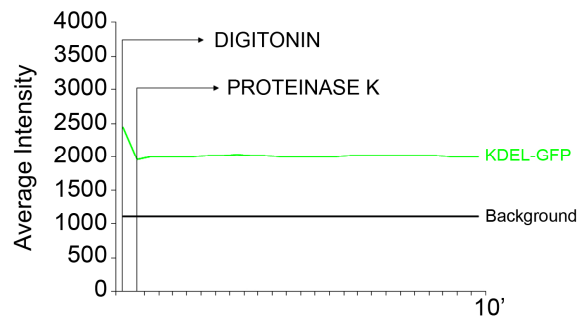
*Supplementary Figure 1:*

Quantification of FPP assay. Fluorescence of different GFPs were quantified in live imaging using a cooled camera (QUANTEM 512 SC) driven by METAMORPH software (Molecular Devices Ltd, Downingtown, PA, USA). Images were collected every 5 seconds for 10 minutes. Decrease in signal intensity after addition of proteinase K is visible, as expected, for ER-GFP (**A**), but not for KDEL-GFP (**B**) and Para2-GFP (**C**), demonstrating that Para2 catalytic domain is protected by ER membrane end exposed into ER lumen.

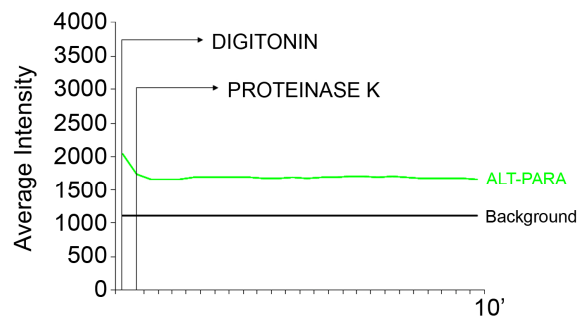
**A**



**B**



**C**



## References

1. Harding AE: **In the hereditary ataxias and related disorders.**; 1984.
2. Salinas S, Proukakis C, Crosby A, Warner TT: **Hereditary spastic paraplegia: clinical features and pathogenetic mechanisms.** *Lancet Neurol* 2008, **7**(12):1127-1138.
3. Reid E. REI: **Scriver's Online Metabolic and Molecular Bases of Inherited Diseases.** In: *Hereditary Spastic Paraplegia.* Edited by Valle B, Vogelstein, Kinzler, Antonarakis, Ballabio; 2010.
4. Park SH, Zhu PP, Parker RL, Blackstone C: **Hereditary spastic paraplegia proteins REEP1, spastin, and atlastin-1 coordinate microtubule interactions with the tubular ER network.** *J Clin Invest* 2010, **120**(4):1097-1110.
5. Botzolakis EJ, Zhao J, Gurba KN, Macdonald RL, Hedera P: **The effect of HSP-causing mutations in SPG3A and NIPA1 on the assembly, trafficking, and interaction between atlastin-1 and NIPA1.** *Mol Cell Neurosci* 2011, **46**(1):122-135.
6. Goytain A, Hines RM, El-Husseini A, Quamme GA: **NIPA1(SPG6), the basis for autosomal dominant form of hereditary spastic paraplegia, encodes a functional Mg<sup>2+</sup> transporter.** *J Biol Chem* 2007, **282**(11):8060-8068.
7. Ito D, Fujisawa T, Iida H, Suzuki N: **Characterization of seipin/BSCL2, a protein associated with spastic paraplegia 17.** *Neurobiol Dis* 2008, **31**(2):266-277.

8. Casari G, De Fusco M, Ciarmatori S, Zeviani M, Mora M, Fernandez P, De Michele G, Filla A, Coccozza S, Marconi R *et al*: **Spastic paraplegia and OXPHOS impairment caused by mutations in paraplegin, a nuclear-encoded mitochondrial metalloprotease.** *Cell* 1998, **93**(6):973-983.
9. Hansen JJ, Durr A, Cournu-Rebeix I, Georgopoulos C, Ang D, Nielsen MN, Davoine CS, Brice A, Fontaine B, Gregersen N *et al*: **Hereditary spastic paraplegia SPG13 is associated with a mutation in the gene encoding the mitochondrial chaperonin Hsp60.** *Am J Hum Genet* 2002, **70**(5):1328-1332.
10. Fink JK: **Hereditary spastic paraplegia.** *Curr Neurol Neurosci Rep* 2006, **6**(1):65-76.
11. Fink JK: **Sporadically occurring neurologic disease: HSP genes and apparently sporadic spastic paraplegia.** *Neurology* 2008, **71**(19):1468-1469.
12. Arlt H, Tauer R, Feldmann H, Neupert W, Langer T: **The YTA10-12 complex, an AAA protease with chaperone-like activity in the inner membrane of mitochondria.** *Cell* 1996, **85**(6):875-885.
13. Banfi S, Bassi MT, Andolfi G, Marchitello A, Zanotta S, Ballabio A, Casari G, Franco B: **Identification and characterization of AFG3L2, a novel paraplegin-related gene.** *Genomics* 1999, **59**(1):51-58.
14. Kremmidiotis G, Gardner AE, Settasatian C, Savoia A, Sutherland GR, Callen DF: **Molecular and functional analyses of the human and mouse genes encoding AFG3L1, a**

- mitochondrial metalloprotease homologous to the human spastic paraplegia protein.** *Genomics* 2001, **76**(1-3):58-65.
15. Neuwald AF, Aravind L, Spouge JL, Koonin EV: **AAA+: A class of chaperone-like ATPases associated with the assembly, operation, and disassembly of protein complexes.** *Genome Res* 1999, **9**(1):27-43.
  16. Leonhard K, Guiard B, Pellecchia G, Tzagoloff A, Neupert W, Langer T: **Membrane protein degradation by AAA proteases in mitochondria: extraction of substrates from either membrane surface.** *Mol Cell* 2000, **5**(4):629-638.
  17. Tatsuta T, Augustin S, Nolden M, Friedrichs B, Langer T: **m-AAA protease-driven membrane dislocation allows intramembrane cleavage by rhomboid in mitochondria.** *EMBO J* 2007, **26**(2):325-335.
  18. Nolden M, Ehses S, Koppen M, Bernacchia A, Rugarli EI, Langer T: **The m-AAA protease defective in hereditary spastic paraplegia controls ribosome assembly in mitochondria.** *Cell* 2005, **123**(2):277-289.
  19. Koppen M, Metodiev MD, Casari G, Rugarli EI, Langer T: **Variable and tissue-specific subunit composition of mitochondrial m-AAA protease complexes linked to hereditary spastic paraplegia.** *Mol Cell Biol* 2007, **27**(2):758-767.
  20. Martinelli P, La Mattina V, Bernacchia A, Magnoni R, Cerri F, Cox G, Quattrini A, Casari G, Rugarli EI: **Genetic interaction between the m-AAA protease isoenzymes reveals novel**

- roles in cerebellar degeneration.** *Hum Mol Genet* 2009, **18**(11):2001-2013.
21. Ferreirinha F, Quattrini A, Pirozzi M, Valsecchi V, Dina G, Broccoli V, Auricchio A, Piemonte F, Tozzi G, Gaeta L *et al*: **Axonal degeneration in paraplegin-deficient mice is associated with abnormal mitochondria and impairment of axonal transport.** *J Clin Invest* 2004, **113**(2):231-242.
  22. Pirozzi M, Quattrini A, Andolfi G, Dina G, Malaguti MC, Auricchio A, Rugarli EI: **Intramuscular viral delivery of paraplegin rescues peripheral axonopathy in a model of hereditary spastic paraplegia.** *J Clin Invest* 2006, **116**(1):202-208.
  23. Koppen M, Bonn F, Ehses S, Langer T: **Autocatalytic processing of m-AAA protease subunits in mitochondria.** *Mol Biol Cell* 2009, **20**(19):4216-4224.
  24. Lorenz H, Hailey DW, Wunder C, Lippincott-Schwartz J: **The fluorescence protease protection (FPP) assay to determine protein localization and membrane topology.** *Nat Protoc* 2006, **1**(1):276-279.
  25. Bulbarelli A, Sprocati T, Barberi M, Pedrazzini E, Borgese N: **Trafficking of tail-anchored proteins: transport from the endoplasmic reticulum to the plasma membrane and sorting between surface domains in polarised epithelial cells.** *J Cell Sci* 2002, **115**(Pt 8):1689-1702.
  26. Hanson PI, Whiteheart SW: **AAA+ proteins: have engine, will work.** *Nat Rev Mol Cell Biol* 2005, **6**(7):519-529.

27. Ito D, Suzuki N: **Seipinopathy: a novel endoplasmic reticulum stress-associated disease.** *Brain* 2009, **132**(Pt 1):8-15.
28. Errico A, Ballabio A, Rugarli EI: **Spastin, the protein mutated in autosomal dominant hereditary spastic paraplegia, is involved in microtubule dynamics.** *Hum Mol Genet* 2002, **11**(2):153-163.
29. Ehses S, Raschke I, Mancuso G, Bernacchia A, Geimer S, Tondera D, Martinou JC, Westermann B, Rugarli EI, Langer T: **Regulation of OPA1 processing and mitochondrial fusion by m-AAA protease isoenzymes and OMA1.** *J Cell Biol* 2009, **187**(7):1023-1036.
30. Coppola M, Pizzigoni A, Banfi S, Bassi MT, Casari G, Incerti B: **Identification and characterization of YME1L1, a novel paraplegin-related gene.** *Genomics* 2000, **66**(1):48-54.
31. Griparic L, Kanazawa T, van der Blik AM: **Regulation of the mitochondrial dynamin-like protein Opa1 by proteolytic cleavage.** *J Cell Biol* 2007, **178**(5):757-764.
32. Deak PM, Wolf DH: **Membrane topology and function of Der3/Hrd1p as a ubiquitin-protein ligase (E3) involved in endoplasmic reticulum degradation.** *J Biol Chem* 2001, **276**(14):10663-10669.
33. Hampton RY, Gardner RG, Rine J: **Role of 26S proteasome and HRD genes in the degradation of 3-hydroxy-3-methylglutaryl-CoA reductase, an integral endoplasmic reticulum membrane protein.** *Mol Biol Cell* 1996, **7**(12):2029-2044.

34. Kreft SG, Wang L, Hochstrasser M: **Membrane topology of the yeast endoplasmic reticulum-localized ubiquitin ligase Doa10 and comparison with its human ortholog TEB4 (MARCH-VI).** *J Biol Chem* 2006, **281**(8):4646-4653.
35. Binns D, Lee S, Hilton CL, Jiang QX, Goodman JM: **Seipin is a discrete homooligomer.** *Biochemistry* 2010, **49**(50):10747-10755.
36. Szymanski KM, Binns D, Bartz R, Grishin NV, Li WP, Agarwal AK, Garg A, Anderson RG, Goodman JM: **The lipodystrophy protein seipin is found at endoplasmic reticulum lipid droplet junctions and is important for droplet morphology.** *Proc Natl Acad Sci U S A* 2007, **104**(52):20890-20895.
37. Blackstone C, O'Kane CJ, Reid E: **Hereditary spastic paraplegias: membrane traffic and the motor pathway.** *Nat Rev Neurosci* 2011, **12**(1):31-42.



# Conclusions

## **SPG4 and Spastin: relevance for translational research**

To better understand the pathogenetic mechanism of Spastin related AD-HSP, we firstly decided to better characterize the SPG4 mutation spectrum. Even if the majority of cases are clearly related to loss-of-function alleles, it is possible that truncated polypeptides may be produced by certain mutations, acting in a dominant negative fashion [1]. In our study we showed that no aberrant proteins were found in cells lines obtained from several patients carrying splice-sites or nonsense mutations, confirming that haplo-insufficiency is the most common cause of the disease. For this reason, down-regulation approaches are the best way to characterize the pathogenesis of HSP in *ex-vivo* studies performed on primary neuronal cell lines [1-3].

Spastin plays a crucial role in neurons. Axons of these cells can reach in humans up to 1m of length and for this reason they are highly dependent on a really efficient transport machinery. Consistently, Spastin is enriched in cellular regions characterized by high cytoskeletal dynamicity like the growth cone and branching points [3-5]. Moreover, *Drosophila* studies report a crucial role of Spastin also in dendritic branching and arbor formation [6]. Down-regulation of Spastin in hippocampal primary neurons causes a severe alteration of the global morphology of the cells, which lose their reproducible and stereotyped shape characterized by one axon, a single apical

dendrite, and several shorter basilar dendrites. The length of the longest process of each neuron was significantly affected when Spastin was knocked down, while dendrite number and length and neurite branching were not altered. This phenotype was also described for a *Zebrafish* model of Spastin knock-down [7]. The alteration in neuronal structure is connected with a strong stabilization of the microtubule network associated to a reduction in microtubule polymerization rate. On the other hand, we also demonstrated that strong, but also milder over-expression of Spastin affects the cytoskeletal dynamics reducing consistently the amount of stable microtubule. All together, these data suggest that Spastin levels are crucial for a correct neurite outgrowth and underline how therapeutic approaches based on over-expression systems cannot be used for HSP patients mutated in SPG4.

Moreover, the existence of two different isoforms of Spastin contribute to complicate the studies of the disease. Even if the full-length isoform is localized to the early secretory pathway while the short isoform can be strongly and preferentially recruited to endosomes [8], both Spastin isoforms can act as microtubule severing proteins [1, 9, 10]. Up to now, it is not yet completely clear the relevance of M1 and M87 Spastin in the disease, but some clues are present showing that the long isoform may play a direct role in the pathogenesis. First of all the full-length protein is more expressed in nervous system [11]. Secondly, a lot of different interactors have been reported as M1 specific, one of which is the HSP protein Atlastin, suggesting a different role of the two isoforms related with

intracellular trafficking [8, 12, 13]. Finally, we described a novel mechanism for regulation of M1 and M87 transcription based on the existence of a cryptic promoter in the first SPG4 gene. This promoter guide the transcription of a RNA encoding only for the shorter Spastin isoform and shows a kind of cellular specific activity [14]. Our data on two polymorphisms reported as phenotype modifier when present in patient carrying SPG4 mutation on the other allele (c. 131C>T and c. 134 C>A) [15-17] demonstrate that only one of these two base substitutions (c. 131C>T) altered the activity of the cryptic promoter. These findings suggest the idea that a change in the amino acidic structure of the protein (S44L and P45Q) is the real responsible for the worsening of the phenotype shown by patients, proving an active relevance of M1 Spastin in the disease [14]. Further studies are needed to clarify the real role of the two Spastin isoforms, but our analysis of transcriptional regulation of SPG4 gene may be used in future for establishing therapeutic approaches based on selective regulation of long and short Spastin.

## **SPG7 and Paraplegin: relevance for translational research**

Identification of mutations in SPG7 directly correlate mitochondrial dysfunction with retrograde degeneration of neuron axons present in AR-HSP patients [18]. Interestingly, also mutations in the other *m*-AAA subunit AFG3L2 cause a neuronal specific cellular phenotype that lead to an Autosomal Dominant form of Spino-Cerebellar Ataxia (SCA28) [19]. Even if both diseases can present common features, the reason why alteration in the same molecular complex leads to different tissue specific cell death remains unclear. In mice, AFG3L1, AFG3L2 and Paraplegin are ubiquitously expressed, but show tissue specific differences in expression levels [20, 21]. This leads to high variability both in *m*-AAA protease total amount, but also in the ratio between homo- and hetero-oligomeric complexes.

In our analysis we demonstrate that, in MEF cells, homo- and hetero-oligomeric *m*-AAA complexes show at least a partial redundancy in terms of mitochondrial morphology and OPA1 processing, pointing out how an almost complete removal of the *m*-AAA is needed to trigger mitochondrial network and cristae impairments [22]. The inability of Paraplegin to form a homo-oligomeric complex can therefore explain why SPG7 mutations are more tolerated in humans than the one in AFG3L2. Patients develop the disease only when a complete loss of Paraplegin occurs, while for AFG3L2 reduced levels of 50% are enough to trigger the pathogenesis. In this second case, in fact, cells will lose both homo- and hetero-oligomeric *m*-AAA complexes [20, 23]. If this redundancy will be also proved in tissues,

demonstrating a close relation between phenotype and total levels of *m*-AAA independently from its subunit composition, we may hypothesize to rescue the SPG7<sup>-/-</sup> mouse phenotype infecting them with AAV viruses carrying AFG3L2 cDNA and reproducing an effect similar or identical to the one obtained with SPG7 cDNA infection [24]. This could also suggest new possible therapeutic strategies in patients treatment, for example by up-regulating the expression levels of AFG3L2, a gene already present in their cells.

Otherwise, the existence of tissue specific unknown substrates for hetero- or homo- oligomeric complexes cannot be excluded and may explain why different tissues show variability in *m*-AAA protease complexes ratio. In this case changes in the level of the other *m*-AAA subunits will not be able rescue the patients phenotype.

Another important findings of our study was to disclose the relation between *m*-AAA protease defects and alterations in OPA1 processing. While *m*-AAA protease was previously described as the responsible for OPA1 cleavage in yeast reconstituted systems [25], we clearly demonstrated that drastic reduction of *m*-AAA subunits levels in MEF cells triggers an accelerated processing/degradation of OPA1 long isoforms. This proteolytic action is performed by OMA1 and lead, as final consequence, to disruption of mitochondrial network due to mitochondrial fragmentation and alteration in cristae morphology [22]. These mitochondrial abnormalities are common to several neurodegenerative diseases and can potentially play a key role in the pathogenesis of HSP and SCA28. Notably, the action of OMA on OPA1 long isoforms occurs also as a consequence to other mitochondrial

stress conditions, suggesting the idea that mitochondrial fragmentation may play a positive role in cellular surveillance on short terms period, but may be detrimental when protracted [22]. This hypothesis fits with the late onset of the diseases, where a prolonged time of *m*-AAA protease deprivation in affected cells cannot be overcome by the immediate OMA1 response. On the other hand, up to now we cannot exclude that OMA1 response does not lead to any beneficial effort for the cells even after short time periods. If this is the case, OMA1 activation may be studied as a target for therapeutic treatments of SPG7 related HSP and AFG3L2 related SCA28.

Finally our last findings evidence the presence of an alternative splicing for the SPG7 gene that encodes a non-mitochondrial form of Paraplegin (Mancuso et al, unpublished data). Remarkably, this splicing is conserved in humans. All the mutations found in SPG7 patients localize to exons that are in common for the two isoforms, opening up the hypothesis that a lack of Paraplegin2 can contribute to patient phenotypes in a non-mitochondrial matter. Interestingly, several HSP have been linked to ER stress conditions and misfolded/aberrant protein accumulation in the ER membrane. Even if the proteolytic function of Paraplegin2 in the ER has still to be empirically proved, the complete identity between Paraplegin and Paraplegin2 permits us to speculate about a possible role of this novel isoform in ER stress related HSPs. Moreover, bioinformatic approaches suggest an enrichment of Paraplegin2 mRNA levels in

specific tissues like retina, opening up the possibility of a role of SPG7 gene in other diseases.

## References

1. Solowska JM, Morfini G, Falnikar A, Himes BT, Brady ST, Huang D, Baas PW: **Quantitative and functional analyses of spastin in the nervous system: implications for hereditary spastic paraplegia.** *J Neurosci* 2008, **28**(9):2147-2157.
2. Riano E, Martignoni M, Mancuso G, Cartelli D, Crippa F, Toldo I, Siciliano G, Di Bella D, Taroni F, Bassi MT *et al*: **Pleiotropic effects of spastin on neurite growth depending on expression levels.** *J Neurochem* 2009, **108**(5):1277-1288.
3. Yu W, Qiang L, Solowska JM, Karabay A, Korulu S, Baas PW: **The microtubule-severing proteins spastin and katanin participate differently in the formation of axonal branches.** *Mol Biol Cell* 2008, **19**(4):1485-1498.
4. Errico A, Claudiani P, D'Addio M, Rugarli EI: **Spastin interacts with the centrosomal protein NA14, and is enriched in the spindle pole, the midbody and the distal axon.** *Hum Mol Genet* 2004, **13**(18):2121-2132.
5. Svenson IK, Kloos MT, Jacon A, Gallione C, Horton AC, Pericak-Vance MA, Ehlers MD, Marchuk DA: **Subcellular localization of spastin: implications for the pathogenesis of hereditary spastic paraplegia.** *Neurogenetics* 2005, **6**(3):135-141.
6. Jinushi-Nakao S, Arvind R, Amikura R, Kinameri E, Liu AW, Moore AW: **Knot/Collier and cut control different aspects of dendrite cytoskeleton and synergize to define final arbor shape.** *Neuron* 2007, **56**(6):963-978.




7. Wood JD, Landers JA, Bingley M, McDermott CJ, Thomas-McArthur V, Gleadall LJ, Shaw PJ, Cunliffe VT: **The microtubule-severing protein Spastin is essential for axon outgrowth in the zebrafish embryo.** *Hum Mol Genet* 2006, **15**(18):2763-2771.
8. Connell JW, Lindon C, Luzio JP, Reid E: **Spastin couples microtubule severing to membrane traffic in completion of cytokinesis and secretion.** *Traffic* 2009, **10**(1):42-56.
9. Roll-Mecak A, Vale RD: **Structural basis of microtubule severing by the hereditary spastic paraplegia protein spastin.** *Nature* 2008, **451**(7176):363-367.
10. White SR, Evans KJ, Lary J, Cole JL, Lauring B: **Recognition of C-terminal amino acids in tubulin by pore loops in Spastin is important for microtubule severing.** *J Cell Biol* 2007, **176**(7):995-1005.
11. Claudiani P, Riano E, Errico A, Andolfi G, Rugarli EI: **Spastin subcellular localization is regulated through usage of different translation start sites and active export from the nucleus.** *Exp Cell Res* 2005, **309**(2):358-369.
12. Evans K, Keller C, Pavur K, Glasgow K, Conn B, Lauring B: **Interaction of two hereditary spastic paraplegia gene products, spastin and atlastin, suggests a common pathway for axonal maintenance.** *Proc Natl Acad Sci U S A* 2006, **103**(28):10666-10671.
13. Sanderson CM, Connell JW, Edwards TL, Bright NA, Duley S, Thompson A, Luzio JP, Reid E: **Spastin and atlastin, two**

- proteins mutated in autosomal-dominant hereditary spastic paraplegia, are binding partners.** *Hum Mol Genet* 2006, **15**(2):307-318.
14. Mancuso G, Rugarli EI: **A cryptic promoter in the first exon of the SPG4 gene directs the synthesis of the 60-kDa spastin isoform.** *BMC Biol* 2008, **6**:31.
  15. Chinnery PF, Keers SM, Holden MJ, Ramesh V, Dalton A: **Infantile hereditary spastic paraparesis due to codominant mutations in the spastin gene.** *Neurology* 2004, **63**(4):710-712.
  16. Svenson IK, Kloos MT, Gaskell PC, Nance MA, Garbern JY, Hisanaga S, Pericak-Vance MA, Ashley-Koch AE, Marchuk DA: **Intragenic modifiers of hereditary spastic paraplegia due to spastin gene mutations.** *Neurogenetics* 2004, **5**(3):157-164.
  17. McDermott CJ, Burness CE, Kirby J, Cox LE, Rao DG, Hewamadduma C, Sharrack B, Hadjivassiliou M, Chinnery PF, Dalton A *et al*: **Clinical features of hereditary spastic paraplegia due to spastin mutation.** *Neurology* 2006, **67**(1):45-51.
  18. Casari G, De Fusco M, Ciarmatori S, Zeviani M, Mora M, Fernandez P, De Michele G, Filla A, Coccozza S, Marconi R *et al*: **Spastic paraplegia and OXPHOS impairment caused by mutations in paraplegin, a nuclear-encoded mitochondrial metalloprotease.** *Cell* 1998, **93**(6):973-983.
  19. Di Bella D, Lazzaro F, Brusco A, Plumari M, Battaglia G, Pastore A, Finardi A, Cagnoli C, Tempia F, Frontali M *et al*: **Mutations**

- in the mitochondrial protease gene AFG3L2 cause dominant hereditary ataxia SCA28.** *Nat Genet* 2010, **42**(4):313-321.
20. Koppen M, Metodiev MD, Casari G, Rugarli EI, Langer T: **Variable and tissue-specific subunit composition of mitochondrial m-AAA protease complexes linked to hereditary spastic paraplegia.** *Mol Cell Biol* 2007, **27**(2):758-767.
21. Martinelli P, La Mattina V, Bernacchia A, Magnoni R, Cerri F, Cox G, Quattrini A, Casari G, Rugarli EI: **Genetic interaction between the m-AAA protease isoenzymes reveals novel roles in cerebellar degeneration.** *Hum Mol Genet* 2009, **18**(11):2001-2013.
22. Ehses S, Raschke I, Mancuso G, Bernacchia A, Geimer S, Tondera D, Martinou JC, Westermann B, Rugarli EI, Langer T: **Regulation of OPA1 processing and mitochondrial fusion by m-AAA protease isoenzymes and OMA1.** *J Cell Biol* 2009, **187**(7):1023-1036.
23. Nolden M, Ehses S, Koppen M, Bernacchia A, Rugarli EI, Langer T: **The m-AAA protease defective in hereditary spastic paraplegia controls ribosome assembly in mitochondria.** *Cell* 2005, **123**(2):277-289.
24. Pirozzi M, Quattrini A, Andolfi G, Dina G, Malaguti MC, Auricchio A, Rugarli EI: **Intramuscular viral delivery of paraplegin rescues peripheral axonopathy in a model of hereditary spastic paraplegia.** *J Clin Invest* 2006, **116**(1):202-208.

25. Duvezin-Caubet S, Koppen M, Wagener J, Zick M, Israel L, Bernacchia A, Jagasia R, Rugarli EI, Imhof A, Neupert W *et al*: **OPA1 processing reconstituted in yeast depends on the subunit composition of the m-AAA protease in mitochondria.** *Mol Biol Cell* 2007, **18**(9):3582-3590.

# Publications

**BMC Biology** 

Research article **Open Access**

**A cryptic promoter in the first exon of the *SPG4* gene directs the synthesis of the 60-kDa spastin isoform**  
Giuseppe Mancuso<sup>1</sup> and Elena I Rugarli<sup>\*1,2</sup>

Address: <sup>1</sup>Division of Biochemistry and Genetics, Istituto Neurologico 'C. Besta', Milan, Italy and <sup>2</sup>Department of Neuroscience and Medical Biotechnologies, University of Milano-Bicocca, Milan, Italy  
Email: Giuseppe Mancuso - giuseppe.mancuso@istituto-besta.it; Elena I Rugarli<sup>\*</sup> - elena.rugarli@unimib.it  
<sup>\*</sup> Corresponding author

**Journal of Neurochemistry** 

JOURNAL OF NEUROCHEMISTRY | 2009 | 108 | 1277-1288 doi: 10.1111/j.1471-4159.2009.05875.x

**Pleiotropic effects of spastin on neurite growth depending on expression levels**

Elena Riano,<sup>\*</sup> Monica Martignoni,<sup>\*</sup> Giuseppe Mancuso,<sup>\*</sup> Daniele Cartelli,<sup>†</sup> Francesca Crippa,<sup>‡</sup> Irene Toldo,<sup>§</sup> Gabriele Siciliano,<sup>¶</sup> Daniela Di Bella,<sup>\*</sup> Franco Taroni,<sup>\*</sup> Maria Teresa Bassi,<sup>‡</sup> Graziella Cappelletti<sup>†</sup> and Elena I. Rugarli<sup>\*\*\*</sup>

Published December 28, 2009 **JCB: Article**

**Regulation of OPA1 processing and mitochondrial fusion by *m*-AAA protease isoenzymes and OMA1**

Sarah Ehnes,<sup>1,2,3</sup> Ines Raschke,<sup>1,2,3</sup> Giuseppe Mancuso,<sup>5</sup> Andrea Bernacchia,<sup>5</sup> Stefan Geimer,<sup>7</sup> Daniel Tondera,<sup>8</sup> Jean-Claude Martinou,<sup>9</sup> Benedikt Westermann,<sup>7</sup> Elena I. Rugarli,<sup>5,6</sup> and Thomas Langer<sup>1,2,3,4</sup>

# Acknowledgments

Like the last time and hopefully for the LAST time, here I am finishing to write a thesis with acknowledgments to people that made all this possible.

The first thanks goes to my parents, to whom all this work is dedicated to. Their help and support were constantly present and even when I had to take important decisions, like moving in Germany, I always had their backing. Thanks a lot for everything.

Second thanks goes for sure to Elena, for all the lessons and the incentives that helped me growing during all the time I spent in her group. The bad think about this job is that we never have a finishing point, but just new starting lines, otherwise I would have been glad to consider AG Rugarli as my final goal.

Then comes Polly, obviously, turned from colleague to friend, then to girlfriend and finally to my wife to be. I don't think there are so many things to say about a person I'm happy to spend (literally) every single minute of my days with. To have her by my side played a key role in successfully finishing this experience, so thanks a lot also to her.

Finally, I must thanks all my past and present colleagues. The Milano's team: Andrev, la Popi, la Ryan, Möni, Ianlu, Pit, Paolina and (almost) all the guys from Besta for all the amazing moments spent in the lab, but specially outside of it. And also the German's team: Jette,

Esther, Eva, Sabrina, Sara, Fede, Dominic and the newcomers. To them the acknowledgment for making me feel a little less far from home. Special mention goes also to AG Langer guys and Thomas himself, for constant support, ideas and some really appreciated dinners.

I finish with an enormous thanks to all my true friends, present in my life now that I'm 900 km far away exactly in the same way they have been when we lived in the same block. With my parents, the reason why I'll not be able to do my job wherever is not Milano. I love you all, guys.

Ok, that's all, but I would like to use this moment also to say some important un-polite words.

No thanks goes to those who made almost impossible to be a scientist in Italy, to those who asked me to choose between work and life, to those who try to boycott talent or force it to escape far away, to those constantly work trying to give no future to young people. Most important, no thanks to all the people that turned my Country into something I don't have to be grateful to after reaching such a result as a PhD degree.

*NB: This part is the only one no one corrected in terms of English, I hope it's not too bad...*

### *Ringraziamenti in italiano*

Come l'ultima volta e spero per l'ULTIMA volta, eccomi qui a concludere la stesura della tesi con i ringraziamenti alle persone che l'hanno resa possibile.

Il primo grazie va sicuramente ai miei genitori, a cui ho dedicato tutto questo lavoro. Il loro aiuto ed il loro supporto sono stati costantemente presenti ed anche nel momento delle scelte importanti, come ad esempio il trasferirmi in Germania, il loro appoggio non è mai mancato. Grazie di tutto.

Il secondo grazie va sicuramente ad Elena, per gli insegnamenti i continui stimoli che mi hanno aiutato a crescere durante tutto il periodo che ho passato nel suo gruppo. Il brutto di questo lavoro è che non c'è mai un punto di arrivo, ma solo nuovi punti di partenza, perché avrei fatto volentieri dell'AG Rugarli il mio traguardo.

Poi c'è la Polly, ovviamente, trasformatasi negli anni da collega, ad amica, a fidanzata a futura sposa. Non credo ci sia molto da scrivere riguardo una persona con cui sono felice di passare (letteralmente) ogni singolo minuto della mia giornata. Averla vicina è stato fondamentale per arrivare alla fine di questa esperienza, quindi grazie mille anche a lei.

Per finire poi, un ringraziamento doveroso va a tutti i miei colleghi passati e presenti. Il team di Milano: Andrev, la Popi, la Ryan, Möni, Ianlu, Pit, Paolina e (quasi)tutti i ragazzi del Besta per i fantastici momenti trascorsi assieme, in laboratorio come soprattutto fuori. E poi il nuovo team teutonico: Jette, Esther, Eva, Sabrina, Sara, Fede,



Dominic e i nuovi arrivati. A loro va il ringraziamento per avermi fatto sentire un po' meno distante da casa. Una menzione speciale va anche al gruppo Langer ed allo stesso Thomas, per il costante supporto, lo scambio di idee ed alcune cene molto apprezzate.

Chiudo con un gigantesco grazie a tutti gli amici veri, presenti oggi che sono a 900 km di distanza esattamente come lo erano quando si viveva nello stesso isolato. Insieme ai miei, la ragione che mi rende impossibile fare questo lavoro ovunque non sia Milano. Vi voglio bene.

Ok, avrei detto tutto, però voglio togliermi un piccolo sassolino dalla scarpa.

Nessun ringraziamento per chi rende la ricerca in Italia impossibile o quasi, per chi costringe ragazzi come me a scegliere tra il lavoro e gli affetti, per chi cerca di boicottare il talento o lo costringe a scappare lontano, per chi lavora quotidianamente nel tentativo di privare i giovani di un futuro. Soprattutto, nessun ringraziamento per chi ha reso possibile che il mio Paese non fosse più qualcosa a cui essere grati dopo il conseguimento di un risultato come può essere il dottorato di ricerca.